Direction of Arrival Estimation for Spinning Antenna Based Electronic Intelligence Systems

By

Fuad Alibrahim

Supervisor: M. R. Inggs

Thesis Presented for the Degree of

DOCTOR OF PHILOSOPHY

In the Department of Electrical Engineering

UNIVERSITY OF CAPE TOWN

March 2021

Declaration

I declare that this thesis is my own, unaided work. It is being submitted for the degree of Doctor of Philosophy in Engineering in the University of Cape Town. It has not been submitted before for any degree or examination in any other university.

Signature of Author: Signed by candidate

ABSTRACT

The spinning directional antenna is the most cost-effective antenna configuration for providing high gain over a wide (multi-octave) radio frequency (RF) range. Thus, it is the appropriate antenna configuration for increasing the intercept range of an electronic intelligence (ELINT) system, which is an important requirement due to the advanced capabilities of modern RF emitters.

An ELINT system employing the spinning antenna configuration is capable of accurately estimating the direction of arrival (DOA) of the received signals, provided that: the antenna's beamwidth is narrow; the received data is fully spread across the antenna mainlobe; the number of data samples is large; the signal to disturbance ratio (SDR) is large. However, the antenna's beamwidth may be wide due to the wide operating RF range and physical constraints; the received data may be partially spread across the antenna mainlobe due to the agility of the received signals, errors in estimating the signals' parameters and missing data samples; the number of data samples may be small; the SDR may be small.

The presence of the aforementioned factors significantly degrades the DOA estimation accuracy. To overcome this problem, we propose the use of biased estimators for estimating the DOA of emitters' signals received by a spinning antenna based ELINT system. The proposed biased DOA estimators were constructed using Bayesian estimation techniques and by performing a linear transformation and an affine transformation on the maximum likelihood (ML) estimator.

Using Monte Carlo simulation and real radar data, we demonstrate that: the proposed biased DOA estimators outperform the mean square error (MSE) limit specified by the popular performance benchmark, the Cramer Rao lower bound (CRLB); the proposed Bayesian DOA estimators are capable of improving the DOA estimation accuracy by merging the information contained in several snapshots (antenna scans). This thus supports the hypothesis that biased DOA estimators are capable of accurately estimating the DOA of emitters' signals received by a spinning antenna based ELINT system.

Improving the spatial resolution of a spinning antenna based system beyond the Rayleigh resolution limit is a research area that was receiving noticeable interest while we were conducting this research. We propose a user parameter-free super-resolution DOA estimator that overcomes the shortcomings of existing super-resolution DOA estimators. This proposed super-resolution DOA estimator was constructed using the sparse Bayesian learning (SBL) technique.

Using Monte Carlo simulation, we demonstrate that the proposed super-resolution DOA estimator outperforms existing super-resolution DOA estimators. This therefore supports the hypothesis that the SBL DOA estimator is capable of reliably resolving signals received by a spinning antenna based system.

CONTENTS

LIST OF FIGURES

LIST OF TABLES

LIST OF ACRONYMS

AML	Asymptotic (large sample size) ML
BB	Barankin bound
BBP	Blair and Brandt-Pearce
BCRLB	Bayesian Cramer Rao lower bound
CRLB	Cramer Rao lower bound
DOA	Direction of arrival
DSP	Digital signal processing
ECM	Electronic counter measure
ELINT	Electronic intelligence
EOB	Electronic order of battle
EP	Electronic protection
ESM	Electronic support measure
EW	Electronic warfare
IAA	Iterative adaptive approach
IFM	Instantaneous frequency measurement
LPI	Low probability of intercept
ML	Maximum likelihood
MMSE	Minimum mean square error
MSE	Mean square error
MVU	Minimum variance unbiased
MW	Moving window
pdf	Probability density function
PDW	Pulse descriptor word
POI	Probability of intercept
RF	Radio frequency
SBL	Sparse Bayesian learning
SDR	Signal to disturbance ratio
SDP	Semidefinite program
SIGINT	Signals intelligence
STFT	Short time Fourier transform

TDOA	Time difference of arrival
TOA	Time of arrival

1. Overview

1.1 Introduction

The use of advanced electronic protection (EP) and low probability of intercept (LPI) techniques by hostile radio frequency (RF) emitters presents significant difficulties to electronic warfare (EW) RF sensors. These techniques enable the RF emitters not only to overcome countermeasures that used to be effective in the past, but also to detect targets well before the EW RF sensors on-board the targets detect the presence of the RF emitters [13], [18], [46]. Furthermore, the intercept range, which is the maximum distance at which an EW RF sensor can detect an emitter's signal and estimate the parameters of the signal, is significantly decreased due to the advanced EP and LPI techniques employed by such hostile RF emitters [13], [18], [46].

These advanced techniques are driving the requirement for a longer intercept range, which motivated the development of architectures for EW RF sensors that reduce the equivalent noise bandwidth as well as the development of innovative signal processing algorithms that provide processing gains [13].

The spinning directional antenna is the most cost-effective antenna configuration for increasing the intercept range of an EW RF sensor [17], but it also provides low probability of intercept (POI) due to the narrow instantaneous spatial coverage. Thus, this antenna configuration is more appropriate for an EW RF sensor that is not time critical, such as an electronic intelligence (ELINT) system.

ELINT is a subfield of signals intelligence (SIGINT), whose objective is to intercept and analyse hostile non-communications RF emissions, primarily from radars, in order to determine the capabilities and vulnerabilities of the adversaries [46], [18].

For an emitter to be usefully intercepted by an EW RF sensor, the emitter's direction of arrival (DOA) must be accurately estimated. This is because the DOA parameter enables the EW RF sensor to track and locate the RF emitters. The DOA parameter indicates in what direction relative to the EW RF sensor the emitter is present [13], and the localisation is typically accomplished by exploiting the DOA estimates produced by several coordinated EW RF sensors or by exploiting several DOA estimates that are produced during the movement of a mobile EW RF sensor. Moreover, the DOA parameter enhances the deinterleaving (sorting) function within an EW RF sensor because the RF emitter is unable to instantly change the DOA parameter.

In spinning antenna based ELINT applications, the DOA estimation accuracy is degraded by: the wide beamwidth of the spinning antenna; the partial spread of the data (slow-time data) across the spinning antenna mainlobe; the small number of data samples (slow-time data); and the small signal to disturbance ratio (SDR).

The wide beamwidth of the spinning antenna is a result of the conflicting design parameters. For example, the size of the antenna aperture needs to be constrained to maintain a reasonable size of the motor and to enable fast spinning so that the spatial domain is searched more quickly [16]. The small aperture size increases the antenna beamwidth, which in turn increases the speed of searching the spatial domain, but it also reduces the intercept range due to the reduced antenna gain [19]. A good compromise can be achieved at high frequencies. However, at low frequencies, the beam will be very wide anyway, due to the small aperture size. Table 1 summarises the major parameters of a spinning antenna.

The partial spread of the data across the spinning antenna mainlobe is typically caused by the agility of the emitters' signals, errors in estimating the signals' parameters and by missing data samples. The agility of the emitters' signals and errors in estimating the signals' parameters may confound the deinterleaving (sorting) function [18], thus causing the data samples that belong to the same emitter to be sorted (deinterleaved) into different groups, which in turn results in the partial spread of the data across the spinning antenna mainlobe. Missing data samples are typically caused by errors in the detection process and by the congested RF domain [17], [31].

A full spread of the data scenario provides more knowledge about the DOA through the antenna boresight directions. Figure 1 shows a full spread scenario and a partial spread scenario.

To the best of our knowledge, no DOA estimators for spinning antenna based ELINT systems have been reported in the literature, although spinning antenna based DOA estimators were reported for other applications (mainly radar) and have been shown to perform adequately with regard to the estimation accuracy (as measured by the mean square error [MSE]) for the corresponding applications. Moreover, the MSEs of some of these estimators have been shown to attain the popular performance benchmark for unbiased estimation techniques, the Cramer Rao lower bound (CRLB) [14].

However, we show in this thesis that the MSE limit specified by the CRLB (assuming zero bias) is insufficient for the kinds of scenarios that spinning antenna based ELINT systems might encounter, i.e., scenarios that are characterised by: the wide beamwidth of the spinning antenna; the partial spread of the data across the spinning antenna mainlobe; the small number of data samples; and the small SDR. In this thesis, we therefore adopt the theory of biased estimation [8]-[12], [26] to obtain DOA estimators that will perform better with regard to the MSE and that will outperform the MSE limit specified by the CRLB. We thus present biased DOA estimators, which exploit how the variance of an estimator can be made smaller at the expense of increasing the bias, while ensuring that the overall MSE is reduced [8]-[12], [26]. These proposed biased DOA estimators exploit the amplitude modulation caused by the spinning of the directional antenna; they were constructed by using minimax estimation techniques [9]-[12] in conjunction with Bayesian estimation techniques [14].

Also, we present recursive versions of the proposed Bayesian DOA estimators that further improve the DOA estimation accuracy by merging the information contained in several snapshots (one antenna scan is defined as a snapshot in this thesis).

Improving the spatial resolution of a spinning antenna based system beyond the Rayleigh resolution limit is a research area that received noticeable interest while we were conducting this research. To the best of our knowledge, the super-resolution DOA estimators currently available in the literature have shortcomings either in terms of performance or the need for tuning user parameters. Tuning the user parameters heuristically is a difficult process, and it influences the performance of the super-resolution DOA estimators.

In this thesis, we therefore adopt the sparse Bayesian learning (SBL) technique because of its ability to handle problems with severely ill-conditioned dictionaries [23]-[24], such as the spinning antenna problem, and this, in turn, results in a user parameter free super-resolution DOA estimator.

Table 1. Specifications of a spinning antenna. (Rockwell Collins. ANT-1040G Spinning DF Antenna Unit). [22].

Frequency (GHz)	Beamwidth (deg)	Gain (dBi)
0.5 – 2	72	6.5
2	20	10.5
4	10.5	14.5
8	5.5	16
12	3.3	19
18	2.4	21
18 – 40	18	15
Spin rates (RPM)		
0 – 200		

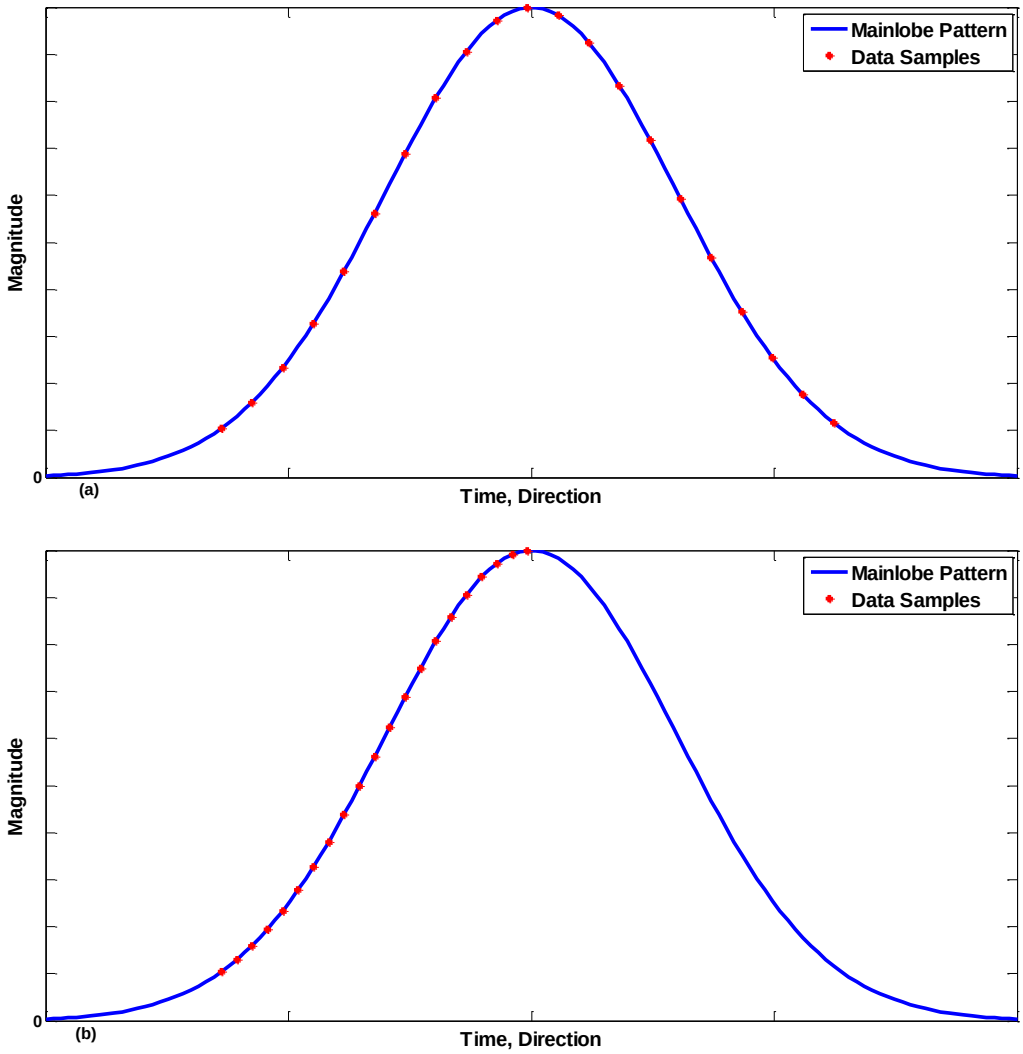

Figure 1. The spread of the data across the spinning antenna mainlobe: (a) Full spread scenario. (b) Partial spread scenario.

1.2 Hypothesis

The hypothesis statement for the biased DOA estimators is expressed as follows:

Biased DOA estimators that were constructed using minimax estimation techniques and Bayesian estimation techniques are capable of accurately estimating the DOA of emitters' signals received by a spinning antenna based ELINT system.

The questions for this hypothesis are:

- Are the biased DOA estimators capable of outperforming the MSE limits specified by the CRLB and the Barankin bound (BB)?
- Are the Bayesian DOA estimators capable of achieving the MSE limit specified by the Bayesian Cramer Rao lower bound (BCRLB)?
- Are the recursive versions of the Bayesian DOA estimators capable of improving the MSE by merging the information contained in several snapshots (antenna scans)?

The hypothesis statement for the super-resolution DOA estimator is expressed as follows:

A super-resolution DOA estimator that was constructed using the SBL technique is capable of adaptively resolving signals received by a spinning antenna based system.

The questions for this hypothesis are:

- Can the SBL DOA estimator performs as well as published super-resolution DOA estimators in terms of MSE and resolution?
- Is the SBL DOA estimator capable of adaptively resolving the received signals using a single snapshot?

1.3 Publications

This research has produced the following publications:

1) F. Alibrahim, and M. Inggs, "Biased estimators for spinning antenna DOA measurements", *IEEE Transactions on Aerospace and Electronic Systems*, Vol. 52, pp. 1499-1513, July 2016.
2) F. Alibrahim, and M. Inggs, "Sparse Bayesian learning for spinning antenna DOA super-resolution", *Electronic Letters*, Vol. 54, pp. 389-391, March 2018.

1.4 Outline

Chapter 2 begins with a brief overview of the factors that influence the choice of an antenna configuration for an EW RF sensor, before briefly discussing the system architecture of a typical spinning antenna based ELINT system.

The system architecture, which consists of a spinning directional antenna and an Omni antenna, is illustrated in Figure 2. These antennas are coupled with a high POI instantaneous frequency measurement (IFM) receiver and long intercept range digital receivers.

The spinning directional antenna provides the ELINT system with high gain, which increases the intercept range, and with selectivity, which isolates signals of interest in a congested environment. Furthermore, the spinning directional antenna is exploited to estimate the DOA parameter.

The Omni antenna provides full spatial coverage and is used to inhibit the skirt and the sidelobes/backlobes of the spinning directional antenna. Furthermore, the Omni antenna is employed to cancel signal fluctuations other than the signal fluctuations due to the spinning of the directional antenna, so that the DOA parameter can be accurately estimated.

The digital receiver is an important technology supporting EW RF sensors. It has the ability to handle several time simultaneous signals and to perform complex tasks, such as channelisation, detection, estimation of signals' parameters, deinterleaving and DOA estimation.

The EW processor performs various tasks, such as the analysis of pulse and burst repetitions intervals, scan pattern analysis, classification and identification.

Chapter 2 concludes with a literature review that focuses on the DOA estimators for spinning antenna based systems.

Chapter 3 begins with a brief overview of the challenges facing modern EW RF sensors. Then, the data model that was used for constructing the DOA estimators and deriving the MSE bounds is presented. Two data models were considered: the complex Gaussian distributed data model and the Rician distributed data model. The latter was considered to support ELINT systems that are only capable of estimating the amplitude (i.e., the magnitude of a complex Gaussian distributed data sample; also referred to as the envelope).

Thereafter, MSE bounds (assuming zero bias) for unbiased estimation techniques (i.e., the CRLB and the BB) are derived and analysed. The analysis of these MSE bounds indicated that the best achievable MSE of any unbiased DOA estimator is insufficient for the kinds of scenarios that spinning antenna based ELINT systems might encounter, i.e., scenarios that are characterised by: the wide beamwidth of the spinning antenna; the partial spread of the data across the spinning antenna mainlobe; the small number of data samples; and the small SDR. Therefore, DOA estimators that provide better MSE are needed.

Chapter 3 concludes by presenting DOA estimators that were constructed using the maximum likelihood (ML) technique. For the complex Gaussian distributed data, the ML estimates are computed by maximising a one-dimensional nonlinear function. For the Rician distributed data, the ML estimates are computed by maximising a two-dimensional nonlinear function. The computational complexity of the two-dimensional nonlinear function was reduced by approximating the two-dimensional nonlinear function to a one-dimensional nonlinear function, based on the fact that the Rician distribution is approximately Gaussian at moderate to high SDR.

Chapter 4 begins with a brief overview of the minimax estimation techniques and the Bayesian estimation techniques that were used to construct the proposed biased DOA estimators.

Thereafter, the proposed biased DOA estimators and the BCRLB are presented:

The proposed minimax DOA estimators were constructed by performing a linear transformation and an affine transformation on an efficient estimator (i.e., an unbiased estimator that attains the CRLB [14]) or a minimum variance unbiased (MVU) estimator (i.e., an estimator with the least variance among the unbiased estimators [14]).

The proposed Bayesian DOA estimators were constructed using the minimum mean square error (MMSE) estimation technique. The MMSE technique is a popular form of Bayesian estimation techniques; it introduces the bias by imposing prior distributions on the parameters to be estimated.

The proposed recursive versions of the Bayesian DOA estimators are based on the sequential form of the MMSE technique.

The BCRLB is derived in Chapter 4 to provide a performance benchmark for the Bayesian DOA estimators.

Chapter 4 concludes by evaluating the DOA estimation accuracy (as measured by the MSE) of the proposed biased DOA estimators using Monte Carlo simulation and real radar data provided by Reutech Radar Systems. The results of this evaluation illustrate that: the proposed biased DOA estimators outperform the CRLB and the BB, and the MSEs of the proposed Bayesian DOA estimators are very close to the BCRLB; the recursive Bayesian DOA estimators improve the DOA estimation accuracy by merging the information contained in several snapshots, and they can handle snapshots that differ with regard to the emitter steering vector.

Chapter 5 begins with a brief overview of the SBL technique and the iterative adaptive approach (IAA) technique. The SBL technique is used to construct the proposed super-resolution DOA estimator, while the IAA technique has been shown to outperform most of the existing super-resolution techniques in the literature in spinning antenna based applications [38], [51]-[53].

Chapter 5 concludes by evaluating the DOA estimation accuracy (as measured by the MSE) and the resolution of the proposed SBL DOA estimator using Monte Carlo simulation. The evaluation results show that: the SBL DOA estimator is capable of adaptively resolving the received signals using a single snapshot; the MSE of the SBL DOA estimator is close to the CRLB; and the SBL DOA estimator outperforms the IAA DOA estimator in terms of resolution and accuracy.

The conclusions are reported in **Chapter 6**: we investigated the problem of estimating the DOA of emitters' signals received by a spinning antenna based ELINT system, where the goal was to improve the DOA estimation accuracy (as measured by the MSE).

By evaluating the CRLB and the BB, we showed that the best achievable MSE of the conventional unbiased estimation techniques is insufficient for the kinds of scenarios that spinning antenna based ELINT systems might encounter, i.e., scenarios that are characterised by: the wide beamwidth of the spinning antenna; the partial spread of the data across the spinning antenna mainlobe; the small number of data samples; and the small SDR. Thus, we proposed the use of biased estimation techniques that improve the MSE by introducing a bias.

We first constructed transformed versions of the ML DOA estimators, where the transformation parameters are computed by solving minimax optimisation problems. Then, we constructed Bayesian DOA estimators that introduce the bias by imposing prior distributions on the parameters to be estimated. Also, we constructed recursive Bayesian DOA estimators that further improve the MSE by merging the information contained in several snapshots (antenna scans). Using Monte Carlo simulation and real radar data provided by Reutech Radar Systems, we demonstrated the advantages of the proposed biased DOA estimators in terms of the MSE for complex Gaussian distributed data and Rician distributed data.

In addition, we investigated the problem of increasing the spatial resolution of a spinning antenna based system beyond the Rayleigh resolution limit, where the goal is to have the ability to adaptively resolve the received signals and to have an adequate performance in terms of accuracy (as measured by the MSE) and resolution.

Our analysis of the literature indicated that existing spinning antenna based super-resolution DOA estimators have shortcomings either in terms of performance or the need for tuning user parameters. Thus, we proposed the use of the SBL technique because of its ability to handle problems with severely ill-conditioned dictionaries, such as the spinning antenna problem, and this in turn, resulted in an adaptive super-resolution DOA estimator.

Using Monte Carlo simulation, we demonstrated that the proposed SBL DOA estimator outperforms the IAA DOA estimator in terms of accuracy and resolution, and that the SBL DOA estimator is capable of adaptively resolving the received signals using a single snapshot.

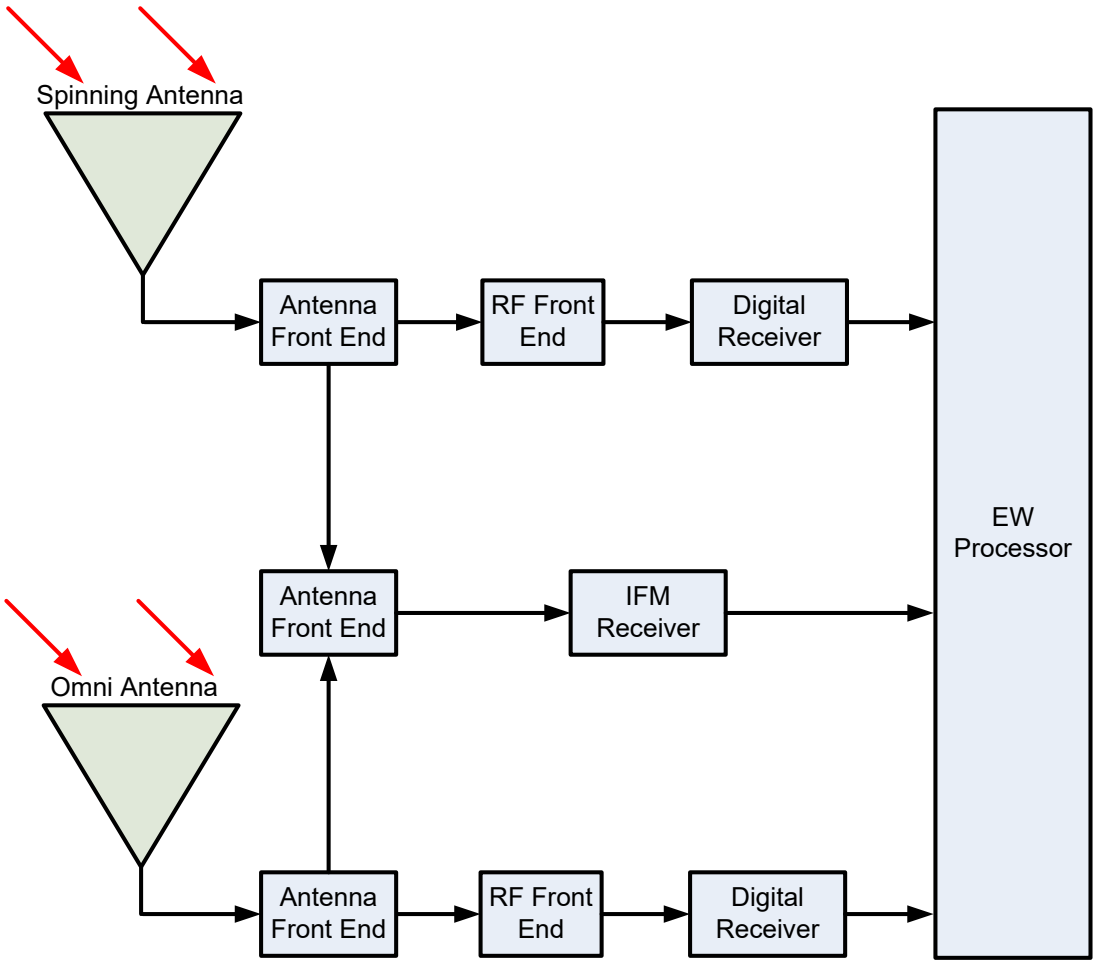

Figure 2. The system architecture of a spinning antenna based ELINT system

2. System architecture and literature review

2.1 Introduction

The type of antenna configuration to be used by an EW RF sensor depends upon several factors, such as: the mission the EW RF sensor is going to perform, the environment in which the EW RF sensor will operate, the physical constraints, and the cost.

In their primary mission, ELINT systems intercept emitters for the purpose of conducting a thorough analysis. The analysis produces the operating specifications, capabilities and vulnerabilities of the intercepted emitter and its associated weapon system [13], [18], [47]. The results obtained from the analysis are then supplied to threat warning systems to enable them to identify emitters [13], [18], [47]. In addition, the results obtained from the analysis are used to design countermeasure techniques [13], [18], [47].

ELINT systems perform other tasks too, such as the tracking of emitters' locations to provide electronic order of battle (EOB) information [13].

ELINT systems must be able to detect sidelobe emissions and emitters deep behind adversarial borders from a stand-off position [13], [18], [47]. This means that the antenna gain must be sufficiently high to meet this specification.

ELINT intercepts are not time critical. This means that the POI performance can be traded for selectivity and increased intercept range by searching the frequency and spatial domains using small intervals (hence low equivalent noise bandwidth and high antenna gain) [13], [18], [47].

Antenna arrays are typically used when high POI, small size and light weight are needed. These advantages are obtained at the cost of decreased intercept range due to the wide spatial coverage and at the cost of hardware complexity due to the additional antenna channels.

In antenna arrays, the monopulse technique is typically used to estimate an emitter's DOA. This technique exploits the difference of the instantaneous amplitude or instantaneous phase between the receiving antenna's channels to estimate the DOA of an emitter [13].

Another monopulse technique is time difference of arrival (TDOA), which exploits the difference of the received signal's time of arrival (TOA) between widely separated sites (airborne or ground based) to estimate the DOA of an emitter [13].

Electronically steered arrays are typically used when fast beam steering, control over beam shape and switching the beam position almost instantaneously are needed. In EW, electronically steered arrays are typically used in electronic counter measure (ECM) applications to provide several beams and the ability to time share a single beam.

Electronic steering might appear to be an optimal solution for an ELINT mission instead of mechanical steering. However, the following should be considered: firstly, ELINT intercepts are not time critical; i.e., a delay in an intercept caused by the mechanical steering of the spinning antenna is acceptable. Therefore, the use of fast electronic steering is not critical for the success of an ELINT mission. Secondly, several wideband electronically steered arrays are needed to achieve full spatial coverage and to cover the required operating frequency range (0.5 – 40 GHz). Thus, the use of electronic steering is cost prohibitive and challenging to implement. Thirdly, wideband beamforming networks (analog, digital or optical) would be required and a sufficient number of radiating elements per array would be needed to achieve the desired antenna gain, which further complicates the design and raises the cost. These factors clearly indicate that mechanical steering suffices and that the use of electronic steering is not critical for the success of an ELINT mission.

Finally, it is noteworthy that in some state-of-the-art platforms, such as the Typhoon aircraft and the F-35 aircraft, the electronic support measure (ESM) systems have dedicated antennas and exploit the active electronically steered arrays that belong to other systems on-board the aircraft, such as the ECM system and the radar.

The abovementioned discussion indicates that the spinning directional antenna is well suited for an ELINT system.

2.2 System architecture

The system architecture of a spinning antenna based ELINT system is illustrated in Figure 2. The system is composed of an Omni antenna and a spinning directional antenna. These antennas are associated with long intercept range digital receivers and a high POI IFM receiver.

The directional antenna can be constantly spinning to survey the spatial domain, or it can be pointed in a particular direction for deep analysis. The Omni antenna provides instantaneous coverage of the whole spatial domain, and captures the scanning patterns of the intercepted emitters.

As illustrated in Figure 3, sidelobes/backlobes detections and mainlobe detections are resolved by positioning the gain of the Omni antenna channel between the peak of the spinning antenna mainlobe and the peak of the spinning antenna sidelobes/backlobes [16]. Thus, mainlobe detection is declared only when the output of the spinning antenna channel is greater than the output of the Omni antenna channel, which in turn must be greater than the sidelobes/backlobes of the spinning antenna [16]. We shall refer to the spatial width of the mainlobe at the points where the output of the spinning antenna channel exceeds the output of the Omni antenna channel as the unambiguous width θ_{um}.

We note here that a detailed description of a sidelobes blanking system is reported in [58].

The IFM receiver provides instantaneous coverage of the whole frequency domain. It provides a fast estimate of the frequency of the received signal in a digital format.

The IFM receiver has a poor dynamic range due to its wide instantaneous frequency range, and it completely fails by producing an erroneous frequency estimate when two or more signals of comparable strength overlap in time [13]. Thus, computer controlled adjustable band-stop filters are typically installed to remove unwanted signals from the IFM receiver input.

We note here that the detection capability of the IFM receiver is degraded by the congested frequency domain.

The IFM receiver, together with the Omni antenna, forms a wide-open EW receiver that is capable of surveying the whole frequency and spatial domains.

The digital receiver is an important technology supporting ELINT applications because of its advanced digital signal processing (DSP) capability and long intercept range [13], [15], [32], [47]. A superheterodyne RF frontend is typically coupled with the digital receiver to downconvert the received signal to an intermediate frequency for digitisation by the digital receiver. The instantaneous bandwidth of the digital receiver is computer controlled with an upper limit set by the digitisation technology.

The digital receiver surveys the frequency domain using adjustable frequency intervals that are computer controlled according to the mission. Also, the digital receiver can be designated in frequency by the IFM receiver.

Channelization is the most used technique to construct the digital receiver because of its ability to resolve several time simultaneous signals in frequency.

Channelization is accomplished by the digital receiver by applying a short time Fourier transform (STFT) to the digitised received signals. The STFT is equivalent to an array of adjacent finite impulse response filters [15]. If a signal presence is detected in one of the STFT parallel outputs, then the signal's parameters (magnitude or complex amplitude, antenna boresight direction, frequency, modulation on pulse, TOA, pulse width, etc.) are estimated and combined to form a pulse descriptor word (PDW).

In the deinterleaving process, PDWs that have similar parameters are considered to originate from the same emitter. Thus, PDWs that belong to the same emitter are extracted from the generated PDWs and then combined together in a single group [47]. We note here that the agility of the received signal and errors in estimating the signal's parameters may cause the PDWs that belong to the same emitter to be deinterleaved (sorted) into different groups, which consequently results in the partial spread of the data across the spinning antenna mainlobe scenarios.

Thereafter, the DOA for each group of PDWs is estimated. To ensure accurate DOA estimation, the Omni antenna channel is typically employed to remove emitters' scanning patterns and other variations so that the data provided by the spinning antenna channel is only proportional to the emitters' DOAs [16].

Parameters, such as the pulse and burst repetition intervals, beam pattern and scanning type, are typically estimated to classify the emitter's mode and hence to identify the emitter.

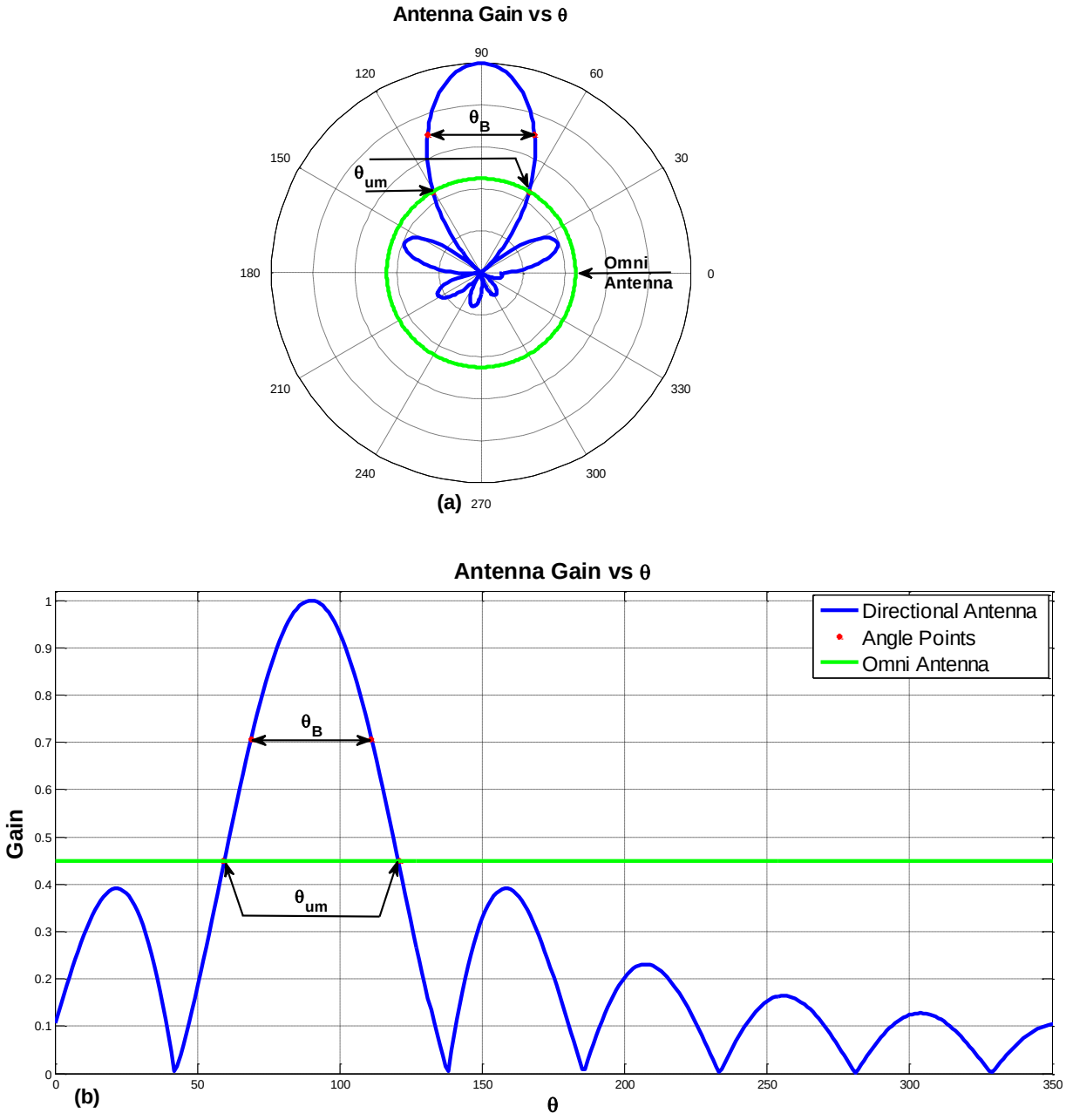

Figure 3. Normalized antenna gain plot of two-channel spinning antenna system illustrating antenna beamwidth θ_B and unambiguous width θ_{um}.

2.3 Literature review

To the best of our knowledge, no DOA estimators for spinning antenna based ELINT systems have been reported in the literature, although spinning antenna based DOA estimators were reported for other applications (mainly radar).

The classical approach to DOA estimation in mechanically steered radars is the moving window (MW) approach [20], in which the DOA is estimated by averaging the antenna

boresight directions associated with the first sample and the last sample of the received data, where this data is received while the radar's illumination sweeps across the target.

The amplitude modulation approach, which was first described by Swerling [7], outperforms the moving window approach at the cost of higher computational complexity [3]. In this approach, the received signal is amplitude modulated by the spinning of the directional antenna, and the peak of the correlation between the received signal and the beam pattern of the spinning antenna determines the received signal's DOA.

In this section, we will survey some of the publications that have looked at the amplitude modulation approach:

- ***Maximum likelihood azimuth estimation applied to SSR & IFF systems [6]:***

  In this work, an estimator to find the DOA of transponders illuminated by a secondary surveillance radar was constructed.

  The constructed estimator, which is based on the amplitude modulation approach, estimates the DOA by convolving the received transponder replies with the first derivative of the antenna beam pattern, and then performs a zero-crossing search.

  The developed DOA estimator provides good estimation accuracy when noise is the only error source. However, the DOA estimation accuracy deteriorates in the case of missed transponder's replies. Thus, a missed replies detector was incorporated into the constructed DOA estimator to combat this problem.

  The performance of the constructed DOA estimator was evaluated and compared with classical DOA estimators using Monte Carlo simulation. It was shown that the constructed DOA estimator is not efficient, but its MSE is very close to the CRLB. Also, it was shown that the constructed DOA estimator outperforms the MW estimator and the accumulator detector at the expense of computational complexity.

- ***Recovery of antenna pattern loss in a search radar [25]:***

  In this work, a signal processing algorithm that provides a detection processing gain for a mechanically steered radar receiver was developed. The processing gain is obtained by recovering the so-called antenna pattern loss, and this enables the radar to increase the detection range without increasing the transmitted power. A detector employing the developed algorithm was shown to outperform a conventional detector by 2.3 dB in SDR.

  A by-product of this work is a DOA estimator that is based on the amplitude modulation approach. This DOA estimator was constructed by approximating the ML technique; it has the following advantages relative to the conventional monopulse:

  1) *It does not require a monopulse feed (for reflector antennas) or a beamforming network (for phased arrays) to be able to estimate the DOA [25].*

2) *It does not require an additional tightly matched receiving channel to be able to estimate the DOA [25].*
3) *It can estimate the DOA even if the targets' DOAs are not within the antenna beamwidth [25].*

The following disadvantages of the constructed DOA estimator relative to the conventional monopulse were mentioned:

1) The DOA estimation accuracy might degrade when the received signal strength fluctuates from sample to sample. For this reason, the radar cannot operate in frequency agility mode [25].
2) It does not work when the received signal saturates the receiver to deny the amplitude modulation caused by the spinning of the antenna [25].

In [5], the DOA estimation accuracy of the DOA estimator constructed in [25] was evaluated using Monte Carlo simulation for a fluctuating target model and a non-fluctuating target model. The DOA estimator was shown to provide adequate estimation accuracy for a non-fluctuating target in the presence of clutter as well as in the absence of clutter. In the case of a fluctuating target, the DOA estimation accuracy was shown to degrade.

- ***DOA estimation by exploiting the amplitude modulation induced by antenna scanning [1]:***

In this work, estimators to find the DOA and complex amplitudes of multiple targets present in the same range-azimuth resolution cell of a surveillance radar were developed. The developed estimators are based on the amplitude modulation approach and were constructed using the ML technique for two target models: multiple targets with unknown deterministic complex amplitudes, and multiple targets with Gaussian distributed random complex amplitudes.

The constructed DOA estimators were suggested as an alternative to the monopulse, because the monopulse requires more hardware and does not work in the presence of multiple targets in the same range-azimuth resolution cell.

The CRLBs for the two target models were derived and were shown to coincide.

The DOA estimation accuracy of the constructed DOA estimators was evaluated using Monte Carlo simulation. For targets with deterministic amplitudes, the DOA estimator was shown to attain the CRLB. For targets with Gaussian distributed random complex amplitudes, the constructed DOA estimator is computationally complex. Thus, it was suggested to use the DOA estimator that was used for the deterministic complex amplitudes model because it is easier to implement. However, it was shown that the DOA estimator for the deterministic complex amplitudes model is not efficient when the target's complex amplitude is Gaussian distributed but the estimator's MSE is close to the CRLB.

- ***Multiple radar targets estimation by exploiting induced amplitude modulation [2]:***

In this work, the ML DOA estimator developed in [1] was extended to consider multiple targets with unknown Doppler frequencies in the same range-azimuth resolution cell. The joint estimation of the Doppler frequencies and DOAs resulted in a computationally complex, multi-dimensional ML estimator.

To reduce the computational complexity, the asymptotic (large sample size) ML (AML) estimator was constructed. It estimates the unknown parameters from the locations of the highest peaks in the likelihood function.

To further reduce the computational complexity, an efficient implementation of the AML, using the RELAX algorithm, was developed. It decouples the multi-dimensional search of the locations of the highest peaks into sequential one-dimensional nonlinear maximisation problems. Thus, the estimator begins by estimating the Doppler frequencies, and then estimating the DOA.

Using Monte Carlo simulation, the estimator was shown to have an MSE very close to the CRLB. However, the Doppler frequency estimate was shown to experience the threshold effect for SDR below 5 dB.

The estimator was shown to be able to resolve multiple targets in the same range-azimuth resolution cell, as long as their Doppler frequencies differ by the inverse of the number of the data samples.

In [48], the performance of the AML-RELAX estimator was evaluated in the case of multiple targets with unknown Gaussian distributed random complex amplitudes. In this case, the estimator is no longer efficient, but its MSE is close to the CRLB, and the estimator was shown to be able to maintain its ability to resolve multiple targets in the same range-azimuth resolution cell. Also, the Doppler frequency estimate was shown to experience the threshold effect for SDR below 20 dB.

- ***Joint Use of Sum and Delta Channels for Multiple Radar Target DOA Estimation [49]:***

In this work, the AML-RELAX estimator developed in [2] was extended to a phased array radar scenario and compared with monopulse estimators.

It was shown that the joint processing of the sum and delta channels of the phased array radar by the AML-RELAX estimator significantly improves the DOA estimation accuracy, but the improvement in Doppler frequency estimation is negligible.

Simulation results illustrated that the AML-RELAX always outperforms the conventional monopulse, and that the conventional monopulse generates an erroneous DOA estimate

when two targets are in the same range-azimuth resolution cell. Also, a modern monopulse estimator, which is the Blair and Brandt-Pearce (BBP) estimator, was compared with the AML-RELAX using Monte Carlo simulation. The BBP estimator is capable of resolving a maximum of two targets in the same range-azimuth resolution cell, provided that their radar cross-sections are a priori known. The AML-RELAX does not require the radar cross-section information to resolve targets and is capable of resolving more than two targets.

In the simulation scenarios, two Swerling 0 targets were considered. The AML-RELAX was employed by a scanning system, while the antenna beam of the system employing the BBP estimator was stationary during the time on target. The AML-RELAX estimator was shown to always outperform the BBP estimator when the two targets differed in the Doppler frequency. For equal Doppler frequencies, the BBP estimator was shown to outperform the AML-RELAX estimator.

- ***Direction-of-arrival estimation in radar systems: moving window against approximate maximum likelihood estimator [3]:***

In this work, the AML estimator developed in [2] was compared with the classical MW estimator using Monte Carlo simulation. It was shown that the AML estimator outperforms the MW estimator in terms of estimation accuracy and that they have a similar detection performance.

With regard to the probability of target splitting, it was shown that the probability of target splitting of the MW is around ten percent, while the probability of target splitting of the AML estimator is lower than three percent.

The comparison concluded that the AML estimator outperforms the MW estimator at the expense of computational complexity.

Improving the spatial resolution beyond the Rayleigh limit is a research area that has received noticeable interest recently, as many super-resolution DOA estimators have been proposed in recent literature. Some of the published super-resolution DOA estimators exploit the knowledge about the spinning antenna beam pattern and the Doppler frequencies to resolve the received signals [1]-[2], [48]-[49]. While other super-resolution DOA estimators assume that the Doppler frequencies are unknown, and while they use a large number of snapshots to resolve the received signals [27]-[30], [34]-[36]. In [4], [37]-[42], [51]-[55], super-resolution DOA estimators that exploit the knowledge about the spinning antenna beam pattern and that can resolve the received signals with a minimum of a single snapshot were proposed.

Unfortunately, the severely ill-conditioned dictionary associated with the spinning antenna problem imposes limitations on the super-resolution DOA estimators. Thus, to the best of our knowledge, the super-resolution DOA estimators currently available in the literature have shortcomings, either in terms of performance or in the need for tuning user parameters.

Tuning the user parameters is a difficult process that is influenced by the parameters of the encountered scenario.

3. Data model and unbiased bounds

3.1 Introduction

Modern RF emitters employ advanced techniques that make it difficult for an EW RF sensor to detect and recognise the RF emitters. For example, modern RF emitters randomise the parameters of their signals to confound the deinterleaving, classification and identification functions within an EW RF sensor [18]. The additional impact of the utility of electronically steered arrays by modern RF emitters further improves the confounding of an EW RF sensor.

Developments that support the randomisation of signals' parameters and the synthesis of complex multifunction signals are commercially available. An example is wide band digital waveform synthesis [18], which allows RF emitters to change the parameters of their signals almost instantaneously with high accuracy.

In addition to the aforementioned difficulties, the RF domain in which an EW RF sensor operates is complex and very dense [31]. Emitters' signals are overlapping and signals of interest might be buried by strong interfering signals. The density of the complex RF domain is typically much higher than the capabilities of an EW RF sensor, which may thus overwhelm the EW RF sensor, leading to a large number of missing data samples [17], [31].

A spinning antenna based ELINT system that is operating in the congested RF environment and competing against modern RF emitters is expected to encounter scenarios that are characterised by the following: the wide beamwidth of the spinning antenna; the partial spread of the data across the spinning antenna mainlobe; the small number of data samples; and the small SDR. These scenarios degrade the DOA estimation accuracy; however, to localise an RF emitter accurately, an accurate DOA estimate is needed [47]. Therefore, it is of prime importance to have a highly accurate DOA estimator.

In this chapter, we will present the data model that will be used to derive the MSE bounds and construct the proposed DOA estimators. Then, we will evaluate the CRLB to investigate the use of unbiased estimation techniques for estimating the DOA of emitters' signals received by a spinning antenna based ELINT system. Finally, we will present the ML estimator for estimating the DOA of emitters' signals received by a spinning antenna based system.

3.2 Data model and notation

3.2.1 Notation

We denote matrices by boldface uppercase letters and vectors by boldface uppercase letters and boldface lowercase letters: thus, $[\boldsymbol{d}]_n$ is the nth element of vector $\boldsymbol{d}$; $[\boldsymbol{R}]_{i:}$ is the ith row of matrix $\boldsymbol{R}$; $[\boldsymbol{R}]_{:i}$ is the ith column of matrix $\boldsymbol{R}$; $[\boldsymbol{R}]_{ie}$ is the element at the ith row and the eth column of matrix $\boldsymbol{R}$; $(\ )^T$ is the transpose operator; $(\ )^H$ is the conjugate-transpose operator; $\boldsymbol{I}$ is the identity matrix; $\odot$ is the Hadamard product or element-wise

multiplication [33]; $Tr(\ \ )$ is the trace operator; $\|\ \ \|_2$ is the l_2 norm. I_0 is the modified zeroth-order Bessel function of the first kind. $\widehat{\ }$ is the estimation operator and $Ex\{\ \ \}$ is the expectation operator. $Re\{\ \ \}$ and $Im\{\ \ \}$ are the real and the imaginary of a complex quantity respectively. $\mathcal{CN}(\boldsymbol{a}, \boldsymbol{R})$ is a multivariate complex normal distribution with mean $\boldsymbol{a}$ and covariance $\boldsymbol{R}$. $\mathcal{N}(\boldsymbol{a}, \boldsymbol{R})$ is a multivariate normal distribution with mean $\boldsymbol{a}$ and covariance $\boldsymbol{R}$.

3.2.2 Data model

Consider the spinning antenna based ELINT system shown in Figure 2, in which the spinning directional antenna, with a beamwidth θ_B, surveys the spatial domain at angular velocity ω_R and receives emitters' signals in the scene. The received emitters' signals are amplitude modulated by the spinning of the directional antenna and embedded in Gaussian disturbance. The digital receiver digitises the received emitters' signals, channelizes them and thus resolves the received signals in frequency, detects the presence of the emitters' signals, estimates their instantaneous parameters, and combines the estimated parameters to form a PDW.

PDWs that have similar parameters are considered to originate from the same emitter. Thus, PDWs that belong to the same emitter are extracted from the generated PDWs and then combined together in a single group. The N complex amplitudes contained in a group of PDWs are collected in an N-dimensional data vector $\boldsymbol{Z}$; the nth sample of the data vector $\boldsymbol{Z}$ is:

$$[\boldsymbol{Z}]_n = b\ G(\theta_{ET}, [\boldsymbol{\theta_{BO}}]_n) + [\boldsymbol{d}]_n \qquad ; n = 1, .. N \tag{1}$$

where G is the spinning antenna beam pattern, $b = b_R + jb_I$ is the received signal complex amplitude, modeled as a deterministic unknown. b_R and b_I are the real and imaginary parts of the received signal complex amplitude b. θ_{ET} is the DOA of the received emitter's signal, $\boldsymbol{d}$ is the complex Gaussian disturbance (thermal noise, interference, etc.), and the N-dimensional column vector $\boldsymbol{\theta_{BO}}$ is the antenna boresight directions vector. $\boldsymbol{\theta_{BO}}$ is related to $\boldsymbol{TOA}$ as follows:

$$\begin{cases} [\boldsymbol{\theta_{BO}}]_n = [\boldsymbol{\theta_{BO}}]_1 + \omega_R\ [\Delta \boldsymbol{TOA}]_n \\ \Delta \boldsymbol{TOA} = \begin{bmatrix} 0 \\ [\boldsymbol{TOA}]_2 - [\boldsymbol{TOA}]_1 \\ \vdots \\ [\boldsymbol{TOA}]_N - [\boldsymbol{TOA}]_1 \end{bmatrix} \end{cases} \tag{2}$$

The vector notation of Equation (1) is given by:

$$\boldsymbol{Z} = b\ \boldsymbol{a}(\theta_{ET}, \boldsymbol{\theta_{BO}}) + \boldsymbol{d} \tag{3}$$

The N-dimensional disturbance vector $\boldsymbol{d}$ has a Gaussian probability density function (pdf) with zero mean and a $N \times N$ dimensional covariance matrix $\boldsymbol{R} = Ex\{\boldsymbol{d}\boldsymbol{d}^{\boldsymbol{H}}\} = \sigma_d^2 \boldsymbol{Q}$, where σ_d^2 is the total disturbance power, and $\boldsymbol{Q}$ is the normalised covariance matrix.

The nth sample of the N-dimensional emitter steering vector $\boldsymbol{a}(\theta_{ET}, \boldsymbol{\theta_{BO}})$ is:

$$[\boldsymbol{a}(\theta_{ET}, \boldsymbol{\theta_{BO}})]_n = G(\theta_{ET}, [\boldsymbol{\theta_{BO}}]_n) \quad ; n = 1 \ldots . N \tag{4}$$

Finally, the pdf of $\boldsymbol{Z}$ conditioned to b and θ_{ET} is as follows:

$$P_{\boldsymbol{Z}}(\boldsymbol{Z}; b, \theta_{ET}) = \frac{1}{\pi^N det(\boldsymbol{R})} exp\Big[-[\boldsymbol{Z} - \boldsymbol{a}(\theta_{ET}, \boldsymbol{\theta_{BO}})\, b]^H \boldsymbol{R^{-1}} [\boldsymbol{Z} - \boldsymbol{a}(\theta_{ET}, \boldsymbol{\theta_{BO}})\, b]\Big] \quad (5)$$

The aforementioned problem formulation is similar to that derived by Farina, Gini and Greco in [1]-[2], when they studied the estimation of radar targets' DOA by using the ML estimator.

In addition, we investigate the problem of estimating the DOA using the amplitude (the magnitude of the complex amplitude) when the Gaussian disturbance is statistically independent (i.e., white Gaussian noise) to support ELINT systems that are only capable of estimating the amplitude $[\boldsymbol{\zeta}]_n = (Re\{[\boldsymbol{Z}]_n\}^2 + Im\{[\boldsymbol{Z}]_n\}^2)^{\frac{1}{2}}$. The amplitude $[\boldsymbol{\zeta}]_n$ of the nth sample of the N-dimensional complex amplitudes vector $\boldsymbol{Z} \in \mathcal{CN}(b\, \boldsymbol{a}(\theta_{ET}, \boldsymbol{\theta_{BO}}), \boldsymbol{R})$ is Rician distributed:

$$P_{[\zeta]_n/[\boldsymbol{Z}]_n}([\boldsymbol{\zeta}]_n; \beta, \theta_{ET}) =$$

$$\frac{2\,[\boldsymbol{\zeta}]_n}{\sigma_d^2} exp\left[\frac{-([\boldsymbol{\zeta}]_n^2 + \beta^2[\boldsymbol{a}(\theta_{ET}, \boldsymbol{\theta_{BO}})]_n^2)}{\sigma_d^2}\right] I_0\left(\frac{2\,[\boldsymbol{\zeta}]_n\, \beta\, [\boldsymbol{a}(\theta_{ET}, \boldsymbol{\theta_{BO}})]_n}{\sigma_d^2}\right) \quad (6)$$

where $\beta = (b_R^2 + b_I^2)^{\frac{1}{2}}$ is the magnitude of the complex amplitude b. We note here that the dependency of $\boldsymbol{a}(\theta_{ET}, \boldsymbol{\theta_{BO}})$ on θ_{ET} and $\boldsymbol{\theta_{BO}}$ was omitted in the following equations for ease of notation.

As shown in Figure 4, the Rician distribution can be approximated to a Gaussian distribution to simplify the derivation of the estimators and MSE bounds. This is because the Rician distribution of $\boldsymbol{\zeta}$ is equivalent to the Rayleigh distribution when there is no signal, and it is approximately Gaussian with mean $\boldsymbol{m_\zeta} \cong \left(\boldsymbol{a} \odot \boldsymbol{a}\, \beta^{\boldsymbol{2}} + \frac{\sigma_d^2}{2}\right)^{\odot\frac{1}{2}}$ at moderate to high SDR, where at very high SDR, the mean becomes $\boldsymbol{m_\zeta} \cong \beta\, \boldsymbol{a}$. This equivalent Gaussian distribution has a covariance matrix $\boldsymbol{C} = \frac{\sigma_d^2}{2} \boldsymbol{I}$ and a pdf given by the following expression:

$$P_{\boldsymbol{\zeta}/\boldsymbol{Z}}(\boldsymbol{\zeta}; \beta, \theta_{ET}) =$$

$$\frac{1}{\sqrt{2\pi^N\, det(\boldsymbol{C})}} exp\left[-\frac{1}{2}\left[\boldsymbol{\zeta} - \left(\boldsymbol{a} \odot \boldsymbol{a}\, \beta^{\boldsymbol{2}} + \frac{\sigma_d^2}{2}\right)^{\odot\frac{1}{2}}\right]^T \boldsymbol{C}^{-1} \left[\boldsymbol{\zeta} - \left(\boldsymbol{a} \odot \boldsymbol{a}\, \beta^{\boldsymbol{2}} + \frac{\sigma_d^2}{2}\right)^{\odot\frac{1}{2}}\right]\right] \quad (7)$$

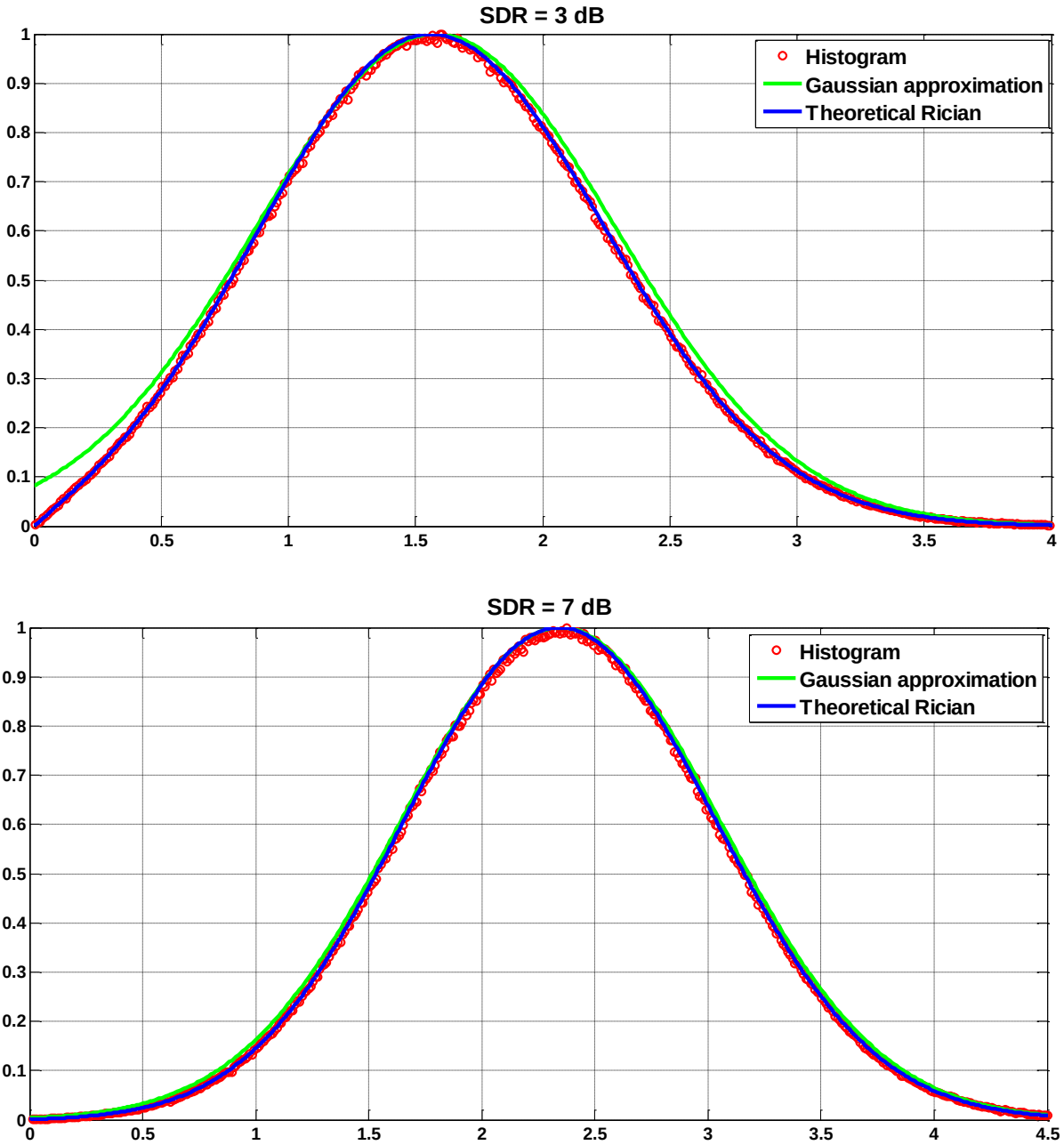

Figure 4. Plots of the Rice distribution versus the Gaussian approximation and the histogram of the magnitude of a complex data at different values of SDR

3.3 The Cramer Rao lower bound

The CRLB is a popular performance benchmark that specifies the best achievable MSE (assuming zero bias) of any unbiased estimator of deterministic parameters in a given data model [14].

The CRLB on the accuracy of DOA estimation in complex Gaussian disturbance has already been derived in the context of radar [1]-[2], and is analysed in this section to investigate the use of unbiased estimation techniques for estimating the DOA of emitters' signals received by a spinning antenna based ELINT system. For complex Gaussian distributed data, as given in

the data model, the 3×1 unknown deterministic parameters vector is $\boldsymbol{\vartheta} = [\theta_{ET}\ b_R\ \ b_I]^T$. The complex Gaussian distributed data vector $\boldsymbol{Z}$ has a mean $\boldsymbol{m_Z} = Ex\{\boldsymbol{Z}\} = (b_R + jb_I)\,\boldsymbol{a}$ and a covariance matrix $\boldsymbol{R}$. The CRLB for each unknown parameter is given by the diagonal elements of the inverse of the Fisher information matrix [14], i.e., $CRLB\ ([\boldsymbol{\vartheta}]_i) = [\boldsymbol{J}^{-1}]_{ii}$. The elements of the 3×3 Fisher information matrix $\boldsymbol{J}$ are obtained as follows:

$$[\boldsymbol{J}]_{ie} = 2\,Re\left\{\frac{\partial \boldsymbol{m_Z^H}}{\partial[\boldsymbol{\vartheta}]_i}\boldsymbol{R}^{-1}\frac{\partial \boldsymbol{m_Z}}{\partial[\boldsymbol{\vartheta}]_e}\right\}; \qquad i,e = 1,2,3 \tag{8}$$

$$\frac{\partial \boldsymbol{m_Z}}{\partial[\boldsymbol{\vartheta}]_i} = \begin{cases}(b_R + jb_I)\,\boldsymbol{a_\theta}\\ \boldsymbol{a}\\ j\,\boldsymbol{a}\end{cases} \tag{9}$$

$\boldsymbol{a_\theta}$ is the gradient, with respect to θ_{ET}, of the emitter steering vector $\boldsymbol{a}$.

For Rician distributed data, as given in the data model, the 2×1 unknown deterministic parameters vector is $\boldsymbol{\vartheta} = [\theta_{ET}\ \beta]^T$. The data vector $\boldsymbol{\zeta}$ is modelled as real Gaussian distributed with mean $\boldsymbol{m_\zeta} = Ex\{\boldsymbol{\zeta}\} \cong \left(\boldsymbol{a} \odot \boldsymbol{a}\,\boldsymbol{\beta^2} + \frac{\sigma_d^2}{2}\right)^{\odot\frac{1}{2}}$ and covariance matrix $\boldsymbol{C}$. The CRLB for each unknown parameter is given by the diagonal elements of the inverse of the Fisher information matrix [14], i.e., $CRLB\ ([\boldsymbol{\vartheta}]_i) = [\boldsymbol{J}^{-1}]_{ii}$. The elements of the 2×2 Fisher information matrix $\boldsymbol{J}$ are obtained as follows:

$$[\boldsymbol{J}]_{ie} = \left\{\frac{\partial \boldsymbol{m_\zeta^T}}{\partial[\boldsymbol{\vartheta}]_i}\,\boldsymbol{C}^{-1}\,\frac{\partial \boldsymbol{m_\zeta}}{\partial[\boldsymbol{\vartheta}]_e}\right\}; \qquad i,e = 1,2 \tag{10}$$

$$\frac{\partial \boldsymbol{m_\zeta}}{\partial[\boldsymbol{\vartheta}]_i} = \begin{cases}\boldsymbol{\beta^2}\,\boldsymbol{a} \odot \boldsymbol{a_\theta} \odot \left(\boldsymbol{a} \odot \boldsymbol{a}\,\boldsymbol{\beta^2} + \dfrac{\sigma_d^2}{2}\right)^{\odot\frac{-1}{2}}\\ \\ \beta\,\boldsymbol{a} \odot \boldsymbol{a} \odot \left(\boldsymbol{a} \odot \boldsymbol{a}\,\boldsymbol{\beta^2} + \dfrac{\sigma_d^2}{2}\right)^{\odot\frac{-1}{2}}\end{cases} \tag{11}$$

We note here that the CRLB is not constant with respect to the DOA.

The CRLB illustrates the best achievable DOA estimation accuracy of any unbiased estimator. A DOA estimation accuracy that is better than 1° is preferable because high accuracy phase interferometric systems are known to have a DOA estimation accuracy that is better than 1° [57].

The CRLB on the accuracy of DOA estimation in uncorrelated complex Gaussian disturbance for the values of the different parameters, as illustrated in Table 2, is shown in Figure 5. The CRLBs shown in Figure 5 illustrate that the DOA estimation accuracy is worse than 1° at large SDR values. Thus, we conclude that the best achievable MSE of any unbiased estimator is insufficient for the kinds of scenarios that spinning antenna based ELINT systems might encounter, i.e., scenarios that are characterised by: the wide beamwidth of the spinning antenna; the partial spread of the data across the spinning antenna mainlobe; the small number of data samples; and the small SDR. This is because the design objective of unbiased estimation techniques does not attempt to minimise the MSE. Thus, there is no

guarantee for a small MSE [9]-[12], where the MSE is the average mean squared difference between the estimate and the true value, and where the MSE consists of estimation errors due to the variance and estimation errors due to the bias [14].

The design objective of unbiased estimation techniques is to construct an estimator that has a zero bias and that, on average, produces the correct value [14]. The advantage of this design objective is that it is easy to solve, and results in a realisable estimator that is easy to implement [14]. However, as previously mentioned, there is no guarantee for a small MSE [8]-[12], [26].

To improve the DOA estimation accuracy, we therefore adopt biased estimation techniques to construct biased DOA estimators that compromise bias for variance so that their MSEs outperform the MSE limit specified by the CRLB [26], [9]-[12]. This will be the subject of the subsequent chapter.

Table 2. Simulation scenarios that are used to evaluate the CRLB. Parameters listed are: spinning antenna beamwidth θ_B, unambiguous width θ_{um}, emitter DOA θ_{ET}, number of data samples N, the product of the pulse repetition interval and angular velocity $PRI\ \omega_R$, and antenna boresight directions vector θ_{BO}.

Scenario	$\theta_B = \theta_{um}$	θ_{ET}	N	$PRI\ \omega_R$	$[\boldsymbol{\theta_{BO}}]_1$	$[\boldsymbol{\theta_{BO}}]_N$
1	30^o	15^o	16	1.9333^o	0^o	29^o
2	30^o	15^o	8	4.1429^o	0^o	29^o
3	30^o	15^o	16	0.9333^o	0^o	14^o
4	30^o	15^o	8	2^o	0^o	14^o

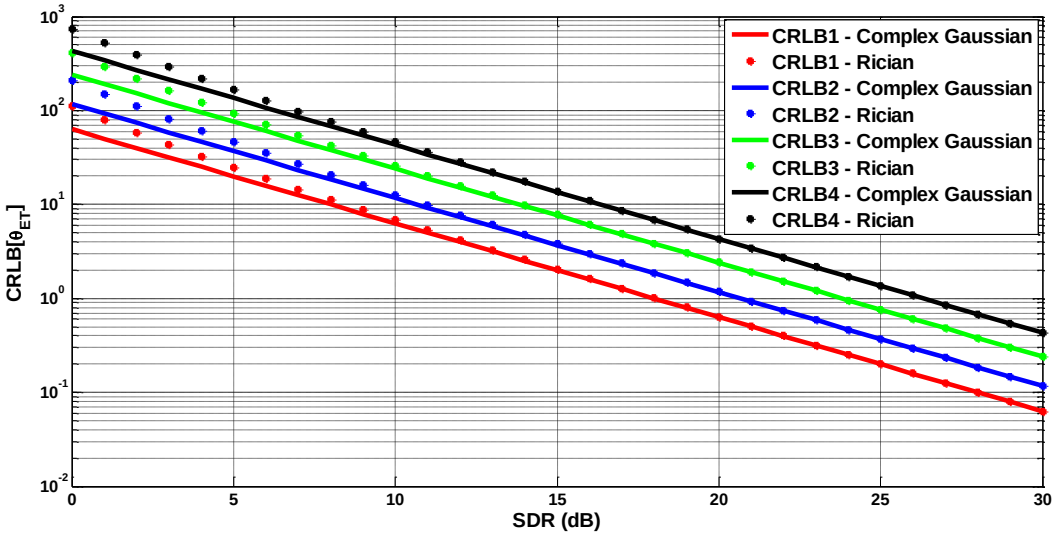

Figure 5. Plots of $CRLB\{\widehat{\theta}_{ET}\}$ with different parameters, as given in Table 2.

3.4 The Barankin bound

Any unbiased estimator experiences the threshold effect in which the MSE of the unbiased estimator deviates substantially from the CRLB below a certain SDR; thus, the use of the CRLB to predict the MSE of the unbiased estimator below the threshold point is invalid [44]. The BB is significantly tighter than the CRLB at low SDR values [44], and is presented in this section to determine the SDR threshold point. The BB on the MSE of any unbiased estimator of $\boldsymbol{\vartheta}$ is given by the diagonal elements of matrix $\boldsymbol{\Lambda}$, i.e., $BB([\boldsymbol{\vartheta}]_i) = [\boldsymbol{\Lambda}]_{ii}$. Where $\boldsymbol{\Lambda}$ is [44]:

$$\boldsymbol{\Lambda} = \boldsymbol{T}\,(\boldsymbol{D} - \mathbf{1}\mathbf{1}^T)^{-1}\,\boldsymbol{T}^T \tag{12}$$

and the matrix $\boldsymbol{T}$ is defined as:

$$\boldsymbol{T} = [\boldsymbol{\vartheta}_1 - \boldsymbol{\vartheta} \quad \boldsymbol{\vartheta}_2 - \boldsymbol{\vartheta} \quad \dots\dots\dots \quad \boldsymbol{\vartheta}_O - \boldsymbol{\vartheta}]; \qquad o = 1 \dots\dots O \tag{13}$$

where $\boldsymbol{\vartheta}_o$ are test points that are chosen to maximise the right-hand side of Equation (12). The vector $\mathbf{1}$, whose elements are equal to 1 is of size O.

For complex Gaussian distributed data, the elements of the Barankin matrix $\boldsymbol{D}$ are given as follows [45]:

$$[\boldsymbol{D}(\boldsymbol{\vartheta})]_{oe} = exp\left[2\,Re\left\{\left(\boldsymbol{m_Z}(\boldsymbol{\vartheta}) - \boldsymbol{m_Z}(\boldsymbol{\vartheta}_o)\right)^H \boldsymbol{R^{-1}}\left(\boldsymbol{m_Z}(\boldsymbol{\vartheta}) - \boldsymbol{m_Z}(\boldsymbol{\vartheta}_e)\right)\right\}\right]; \quad o, e = 1,2, \dots, O \tag{14}$$

For Rician distributed data, the elements of the Barankin matrix $\boldsymbol{D}$ are given as follows [45]:

$$[\boldsymbol{D}(\boldsymbol{\vartheta})]_{oe} = exp\left[\left(\boldsymbol{m_\zeta}(\boldsymbol{\vartheta}) - \boldsymbol{m_\zeta}(\boldsymbol{\vartheta}_o)\right)^T \boldsymbol{C^{-1}}\left(\boldsymbol{m_\zeta}(\boldsymbol{\vartheta}) - \boldsymbol{m_\zeta}(\boldsymbol{\vartheta}_e)\right)\right]; \quad o, e = 1,2, \dots., O \tag{15}$$

The BB on the accuracy of DOA estimation in uncorrelated complex Gaussian disturbance for different parameters values as listed in Table 3, is shown in Figure 6. The BBs illustrated in Figure 6 show that the threshold effect occurs at very small SDR values, even when the number of data samples is small.

Table 3. Simulation scenarios that are used to evaluate the BB. Parameters listed are: spinning antenna beamwidth θ_B, unambiguous width θ_{um}, emitter DOA θ_{ET}, number of data samples N, the product of the pulse repetition interval and angular velocity ($PRI\ \omega_R$), and antenna boresight directions vector $\boldsymbol{\theta_{BO}}$.

Scenario	$\theta_B = \theta_{um}$	θ_{ET}	N	$PRI\ \omega_R$	$[\boldsymbol{\theta_{BO}}]_1$	$[\boldsymbol{\theta_{BO}}]_N$
1	30°	15°	4	7.5°	0°	22.5°
2	30°	15°	32	0.9375°	0°	29.0625°

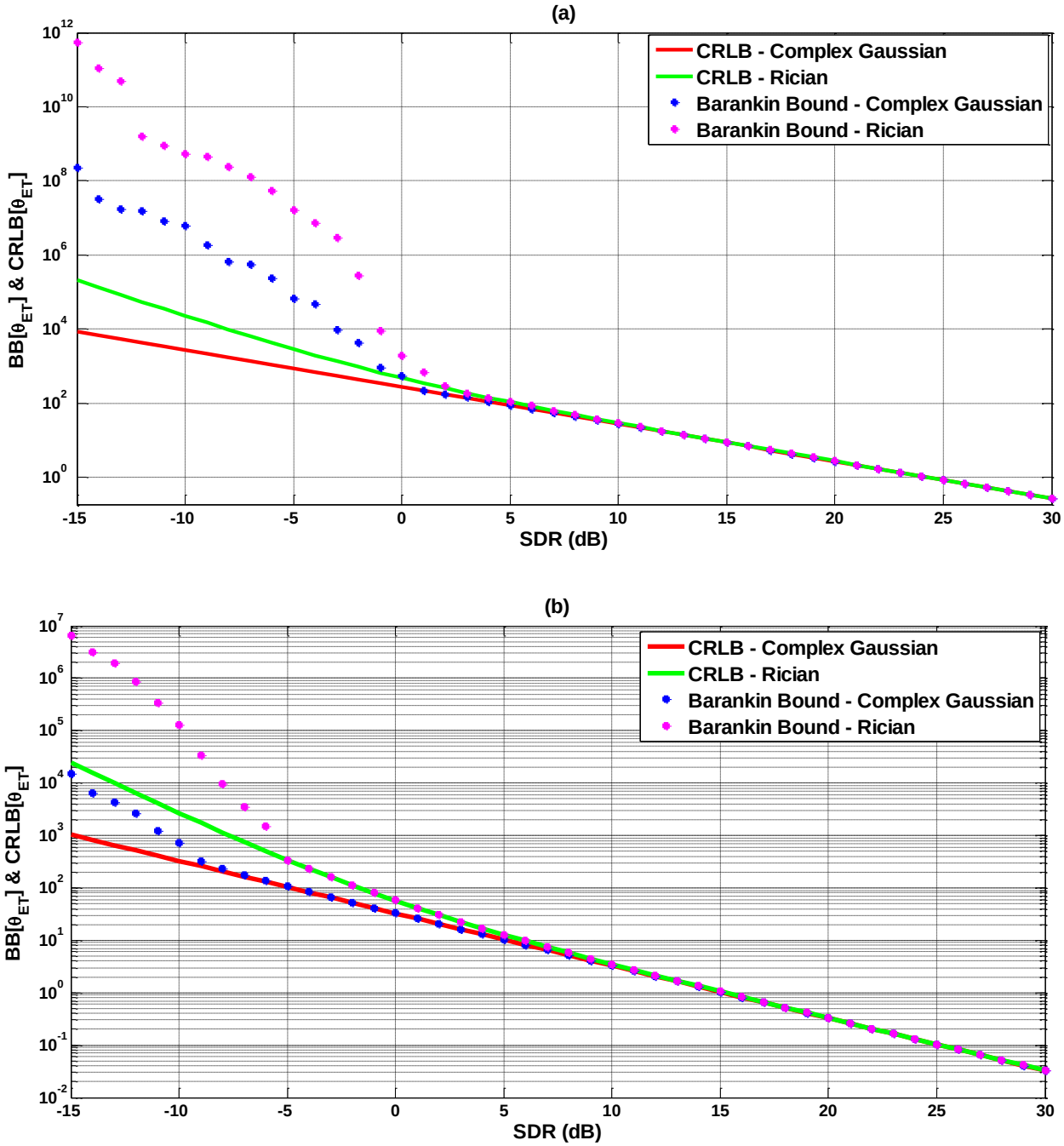

Figure 6. Plots of $CRLB\{\widehat{\theta}_{ET}\}$ and $BB\{\widehat{\theta}_{ET}\}$ with different parameters, as given in Table 3: (a) First scenario. (b) Second scenario.

3.5 The maximum likelihood estimator

The ML technique in which the estimate is given by the value that maximises the likelihood of the observed data is a well-known and widely used technique for constructing asymptotically efficient estimators and in many cases is capable of constructing efficient estimators for a small number of data samples.

The ML estimator for estimating the DOA of signals received by a spinning antenna based system has already been derived in the context of radar; it exploits the knowledge of the

antenna beam pattern and the amplitude modulation induced by the spinning of the directional antenna [1]-[2].

For complex Gaussian distributed data, the ML DOA estimator is obtained by maximising the expression given in Equation (5) with respect to the unknown deterministic parameters b and θ_{ET}. After some simplification, the ML DOA estimator is given by the following expression:

$$\begin{cases} \hat{b} & = \dfrac{\boldsymbol{a^H\, R^{-1}\, Z}}{\boldsymbol{a^H\, R^{-1}\, a}} \\ \hat{\theta}_{ET} & = \underset{\theta_{ET}}{arg\ max}\ \dfrac{|\boldsymbol{Z^H\, R^{-1}\, a}|^2}{\boldsymbol{a^H\, R^{-1}\, a}} \end{cases} \tag{16}$$

For Rician distributed data, the ML DOA estimator is obtained by maximising the expression given in Equation (6) with respect to the unknown parameters β and θ_{ET}. After some simplification, the ML DOA estimator is given by the following expression:

$$(\hat{\theta}_{ET}, \hat{\beta}) = \underset{\beta,\ \theta_{ET}}{arg\ max} \sum_{n=1}^{N} \left(\log I_0 \left(\frac{2\,[\boldsymbol{\zeta}]_n\, \beta\, [\boldsymbol{a}]_n}{\sigma_d^2} \right) - \frac{\beta^2\, [\boldsymbol{a}]_n^2}{\sigma_d^2} \right) \tag{17}$$

The ML DOA estimator given in Equation (17) requires the computation of a two-dimensional nonlinear maximisation function. A simpler DOA estimator can be obtained by maximising the equivalent Gaussian pdf given in Equation (7) with respect to the unknown deterministic parameters β and θ_{ET}. After some simplification, the ML DOA estimator is given by the following expression:

$$\left(\hat{\theta}_{ET}, \hat{\beta}\right) =$$

$$\underset{\beta,\ \theta_{ET}}{arg\ max} \left[2\ \boldsymbol{\zeta^T} \left(\boldsymbol{a} \odot \boldsymbol{a}\, \beta^2 + \frac{\sigma_d^2}{2} \right)^{\odot \frac{1}{2}} \right] - \left[\left(\boldsymbol{a} \odot \boldsymbol{a}\, \beta^2 + \frac{\sigma_d^2}{2} \right)^{\odot \frac{1}{2}} \right]^T \left[\left(\boldsymbol{a} \odot \boldsymbol{a}\, \beta^2 + \frac{\sigma_d^2}{2} \right)^{\odot \frac{1}{2}} \right] \tag{18}$$

The ML DOA estimator given in Equation (18) also requires the computation of a two-dimensional nonlinear maximisation function, but it is easier to implement than the ML DOA estimator given in Equation (17). A suboptimal estimator for β can be used to further reduce the computational complexity to a one-dimensional nonlinear function by exploiting the fact that the mean equals to $\boldsymbol{m_\zeta} \cong \beta\, \boldsymbol{a}$ at high SDR, and then the equivalent Gaussian pdf becomes as follows:

$$P_{\zeta/z}(\boldsymbol{\zeta}; \beta, \theta_{ET}) = \frac{1}{\sqrt{2\pi^N\ det(\boldsymbol{C})}}\ exp\left[-\frac{1}{2}\, [\boldsymbol{\zeta} - \beta\, \boldsymbol{a}]^T\, \boldsymbol{C}^{-1}\, [\boldsymbol{\zeta} - \beta\, \boldsymbol{a}] \right] \tag{19}$$

Then, the suboptimal estimator for β is obtained by maximising the expression given in Equation (19) with respect to the unknown deterministic parameters β and θ_{ET}. After some simplification, the estimator for β is given by the following expression:

$$\hat{\beta} = \frac{\boldsymbol{a^T\, \zeta}}{\boldsymbol{a^T\, a}} \tag{20}$$

By substituting the estimator given in Equation (20) into Equation (18), the ML DOA estimator for Rician distributed data is given by the following expression:

$$\hat{\theta}_{ET} = \underset{\theta_{ET}}{arg\,max} \left[\mathbf{2}\ \boldsymbol{\zeta}^{\boldsymbol{T}} \left(\boldsymbol{a} \odot \boldsymbol{a} \left| \frac{\boldsymbol{a}^{\boldsymbol{T}}\boldsymbol{\zeta}}{\boldsymbol{a}^{\boldsymbol{T}}\boldsymbol{a}} \right|^{\mathbf{2}} + \frac{\sigma_d^2}{2} \right)^{\odot \frac{1}{2}} \right] -$$

$$\left[\left(\boldsymbol{a} \odot \boldsymbol{a} \left| \frac{\boldsymbol{a}^{\boldsymbol{T}}\boldsymbol{\zeta}}{\boldsymbol{a}^{\boldsymbol{T}}\boldsymbol{a}} \right|^{\mathbf{2}} + \frac{\sigma_d^2}{2} \right)^{\odot \frac{1}{2}} \right]^{T} \left[\left(\boldsymbol{a} \odot \boldsymbol{a} \left| \frac{\boldsymbol{a}^{\boldsymbol{T}}\boldsymbol{\zeta}}{\boldsymbol{a}^{\boldsymbol{T}}\boldsymbol{a}} \right|^{\mathbf{2}} + \frac{\sigma_d^2}{2} \right)^{\odot \frac{1}{2}} \right] \tag{21}$$

In the next chapter, the ML DOA estimators presented in this section shall be modified using biased estimation techniques to improve their MSEs beyond the MSE limit specified by the CRLB.

3.6 Summary

In this chapter, the data model for estimating the DOA of emitters' signals received by a spinning antenna based ELINT system was presented. Two types of data were considered: 1) complex Gaussian distributed data, and 2) Rician distributed data.

The CRLB for the presented data model was derived and analysed, and the BB was derived to validate the CRLB. The analysis of these MSE bounds have shown that the best achievable MSE of any unbiased DOA estimator is insufficient for the kinds of scenarios that spinning antenna based ELINT systems might encounter; thus, it can be concluded that DOA estimators that provide better MSE are needed.

The ML DOA estimators for the two data types were derived in this chapter, and in the next chapter, the ML DOA estimators shall be modified to enhance their MSEs.

4. Biased estimation

4.1 Introduction

The design objective of unbiased estimation techniques is to construct an estimator by constraining to zero the MSE's component (the bias) that depends on the unknown parameter of interest, and then attempting to minimise the deviation of the estimate from its average value [14]. This design objective is widely used because of its simplicity and the ability to construct a realisable estimator that does not depend on the unknown parameter of interest.

In the previous chapter, we showed, by evaluating the CRLB, that the best achievable MSE of any unbiased DOA estimator is insufficient for the kinds of scenarios that spinning antenna based ELINT systems might encounter. The reason for this is that the design objective of unbiased estimation techniques does not attempt to minimise the MSE [14], [9], and thus there is no guarantee for a small MSE.

To achieve our goal, which is to improve the DOA estimation accuracy (as measured by the MSE) beyond the MSE limit specified by the CRLB, the realistic approach would be to employ estimation techniques that directly attempt to minimise the MSE. Unfortunately, doing so would lead to an unrealisable estimator that depends on the unknown parameter of interest [14]. To overcome this problem, we employed biased estimation techniques that compromised bias for variance to reduce the overall MSE [8]-[12], [26].

In the first biased estimation technique, presented in [9]-[12], MSE bounds that outperform the conventional CRLB were designed by performing a linear transformation or an affine transformation on the CRLB, where the transformation parameters that compromise bias for variance to obtain the largest reduction in MSE are found by solving a minimax optimisation problem. A biased estimator that outperforms the CRLB can then be constructed by performing a linear transformation or an affine transformation on an efficient estimator using the obtained transformation parameters.

In the second biased estimation technique, which is a Bayesian estimation technique [14], the MSE is improved by imposing a prior distribution on the unknown parameter of interest. Thus, randomness is introduced through the observed data, and the prior distributions are adopted to impose certain constraints [43]. In this setting, the estimate is computed by combining the prior distribution with the information provided by the observed data. Furthermore, the Bayesian estimator makes a compromise between the prior distribution and the observed data, based on how much information is provided by the observed data. This mechanism compromises bias for variance to reduce the overall MSE.

In this chapter, we thus construct biased DOA estimators for both complex Gaussian distributed data and Rician distributed data, using the abovementioned estimation techniques. We first consider the case in which the DOA is estimated using a single snapshot, and then consider the case in which the DOA is estimated using several snapshots. In the latter case,

we construct recursive Bayesian DOA estimators that are capable of merging the information contained in these several snapshots. We also derive the BCRLB to provide a performance benchmark for the Bayesian DOA estimators.

To demonstrate the MSE enhancement provided by the proposed DOA estimators, we compare the proposed biased DOA estimators with the CRLB, the BB and the BCRLB using Monte Carlo simulation and real radar data provided by Reutech Radar Systems [50]. We also demonstrate through Monte Carlo simulation that merging the information contained in several snapshots using the recursive Bayesian DOA estimators can often enhance the MSE over a single snapshot.

4.2 The linearly transformed estimator

In this section, we will present the framework for constructing an MSE bound with linear bias that outperforms the CRLB and the minimax estimator that attains this MSE bound [10], [12].

To construct a minimax estimator that outperforms the CRLB, the corresponding MSE bound should be constructed first, before constructing the minimax estimator that attains this MSE bound [10], [12].

If $\widehat{\boldsymbol{\theta}}$ is an arbitrary estimator of $\boldsymbol{\theta}$ with bias $\boldsymbol{B}$, then the covariance of $\widehat{\boldsymbol{\theta}}$ must satisfy:

$$\boldsymbol{COV} \geq (\boldsymbol{I} + \boldsymbol{B}_{\boldsymbol{\theta}})\, \boldsymbol{J}^{-1}\, (\boldsymbol{I} + \boldsymbol{B}_{\boldsymbol{\theta}})^{\boldsymbol{T}} \tag{22}$$

where $\boldsymbol{B}_{\boldsymbol{\theta}}$ is the bias gradient matrix with respect to $\boldsymbol{\theta}$. If $\boldsymbol{B}_{\boldsymbol{\theta}} = \boldsymbol{0}$ then the right side of Equation (22) becomes $\boldsymbol{J}^{-1}$, which is the CRLB.

The MSE of the estimator $\widehat{\boldsymbol{\theta}}$ is the sum of the covariance and the squared norm of the bias [10], [12]:

$$MSE = Ex\left\{\left\|\widehat{\boldsymbol{\theta}} - \boldsymbol{\theta}\right\|^2\right\} = \|\boldsymbol{B}\|^2 + Tr(\boldsymbol{COV}) \tag{23}$$

If we assume that $\widehat{\boldsymbol{\theta}}$ attains the CRLB, and if we use the covariance given in Equation (22) in Equation (23), then the MSE is as follows [10], [12]:

$$MSE = \|\boldsymbol{B}\|^2 + Tr\left((\boldsymbol{I} + \boldsymbol{B}_{\boldsymbol{\theta}})\, \boldsymbol{J}^{-1}\, (\boldsymbol{I} + \boldsymbol{B}_{\boldsymbol{\theta}})^{\boldsymbol{T}}\right) \tag{24}$$

If we use a linear bias function of the form $\boldsymbol{B} = \boldsymbol{M}\,\boldsymbol{\theta}$ for some matrix $\boldsymbol{M}$, then the MSE bound becomes [10], [12]:

$$MSE(\boldsymbol{M}, \boldsymbol{\theta}) = \boldsymbol{\theta}^T\, \boldsymbol{M}^T\, \boldsymbol{M}\, \boldsymbol{\theta} + Tr\left((\boldsymbol{I} + \boldsymbol{M})\, \boldsymbol{J}^{-1}\, (\boldsymbol{I} + \boldsymbol{M})^{\boldsymbol{T}}\right) \tag{25}$$

We note here that, in the case when the CRLB cannot be attained (i.e., an efficient estimator does not exist), then the variance of an MVU estimator can be used to replace $\boldsymbol{J}^{-1}$ in the derived MSE bound [10], [12].

A minimax estimator whose MSE is given by Equation (25), is a linear transformation of $\widehat{\boldsymbol{\theta}}$ [10], [12]:

$$\widehat{\boldsymbol{\theta}}_{\boldsymbol{b}} = (\boldsymbol{I} + \boldsymbol{M})\,\widehat{\boldsymbol{\theta}} \tag{26}$$

The goal is to find an $\boldsymbol{M}$ such that $MSE(\boldsymbol{M}, \boldsymbol{\theta})$ outperforms $MSE(\boldsymbol{0}, \boldsymbol{\theta})$ for all values of $\boldsymbol{\theta}$. Moreover, there should not be another $\boldsymbol{M}$ that results in a larger reduction in MSE. If the optimal $\boldsymbol{M}$ depends on the unknown parameter $\boldsymbol{\theta}$, then $\boldsymbol{M}$ can be calculated by solving the following minimax optimisation problem [10], [12]:

$$\boldsymbol{M} = \min_{\boldsymbol{M}} \max_{\boldsymbol{\theta}} \{MSE(\boldsymbol{M}, \boldsymbol{\theta}) - MSE(\boldsymbol{0}, \boldsymbol{\theta})\} \tag{27}$$

If $\boldsymbol{\theta}$ becomes a scalar, then Equations (25), (26) and (27) are as follows [10], [12]:

$$MSE(m, \theta) = J^{-1}\,(1 + m)^2 + m^2\theta^2 \tag{28}$$

$$\hat{\theta}_b = (1 + m)\,\hat{\theta} \tag{29}$$

$$m = \min_{m} \max_{\theta} \{MSE(m, \theta) - MSE(0, \theta)\} \tag{30}$$

From Equation (29), we conclude that m must lie in the interval $-1 \leq m < 0$ to obtain a reduction in the MSE [10], [12]. The bias $m^2\theta^2$ increases as m decreases toward -1, while the variance $J^{-1}\,(1 + m)^2$ decreases.

If θ lies in a known interval, then the interval can be written as a quadratic constraint Q_c [10], [12]:

$$Q_c = \{\theta : \theta^T A_1 \theta + 2\, b_1 \theta + c_1 \leq 0\} \tag{31}$$

For our problem, the interval and the values of A_1, b_1 and c_1 are as follows:

$$max(\boldsymbol{\theta_{BO}}) - \frac{\theta_{um}}{2} \leq \theta \leq min(\boldsymbol{\theta_{BO}}) + \frac{\theta_{um}}{2} \tag{32}$$

$$A_1 = 1$$

$$b_1 = -\frac{[\boldsymbol{\theta_{BO}}]_N + [\boldsymbol{\theta_{BO}}]_1}{2} \tag{33}$$

$$c_1 = \left(max(\boldsymbol{\theta_{BO}}) - \frac{\theta_{um}}{2}\right)\left(min(\boldsymbol{\theta_{BO}}) + \frac{\theta_{um}}{2}\right)$$

The minimax optimisation problem can be solved by known algorithms for solving minimax optimisation problems [10]. To simplify the computation, the problem can be formulated as semidefinite programs (SDPs), as suggested in [10]. The first step is to convert the $CRLB(\theta)$ to a quadratic form [10], [12]:

$$CRLB(\theta) = B_1\,\theta\,\theta^T\,B_1^T + (C_1\,\theta\,z_1^T + z_1\,\theta^T\,C_1^T) + A_2 \tag{34}$$

The optimal value of m is given by the following [10], [12]:

$$m = -S(\Pi, w)\,(S(\Pi, w) + \Pi)^{-1} \tag{35}$$

where $S(\Pi, w)$ is given by [10], [12]:

$$S(\Pi, w) = B_1 \, \Pi \, B_1^T + (C_1 \, w^T \, z_1^T + z_1 \, w \, C_1^T) + A_2 \tag{36}$$

where Π and w are the solutions to the following semidefinite programming (SDP) problem [10], [12]:

$$\begin{cases} \underset{Y, w, \Pi}{min} \quad Tr(Y) \\ s.t. \quad \begin{bmatrix} Y & S(\Pi, w) \\ S(\Pi, w) & S(\Pi, w) + \Pi \end{bmatrix} \geq 0 \\ \quad \begin{bmatrix} \Pi & w \\ w & 1 \end{bmatrix} \geq 0 \\ \quad \Pi \, A_1 + 2 \, w \, b_1 + c_1 \leq 0 \end{cases} \tag{37}$$

We note here that the OPTI Toolbox [21] was used to solve Equation (37).

We note here that, in the case of a constant $CRLB$ (constant with respect to the unknown parameter to be estimated), m equals to [10], [12]:

$$m = -\frac{CRLB(\theta)}{CRLB(\theta) + V^2} \tag{38}$$

where V is the upper limit of the interval specifying θ.

We note here that, in our problem, we replace the arbitrary estimator $\widehat{\boldsymbol{\theta}}$ with the ML DOA estimator presented in Section 3.5.

4.3 The affine transformed estimator

A reduction in the MSE that outperforms the linear approach can be obtained by allowing for an affine bias of the form $\boldsymbol{B} = \boldsymbol{M}\,\boldsymbol{\theta} + \boldsymbol{U}$ for some matrices $\boldsymbol{M}$ and $\boldsymbol{U}$ [11], [12], thus the MSE bound given in Equation (24) becomes [11], [12]:

$$MSE(\boldsymbol{M}, \boldsymbol{U}, \boldsymbol{\theta}) = (\boldsymbol{M}\,\boldsymbol{\theta} + \boldsymbol{U})^T (\boldsymbol{M}\,\boldsymbol{\theta} + \boldsymbol{U}) + Tr\left((\boldsymbol{I} + \boldsymbol{M})\,\boldsymbol{J}^{-1}\,(\boldsymbol{I} + \boldsymbol{M})^{\boldsymbol{T}}\right) \tag{39}$$

An estimator whose MSE is given by Equation (39) is an affine transformation of $\widehat{\boldsymbol{\theta}}$ [11], [12]:

$$\widehat{\boldsymbol{\theta}}_{\boldsymbol{b}} = (\boldsymbol{I} + \boldsymbol{M})\,\widehat{\boldsymbol{\theta}} + \boldsymbol{U} \tag{40}$$

The goal is to find an $\boldsymbol{M}$ and $\boldsymbol{U}$ such that $MSE(\boldsymbol{M}, \boldsymbol{U}, \boldsymbol{\theta})$ outperforms $MSE(\boldsymbol{0}, \boldsymbol{0}, \boldsymbol{\theta})$ for all values of $\boldsymbol{\theta}$. Moreover, there should not be another $\boldsymbol{M}$ and $\boldsymbol{U}$ that result in a larger reduction in MSE. If the optimal $\boldsymbol{M}$ and $\boldsymbol{U}$ depend on the unknown parameter $\boldsymbol{\theta}$, then $\boldsymbol{M}$ and $\boldsymbol{U}$ can be calculated by solving the following minimax optimisation problem [11], [12]:

$$(\boldsymbol{M}, \boldsymbol{U}) = \underset{\boldsymbol{M}, \boldsymbol{U}}{min} \; \underset{\boldsymbol{\theta}}{max} \{MSE(\boldsymbol{M}, \boldsymbol{U}, \boldsymbol{\theta}) - MSE(\boldsymbol{0}, \boldsymbol{0}, \boldsymbol{\theta})\} \tag{41}$$

If $\boldsymbol{\theta}$ becomes a scalar, then Equations (39), (40) and (41) become [11], [12]:

$$MSE(m, u, \theta) = J^{-1}\,(1 + m)^2 + (m\,\theta + u)^2 \tag{42}$$

$$\hat{\theta}_b = (1 + m)\,\hat{\theta} + u \tag{43}$$

$$(m,u) = \min_{m,u} \max_{\theta} \{MSE(m,u,\theta) - MSE(0,0,\theta)\} \tag{44}$$

The steps used in the previous section are used to solve the minimax optimisation problem. The optimal values of m and u are given by the following [11], [12]:

$$m = -S(\Pi, w)\,(S(\Pi, w) + \Pi - w\,w^T)^{-1} \tag{45}$$

$$u = \frac{1}{1 - w^T\,(S(\Pi, w) + \Pi)^{-1}\,w}\,S(\Pi, w)\,(S(\Pi, w) + \Pi)^{-1}\,w \tag{46}$$

where $S(\Pi, w)$ is given by [11], [12]:

$$S(\Pi, w) = B_1\,\Pi\,B_1^T + (C_1\,w\,z_1^T + z_1\,w\,C_1^T) + A_2 \tag{47}$$

Where Π and w are the solution to the following SDP [11], [12]:

$$\begin{cases} \min\limits_{Y,w,\Pi} & Tr(Y) \\ s.t. & \begin{bmatrix} Y & S(\Pi,w) & 0 \\ S(\Pi,w) & S(\Pi,w)+\Pi & w \\ 0 & w & 1 \end{bmatrix} \geq 0 \\ & \begin{bmatrix} \Pi & w \\ w & 1 \end{bmatrix} \geq 0 \\ & \Pi\,A_1 + 2\,w\,b_1 + c_1 \leq 0 \end{cases} \tag{48}$$

We note here that the OPTI Toolbox [21] was used to solve Equation (48).

In the case of a constant $CRLB$ (constant with respect to the unknown parameter to be estimated), m and u equal to [11], [12]:

$$m = -\frac{CRLB(\theta)}{CRLB(\theta) + b_1^T b_1 - c_1} \tag{49}$$

$$u = -\frac{CRLB(\theta)}{CRLB(\theta) + b_1^T b_1 - c_1}\,b_1 \tag{50}$$

We note here that, in our problem, we replace the arbitrary estimator $\widehat{\boldsymbol{\theta}}$ with the ML DOA estimator presented in Section 3.5.

4.4 The minimum mean square error estimator

Bayesian estimation techniques for deterministic parameters improve the estimation accuracy by incorporating prior information (through prior distributions) about the unknown parameter of interest [14]. Thus, randomness is introduced through the observed data and the prior distributions are adopted to impose certain constraints [43]. Moreover, the knowledge obtained from combining the prior distribution with the observed data is described by the posterior probability distribution [14].

In this thesis, the MMSE estimation technique [14], which is a well-known and popular form of Bayesian estimation techniques, is employed to improve the DOA estimation accuracy beyond the MSE limit specified by the CRLB.

An MMSE estimator relies on the prior information and the observed data to compute the estimate. If the prior information is less informative than the observed data, then the estimator will depend less on the prior information and more on the observed data [14]. An important consideration in MMSE estimation is the accuracy of the prior probability distribution. An inaccurate prior probability distribution will degrade the estimation accuracy [14].

A closed form of the MMSE estimator can be obtained if both the data and the prior probability distribution are Gaussian [14]. Thus, the MMSE estimator, which is the mean of the posterior probability distribution, is given by:

$$Ex\{\boldsymbol{\vartheta}|\boldsymbol{Z}\} = \boldsymbol{\mu} + \boldsymbol{\Gamma}\,\boldsymbol{H}^H\,(\boldsymbol{H}\,\boldsymbol{\Gamma}\,\boldsymbol{H}^H + \boldsymbol{R})^{-1}(\boldsymbol{Z} - \boldsymbol{H}\,\boldsymbol{\mu}) \tag{51}$$

where $\boldsymbol{H}$ is a known $N \times K$ matrix, $\boldsymbol{\vartheta}$ is K-dimensional unknown parameters vector with a prior probability distribution given by the pdf $\mathcal{N}(\boldsymbol{\mu}, \boldsymbol{\Gamma})$. K is the number of the unknown parameters and $\boldsymbol{\mu}$ is the prior mean.

4.4.1 The minimum mean square error estimator for complex Gaussian distributed data

For complex Gaussian distributed data, the relationship between the data and the DOA is nonlinear. This is a problem, and it is solved by seeking an approximate solution based on linearisation [14]. Thus, the MMSE estimator is constructed by performing linearisation approximation around the prior mean, Equation (5) and Equation (51). Thus, the MMSE estimator of the 3×1 unknown parameter vector $\boldsymbol{\vartheta} = [\theta_{ET}\ b_R\ \ b_I]^T$ is given by:

$$\widehat{\boldsymbol{\vartheta}} = \boldsymbol{\mu} + \boldsymbol{\Gamma}\,\boldsymbol{H}^H(\boldsymbol{H}\,\boldsymbol{\Gamma}\,\boldsymbol{H}^H + \boldsymbol{R})^{-1}\big(\boldsymbol{Z} - \boldsymbol{m_Z}(\boldsymbol{\mu})\big) \tag{52}$$

The prior mean is $\boldsymbol{\mu} = \left[\theta_\mu\ \ b_{\mu R}\ \ b_{\mu I}\right]^T$. Matrix $\boldsymbol{H}$ is found by linearising the function that transforms the parameters to the ideal data samples $\boldsymbol{H} = \frac{\partial \boldsymbol{m_Z}}{\partial \boldsymbol{\vartheta}}\Big|_{\boldsymbol{\vartheta}=\boldsymbol{\mu}}$. Thus, the columns of the matrix $\boldsymbol{H}$ and the diagonal elements of the diagonal matrix $\boldsymbol{\Gamma}$ are given by the following:

$$\begin{cases} [\boldsymbol{H}]_{:1} = \left(b_{\mu R} + j b_{\mu I}\right) \boldsymbol{a_\theta}\left(\theta_\mu\,, \boldsymbol{\theta_{BO}}\right) \\ [\boldsymbol{H}]_{:2} = \boldsymbol{a}\left(\theta_\mu\,, \boldsymbol{\theta_{BO}}\right) \\ [\boldsymbol{H}]_{:3} = j\ \boldsymbol{a}\left(\theta_\mu\,, \boldsymbol{\theta_{BO}}\right) \\ [\boldsymbol{\Gamma}]_{11} = v^2 \\ [\boldsymbol{\Gamma}]_{22} = \left(b_{\mu R} - b_{vR}\right)^2 \\ [\boldsymbol{\Gamma}]_{33} = \left(b_{\mu I} - b_{vI}\right)^2 \end{cases} \tag{53}$$

The prior probability distribution is represented by a pdf. Our empirical experience is that the pdf parameter values that result in a good bias-variance trade-off are obtained as follows:

$$\begin{cases} \theta_\mu = \dfrac{[\boldsymbol{\theta_{BO}}]_N + [\boldsymbol{\theta_{BO}}]_1}{2} \\ v = \dfrac{1}{2}\left(\theta_{um} - \left(max(\boldsymbol{\theta_{BO}}) - min(\boldsymbol{\theta_{BO}})\right)\right) \\ b_{\mu R} = Re\left\{\dfrac{\boldsymbol{a}(\theta_\mu, \boldsymbol{\theta_{BO}})^{\boldsymbol{H}}\, \boldsymbol{R^{-1}}\, \boldsymbol{Z}}{\boldsymbol{a}(\theta_\mu, \boldsymbol{\theta_{BO}})^{\boldsymbol{H}}\, \boldsymbol{R^{-1}}\, \boldsymbol{a}(\theta_\mu, \boldsymbol{\theta_{BO}})}\right\} \\ b_{\mu I} = Im\left\{\dfrac{\boldsymbol{a}(\theta_\mu, \boldsymbol{\theta_{BO}})^{\boldsymbol{H}}\, \boldsymbol{R^{-1}}\, \boldsymbol{Z}}{\boldsymbol{a}(\theta_\mu, \boldsymbol{\theta_{BO}})^{\boldsymbol{H}}\, \boldsymbol{R^{-1}}\, \boldsymbol{a}(\theta_\mu, \boldsymbol{\theta_{BO}})}\right\} \\ b_{vR} = Re\left\{\dfrac{\boldsymbol{a}(\theta_\mu + v, \boldsymbol{\theta_{BO}})^{\boldsymbol{H}}\, \boldsymbol{R^{-1}}\, \boldsymbol{Z}}{\boldsymbol{a}(\theta_\mu + v, \boldsymbol{\theta_{BO}})^{\boldsymbol{H}}\, \boldsymbol{R^{-1}}\, \boldsymbol{a}(\theta_\mu + v, \boldsymbol{\theta_{BO}})}\right\} \\ b_{vI} = Im\left\{\dfrac{\boldsymbol{a}(\theta_\mu + v, \boldsymbol{\theta_{BO}})^{\boldsymbol{H}}\, \boldsymbol{R^{-1}}\, \boldsymbol{Z}}{\boldsymbol{a}(\theta_\mu + v, \boldsymbol{\theta_{BO}})^{\boldsymbol{H}}\, \boldsymbol{R^{-1}}\, \boldsymbol{a}(\theta_\mu + v, \boldsymbol{\theta_{BO}})}\right\} \end{cases} \tag{54}$$

where θ_μ is the average of the antenna boresight direction associated with the first data sample and the antenna boresight direction associated with the last data sample, v is the unambiguous width minus the span of the data across the mainlobe divided by two. $b_{\mu R}$, $b_{\mu I}$, b_{vR} and b_{vI} are the complex amplitude parts that are calculated at directions θ_μ and $\theta_\mu + v$.

A Bayesian estimator for deterministic parameters exploits the prior knowledge (represented by the prior pdf) to trades bias for variance in attempt to reduce the overall MSE [14], [43].

The antenna boresight directions vector $\boldsymbol{\theta_{BO}}$ provides useful information that is used to set the prior pdf parameters. The MMSE DOA estimator compromises between this information (prior pdf) and that contributed by the amplitude modulated data to produce the DOA estimate [14].

The MMSE DOA estimator depends on the prior pdf as well as the amplitude modulated data to produce the DOA estimate [14]. If the amplitude modulated data is strong relative to that of the prior pdf, then the estimator will ignore the prior pdf [14]. Otherwise, the estimator will be biased towards the prior pdf [14].

4.4.2 The minimum mean square error estimator for Rician distributed data

For Rician distributed data, the MMSE estimator is constructed by employing the steps used in Section 4.4.1. Thus, the MMSE estimator of the 2×1 unknown parameter vector $\boldsymbol{\vartheta} = [\theta_{ET}\ \beta]^T$ is:

$$\widehat{\boldsymbol{\vartheta}} = \boldsymbol{\mu} + \boldsymbol{\Gamma}\, \boldsymbol{H}^T (\boldsymbol{H}\, \boldsymbol{\Gamma}\, \boldsymbol{H}^T + \boldsymbol{C})^{-1} \left(\boldsymbol{\zeta} - \boldsymbol{m}_\zeta(\boldsymbol{\mu})\right) \tag{55}$$

The prior mean is $\boldsymbol{\mu} = \left[\theta_\mu \;\; \beta_\mu\right]^T$. Matrix $\boldsymbol{H}$ is found by linearising the function that transforms the parameters to the ideal data samples $\boldsymbol{H} = \frac{\partial \boldsymbol{m}_\zeta}{\partial \boldsymbol{\vartheta}}\Big|_{\boldsymbol{\vartheta}=\boldsymbol{\mu}}$. Thus, the columns of the matrix $\boldsymbol{H}$ and the diagonal elements of the diagonal matrix $\boldsymbol{\Gamma}$ are given by the following:

$$\begin{cases} [\boldsymbol{H}]_{:1} = \beta_\mu^2 \;\; \boldsymbol{a} \odot \boldsymbol{a_\theta} \odot \left(\boldsymbol{a} \odot \boldsymbol{a}\, \beta_\mu^2 + \dfrac{\sigma_d^2}{2} \right)^{\odot \frac{-1}{2}} \\ [\boldsymbol{H}]_{:2} = \beta_\mu \, \boldsymbol{a} \odot \boldsymbol{a} \odot \left(\boldsymbol{a} \odot \boldsymbol{a}\, \beta_\mu^2 + \dfrac{\sigma_d^2}{2} \right)^{\odot \frac{-1}{2}} \\ [\boldsymbol{\Gamma}]_{11} = \; v^2 \\ [\boldsymbol{\Gamma}]_{22} = \; \left(\beta_\mu - \beta_v\right)^2 \end{cases} \tag{56}$$

We note here that the dependency of $\boldsymbol{a}\left(\theta_\mu, \boldsymbol{\theta_{BO}}\right)$ and $\boldsymbol{a_\theta}\left(\theta_\mu, \boldsymbol{\theta_{BO}}\right)$ on θ_μ and $\boldsymbol{\theta_{BO}}$ was omitted from Equation (56) for ease of notation. θ_μ and v are calculated using Equation (54), and β_μ and β_v are given by the following:

$$\begin{cases} \beta_\mu = \dfrac{\boldsymbol{a}\left(\theta_\mu, \boldsymbol{\theta_{BO}}\right)^T \boldsymbol{\zeta}}{\boldsymbol{a}\left(\theta_\mu, \boldsymbol{\theta_{BO}}\right)^T \boldsymbol{a}\left(\theta_\mu, \boldsymbol{\theta_{BO}}\right)} \\ \beta_v = \dfrac{\boldsymbol{a}\left(\theta_\mu + v, \boldsymbol{\theta_{BO}}\right)^T \boldsymbol{\zeta}}{\boldsymbol{a}\left(\theta_\mu + v, \boldsymbol{\theta_{BO}}\right)^T \boldsymbol{a}\left(\theta_\mu + v, \boldsymbol{\theta_{BO}}\right)} \end{cases} \tag{57}$$

4.5 The Bayesian Cramer Rao lower bound

In this section, the BCRLB is derived to provide a performance benchmark for the MMSE estimators. The BCRLB is given by the following [43]:

$$\begin{cases} BCRLB\left(\left[\widehat{\boldsymbol{\vartheta}}\right]_i\right) \geq \left[\boldsymbol{W}\, \boldsymbol{I_B^{-1}}\, \boldsymbol{W}\right]_{ii}; \quad i = 1, \ldots . K \\ \boldsymbol{W} = \boldsymbol{1} + \dfrac{\partial \boldsymbol{B}\left(\widehat{\boldsymbol{\vartheta}}\right)}{\partial \boldsymbol{\vartheta}} + \boldsymbol{B}\left(\widehat{\boldsymbol{\vartheta}}\right) \dfrac{\partial \ln p(\boldsymbol{\vartheta})^T}{\partial \boldsymbol{\vartheta}} \\ \boldsymbol{I_B} = \boldsymbol{J} + \dfrac{\partial \ln p(\boldsymbol{\vartheta})}{\partial \boldsymbol{\vartheta}} \dfrac{\partial \ln p(\boldsymbol{\vartheta})^T}{\partial \boldsymbol{\vartheta}} \end{cases} \tag{58}$$

4.5.1 The Bayesian Cramer Rao lower bound for complex Gaussian distributed data

For complex Gaussian distributed data, the bias $\boldsymbol{B}\left(\widehat{\boldsymbol{\vartheta}}\right) = Ex\left\{\widehat{\boldsymbol{\vartheta}}\right\} - \boldsymbol{\vartheta}$ of the MMSE estimator is given by the following:

$$\boldsymbol{B}\left(\widehat{\boldsymbol{\vartheta}}\right) = \boldsymbol{\mu} - \boldsymbol{\vartheta} + \boldsymbol{\Gamma}\, \boldsymbol{H}^H (\boldsymbol{H}\, \boldsymbol{\Gamma}\, \boldsymbol{H}^H + \boldsymbol{R})^{-1} \left(b\, \boldsymbol{a} - \boldsymbol{m_Z}(\boldsymbol{\mu})\right) \tag{59}$$

The dependency of $\boldsymbol{a}(\theta_{ET}, \boldsymbol{\theta_{BO}})$ on θ_{ET} and $\boldsymbol{\theta_{BO}}$ was omitted from Equation (59) for ease of notation.

The derivative of $\boldsymbol{B}(\widehat{\boldsymbol{\vartheta}})$ with respect to $\boldsymbol{\vartheta}$ is given by:

$$\frac{\partial \boldsymbol{B}(\widehat{\boldsymbol{\vartheta}})}{\partial \boldsymbol{\vartheta}} = -\boldsymbol{I} + [\boldsymbol{\Psi}\, b\, \boldsymbol{a}_{\boldsymbol{\theta}}(\theta_{ET}, \boldsymbol{\theta_{BO}}) \quad \boldsymbol{\Psi}\, \boldsymbol{a}(\theta_{ET}, \boldsymbol{\theta_{BO}}) \quad \boldsymbol{\Psi}\, j\boldsymbol{a}(\theta_{ET}, \boldsymbol{\theta_{BO}})] \tag{60}$$

where matrix $\boldsymbol{\Psi} = \boldsymbol{\Gamma}\, \boldsymbol{H}^H(\boldsymbol{H}\, \boldsymbol{\Gamma}\, \boldsymbol{H}^H + \boldsymbol{R})^{-1}$. The derivative of the prior Gaussian pdf natural logarithm is calculated as follows:

$$\begin{cases} \dfrac{\partial \ln p(\boldsymbol{\vartheta})}{\partial [\boldsymbol{\vartheta}]_1} = \dfrac{\theta_\mu - \theta_{ET}}{[\boldsymbol{\Gamma}]_{11}} \\ \dfrac{\partial \ln p(\boldsymbol{\vartheta})}{\partial [\boldsymbol{\vartheta}]_2} = \dfrac{b_{\mu R} - b_R}{[\boldsymbol{\Gamma}]_{22}} \\ \dfrac{\partial \ln p(\boldsymbol{\vartheta})}{\partial [\boldsymbol{\vartheta}]_3} = \dfrac{b_{\mu I} - b_I}{[\boldsymbol{\Gamma}]_{33}} \end{cases} \tag{61}$$

The matrices $\boldsymbol{H}$ and $\boldsymbol{\Gamma}$ are calculated using Equation (53) and the pdf parameters are given by the following:

$$\begin{cases} \theta_\mu = \dfrac{[\boldsymbol{\theta_{BO}}]_N + [\boldsymbol{\theta_{BO}}]_1}{2} \\ v = \dfrac{1}{2}\left(\theta_{um} - \left(max(\boldsymbol{\theta_{BO}}) - min(\boldsymbol{\theta_{BO}})\right)\right) \\ b_{\mu R} = Re\left\{ \dfrac{\boldsymbol{a}(\theta_\mu, \boldsymbol{\theta_{BO}})^{\boldsymbol{H}}\, \boldsymbol{R^{-1}}\, b\, \boldsymbol{a}(\theta_{ET}, \boldsymbol{\theta_{BO}})}{\boldsymbol{a}(\theta_\mu, \boldsymbol{\theta_{BO}})^{\boldsymbol{H}}\, \boldsymbol{R^{-1}}\, \boldsymbol{a}(\theta_\mu, \boldsymbol{\theta_{BO}})} \right\} \\ b_{\mu I} = Im\left\{ \dfrac{\boldsymbol{a}(\theta_\mu, \boldsymbol{\theta_{BO}})^{\boldsymbol{H}}\, \boldsymbol{R^{-1}}\, b\, \boldsymbol{a}(\theta_{ET}, \boldsymbol{\theta_{BO}})}{\boldsymbol{a}(\theta_\mu, \boldsymbol{\theta_{BO}})^{\boldsymbol{H}}\, \boldsymbol{R^{-1}}\, \boldsymbol{a}(\theta_\mu, \boldsymbol{\theta_{BO}})} \right\} \\ b_{vR} = Re\left\{ \dfrac{\boldsymbol{a}(\theta_\mu + v, \boldsymbol{\theta_{BO}})^{\boldsymbol{H}}\, \boldsymbol{R^{-1}}\, b\, \boldsymbol{a}(\theta_{ET}, \boldsymbol{\theta_{BO}})}{\boldsymbol{a}(\theta_\mu + v, \boldsymbol{\theta_{BO}})^{\boldsymbol{H}}\, \boldsymbol{R^{-1}}\, \boldsymbol{a}(\theta_\mu + v, \boldsymbol{\theta_{BO}})} \right\} \\ b_{vI} = Im\left\{ \dfrac{\boldsymbol{a}(\theta_\mu + v, \boldsymbol{\theta_{BO}})^{\boldsymbol{H}}\, \boldsymbol{R^{-1}}\, b\, \boldsymbol{a}(\theta_{ET}, \boldsymbol{\theta_{BO}})}{\boldsymbol{a}(\theta_\mu + v, \boldsymbol{\theta_{BO}})^{\boldsymbol{H}}\, \boldsymbol{R^{-1}}\, \boldsymbol{a}(\theta_\mu + v, \boldsymbol{\theta_{BO}})} \right\} \end{cases} \tag{62}$$

4.5.2 The Bayesian Cramer Rao lower bound for Rician distributed data

For Rician distributed data, the bias $\boldsymbol{B}(\widehat{\boldsymbol{\vartheta}}) = Ex\{\widehat{\boldsymbol{\vartheta}}\} - \boldsymbol{\vartheta}$ of the MMSE estimator is given by the following:

$$\boldsymbol{B}(\widehat{\boldsymbol{\vartheta}}) = \boldsymbol{\mu} - \boldsymbol{\vartheta} + \boldsymbol{\Gamma}\, \boldsymbol{H}^T(\boldsymbol{H}\, \boldsymbol{\Gamma}\, \boldsymbol{H}^T + \boldsymbol{C})^{-1}\left(\left(\boldsymbol{a} \odot \boldsymbol{a}\ \beta^2 + \frac{\sigma_d^2}{2}\right)^{\odot\frac{1}{2}} - \boldsymbol{m}_\zeta(\boldsymbol{\mu})\right) \tag{63}$$

The dependency of $\boldsymbol{a}(\theta_{ET}, \boldsymbol{\theta_{BO}})$ on θ_{ET} and $\boldsymbol{\theta_{BO}}$ was omitted from Equation (63) for ease of notation. The derivative of $\boldsymbol{B}(\widehat{\boldsymbol{\vartheta}})$ with respect to $\boldsymbol{\vartheta}$ is given by the following:

$$\frac{\partial \boldsymbol{B}(\hat{\boldsymbol{\vartheta}})}{\partial \boldsymbol{\vartheta}} =$$

$$-\boldsymbol{I} + \left[\boldsymbol{\Psi}\left(\beta^2 \boldsymbol{a} \odot \boldsymbol{a}_{\boldsymbol{\theta}} \odot \left(\boldsymbol{a} \odot \boldsymbol{a}\,\beta^2 + \frac{\sigma_d^2}{2}\right)^{\odot \frac{-1}{2}}\right) \quad \boldsymbol{\Psi}\left(\beta\, \boldsymbol{a} \odot \boldsymbol{a} \odot \left(\boldsymbol{a} \odot \boldsymbol{a}\,\beta^2 + \frac{\sigma_d^2}{2}\right)^{\odot \frac{-1}{2}}\right)\right] \quad (64)$$

where matrix $\boldsymbol{\Psi} = \boldsymbol{\Gamma}\,\boldsymbol{H}^T(\boldsymbol{H}\,\boldsymbol{\Gamma}\,\boldsymbol{H}^T + \boldsymbol{C})^{-1}$ and the dependency of $\boldsymbol{a}(\theta_{ET}, \boldsymbol{\theta_{BO}})$ and $\boldsymbol{a_{\theta}}(\theta_{ET}, \boldsymbol{\theta_{BO}})$ on θ_{ET} and $\boldsymbol{\theta_{BO}}$ were omitted from Equation (64) for ease of notation. The derivative of the prior Rician pdf natural logarithm is given by:

$$\begin{cases} \dfrac{\partial \ln p(\boldsymbol{\vartheta})}{\partial [\boldsymbol{\vartheta}]_1} = \dfrac{\theta_\mu - \theta_{ET}}{[\boldsymbol{\Gamma}]_{11}} \\ \dfrac{\partial \ln p(\boldsymbol{\vartheta})}{\partial [\boldsymbol{\vartheta}]_2} = \dfrac{\beta_\mu - \beta}{[\boldsymbol{\Gamma}]_{22}} \end{cases} \quad (65)$$

The matrices $\boldsymbol{H}$ and $\boldsymbol{\Gamma}$ are calculated using Equation (56). θ_μ and v are calculated using Equation (62), and β_μ and β_v are given by the following:

$$\begin{cases} \beta_\mu = \dfrac{\boldsymbol{a}(\theta_\mu, \boldsymbol{\theta_{BO}})^{\boldsymbol{T}} \left(\boldsymbol{a} \odot \boldsymbol{a}\,\boldsymbol{\beta^2} + \frac{\sigma_d^2}{2}\right)^{\odot \frac{1}{2}}}{\boldsymbol{a}(\theta_\mu, \boldsymbol{\theta_{BO}})^{\boldsymbol{T}}\, \boldsymbol{a}(\theta_\mu, \boldsymbol{\theta_{BO}})} \\ \beta_v = \dfrac{\boldsymbol{a}(\theta_\mu + v, \boldsymbol{\theta_{BO}})^{\boldsymbol{T}} \left(\boldsymbol{a} \odot \boldsymbol{a}\,\boldsymbol{\beta^2} + \frac{\sigma_d^2}{2}\right)^{\odot \frac{1}{2}}}{\boldsymbol{a}(\theta_\mu + v, \boldsymbol{\theta_{BO}})^{\boldsymbol{T}}\, \boldsymbol{a}(\theta_\mu + v, \boldsymbol{\theta_{BO}})} \end{cases} \quad (66)$$

The dependency of $\boldsymbol{a}(\theta_{ET}, \boldsymbol{\theta_{BO}})$ on θ_{ET} and $\boldsymbol{\theta_{BO}}$ was omitted from Equation (66) for ease of notation.

4.6 The recursive minimum mean square error estimator

If we assume that several data vectors that belong to the same emitter have been collected by the spinning antenna based ELINT system shown in Figure 2, where a single data vector corresponds to a single snapshot, then it would be beneficial to have a DOA estimator for merging the information contained in each snapshot in order to improve the DOA estimation accuracy.

To the best of our knowledge of the literature, DOA estimators that exploit several snapshots do not provide adequate estimation accuracy, and they are designed with a common dictionary of steering vectors for all the snapshots. In other words, these estimators assume that the snapshots have an equal emitter steering vector.

In ELINT applications, it is likely that the snapshots will differ with regard to the emitter steering vector due to the agility of the received signal, errors in estimating the signal's parameters and missing data samples. Missing data samples occur for a variety of reasons, such as errors in the detection process and the density of the operating RF

environment [17], [31]. Thus, having the ability to process several snapshots that differ with regard to the emitter steering vector can be valuable.

In this section, we therefore present a recursive version of the MMSE DOA estimator to further improve the accuracy of estimating the DOA of emitters' signals received by a spinning antenna based ELINT system. The proposed recursive MMSE DOA estimator is based on the sequential form of the MMSE estimator [14], and is designed by taking into consideration the signal processing chain of modern ELINT systems. Thus, the recursive MMSE DOA estimator is supposed to receive deinterleaved data that belong to the same emitter, before then outputting the DOA estimate. It is also assumed that the host ELINT system is capable of identifying the snapshots that belong to the same emitter.

The recursive MMSE DOA estimator improves the DOA estimation accuracy by merging the information contained in several snapshots, and it is capable of processing snapshots that differ in terms of the emitter steering vector and SDR. The recursive MMSE DOA estimator is efficient in terms of computations and memory storage because it reuses the estimate from the previous snapshot rather than accumulating the consecutive snapshots. Also, the recursive MMSE DOA estimator exploits the DOA estimate and the error covariance from the previous snapshot to compute the pdf parameters of the subsequent snapshot.

4.6.1 Flowchart of the recursive estimator

The recursive MMSE DOA estimator extends the MMSE DOA estimators presented in the previous sections to the case where the DOA estimate is updated in time as a new snapshot arrives. In doing so, it computes the prior pdf parameters for the corresponding snapshot based on the estimate for the previous snapshot and so is based on the sequential form of the MMSE estimator [14]. The derivation of the sequential MMSE estimator is discussed in [14].

Figure 7 is a flowchart of the proposed recursive MMSE DOA estimator, where the subscript f illustrates the recursive execution of the estimator and it starts from 1. The estimator receives a new data vector (snapshot), and outputs the DOA estimate $\hat{\theta}_{ET}$.

The initial values of the prior pdf parameters $\theta_{\mu 0}$ and v_0 for the new data vector are computed in the first and the second steps, using the equations shown in the flowchart.

In the third step, the prior pdf parameters θ_μ and v for the new data vector are computed using the results obtained from the previous snapshot and the initial values $\theta_{\mu 0}$ and v_0. In the third step, the median is applied to situate θ_μ in the interval: $\theta_{\mu 0} - v_0 \leq \theta_\mu \leq \theta_{\mu 0} + v_0$

In the fourth step, matrices $\boldsymbol{\Gamma}$ and $\boldsymbol{H}$, and the complex amplitude b or magnitude β are computed.

In the fifth step, the vector of unknown parameters $\boldsymbol{\vartheta}$ and the error covariance $\boldsymbol{P}$ are computed. The error covariance is a measure of the accuracy of the estimate and hence it is

used in conjunction with the DOA estimate to compute the pdf parameters of the subsequent snapshot.

For complex Gaussian distributed data, the error covariance is given by the following [14]:

$$\boldsymbol{P} = \boldsymbol{\Gamma} - \boldsymbol{\Gamma}\,\boldsymbol{H}^{H}(\boldsymbol{H}\,\boldsymbol{\Gamma}\,\boldsymbol{H}^{H} + \boldsymbol{R})^{-1}\;\boldsymbol{H}\,\boldsymbol{\Gamma} \tag{67}$$

For Rician distributed data, the error covariance is given by the following [14]:

$$\boldsymbol{P} = \boldsymbol{\Gamma} - \boldsymbol{\Gamma}\,\boldsymbol{H}^{T}(\boldsymbol{H}\,\boldsymbol{\Gamma}\,\boldsymbol{H}^{T} + \boldsymbol{C})^{-1}\;\boldsymbol{H}\,\boldsymbol{\Gamma} \tag{68}$$

We note here that, if the parameters are evolving in time, then a prediction step that is similar to what is implemented in tracking applications should be included. The purpose of this step is to propagate the state of the parameters from one time instance to the next time instance, according to a model that describes the intercept dynamics [14]. In other words, the prediction step predicts how the parameters will vary from one time instance to the next time instance.

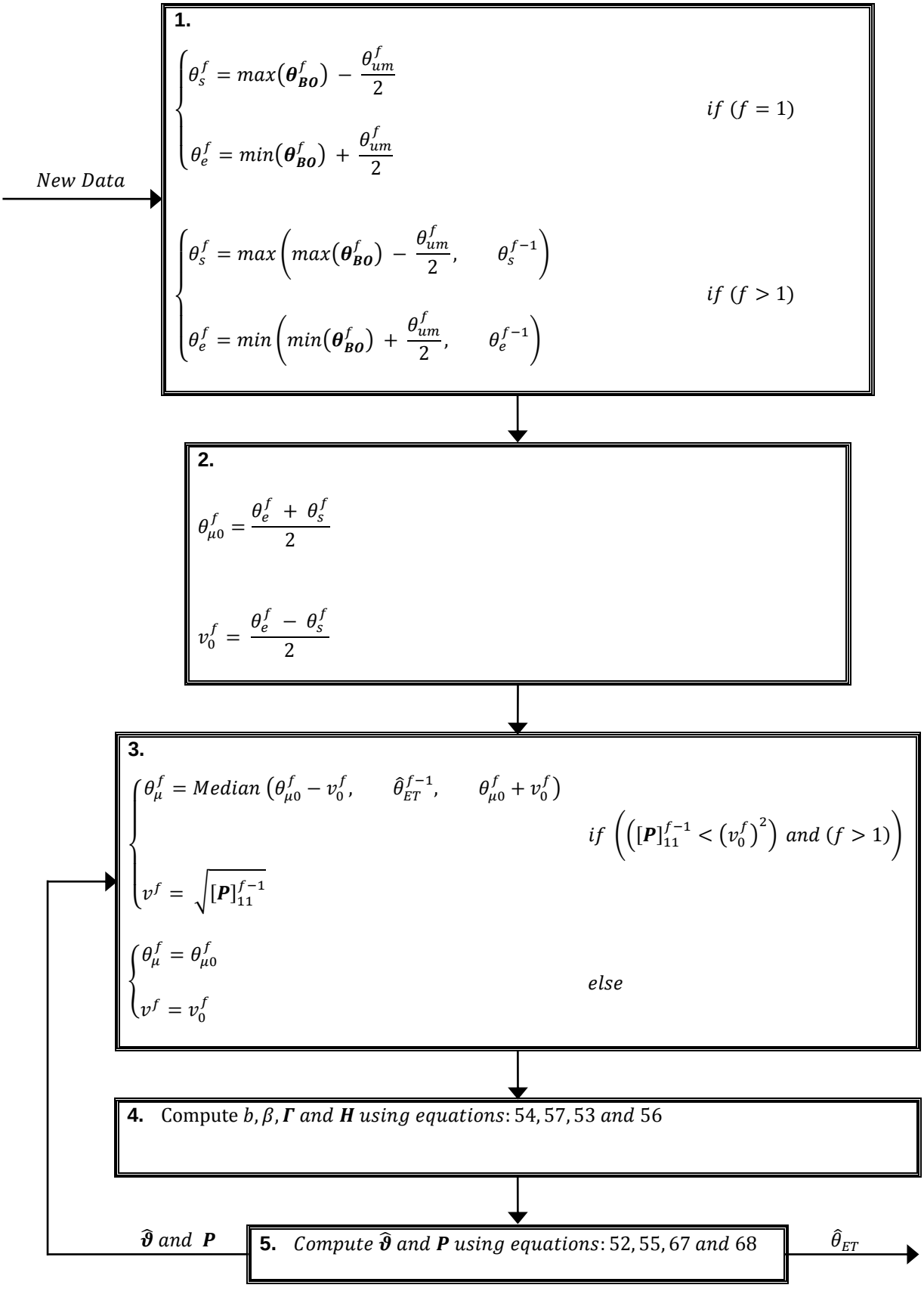

Figure 7. Flowchart of the proposed recursive MMSE DOA estimator

4.7 Performance analysis

In this section, we evaluate the DOA estimation accuracy of the DOA estimators using Monte Carlo simulation and real radar data provided by Reutech Radar Systems [50]. We compare the constructed biased DOA estimators to the CRLB, the BB and the BCRLB. We use the MSE, which is the direct measure of estimation error [12] as a performance criterion. The MSE is given by the following:

$$MSE = Ex\left\{\left(\hat{\theta}_{ET} - \theta_{ET}\right)^2\right\} \tag{69}$$

4.7.1 Monte Carlo simulation

In the Monte Carlo simulations, the beam pattern of the spinning antenna is Gaussian, and the disturbance consists of complex white Gaussian noise with zero mean. The disturbance covariance matrix is assumed to be *a priori* known. In practice, however, the disturbance covariance matrix is typically estimated from the data (preferably, signal free data). The complex amplitude is fixed and the SDR is scaled to calculate the disturbance power $\sigma_d^2 = \frac{b^2}{SDR}$.

4.7.1.1 The nonrecursive estimators

The parameters of the simulation scenarios are illustrated in Table 4. The first and the second simulation scenarios are a full spread of the data across the spinning antenna mainlobe scenarios, while the third and the fourth simulation scenarios are a partial spread of the data across the spinning antenna mainlobe scenarios.

Table 4. Simulation scenarios that are used to evaluate the nonrecursive DOA estimators. Parameters listed are: spinning antenna beamwidth θ_B, unambiguous width θ_{um}, emitter DOA θ_{ET}, number of data samples N, the product of the pulse repetition interval and angular velocity $PRI\ \omega_R$, and antenna boresight directions vector $\boldsymbol{\theta_{BO}}$.

Scenario	$\theta_B = \theta_{um}$	θ_{ET}	N	$PRI\ \omega_R$	$[\boldsymbol{\theta_{BO}}]_1$	$[\boldsymbol{\theta_{BO}}]_N$
1	30^o	15^o	32	0.9375^o	0^o	29.0625^o
2	25^o	12.5^o	32	0.7813^o	0^o	24.2188^o
3	25^o	12.5^o	16	1^o	0^o	15^o
4	25^o	12.5^o	8	2.5714^o	0^o	18^o

In Figure 8, the MSE of the two-dimensional ML DOA estimator in Equation (17) is compared to the MSE of the approximated ML DOA estimator in Equation (21), using the first simulation scenario. It is evident from Figure 8 that the loss in estimation accuracy due to the approximation is negligible.

In Figure 9 and Figure 10, the MSE, bias and variance of the nonrecursive DOA estimators are illustrated for the second simulation scenario, which is a full spread of the data across the

spinning antenna mainlobe scenario. In this scenario, the affine transformed ML estimator and the MMSE estimator provide a significant improvement in terms of MSE. Also, it is shown in Figure 10 that the bias dominates the MSE and the variance converges to zero.

In Figure 11 to Figure 14, the MSE, bias and variance of the DOA estimators are illustrated for the third and the fourth simulation scenarios, which are a partial spread of the data across the spinning antenna mainlobe scenarios. The improvement in terms of the MSE provided by the affine transformed ML estimator and the MMSE estimator is good, but not as significant as in the second simulation scenario. Figure 12 and Figure 14 show that the bias increases and the variance decreases, as the SDR decreases.

We note here that Equation (59) and Equation (63) were used to compute the theoretical bias in Figure 10, Figure 12 and Figure 14.

The simulation results illustrate that the biased DOA estimators did not experience the threshold effect even for a small number of data samples and/or small SDR. These results are in agreement with the fact that the BB did not deviate from the CRLB. Also, the simulation results illustrate that the biased DOA estimators outperform the CRLB and the BB, and that the MSE of the MMSE estimator is close to the BCRLB. The MMSE estimator and the affine transformed ML estimator are shown to have the best MSE for a small SDR and/or a small number of data samples.

We note here that the biased DOA estimators can resolve closely spaced emitters, if the emitters' frequencies differ.

When compared to the other estimators, the MMSE estimator does not require the computation over a predefined grid, thus the MMSE estimator has less computational complexity and is easier to implement.

Our empirical experience is that the optimal values of the transformation parameters m and u obtained by Equation (35), Equation (45) and Equation (46) always conform to the optimal values of m and u for $\theta = min(\boldsymbol{\theta_{BO}}) + \theta_{um}/2$, provided that the antenna mainlobe is symmetrical around its peak. This means that the transformation parameters for the linearly transformed ML estimator can be calculated directly using Equation (38):

$$m = -\frac{CRLB\left(min(\boldsymbol{\theta_{BO}}) + \frac{\theta_{um}}{2}\right)}{CRLB\left(min(\boldsymbol{\theta_{BO}}) + \frac{\theta_{um}}{2}\right) + \left(min(\boldsymbol{\theta_{BO}}) + \frac{\theta_{um}}{2}\right)^2} \tag{70}$$

It also means that the transformation parameters for the affine transformed ML estimator can be calculated directly using Equation (49) and Equation (50):

$$m = -\frac{CRLB\left(min(\boldsymbol{\theta_{BO}}) + \frac{\theta_{um}}{2}\right)}{CRLB\left(min(\boldsymbol{\theta_{BO}}) + \frac{\theta_{um}}{2}\right) + b_1^T b_1 - c_1} \tag{71}$$

$$u = -\frac{CRLB\left(min(\boldsymbol{\theta_{BO}}) + \frac{\theta_{um}}{2}\right)}{CRLB\left(min(\boldsymbol{\theta_{BO}}) + \frac{\theta_{um}}{2}\right) + b_1^T b_1 - c_1} b_1 \tag{72}$$

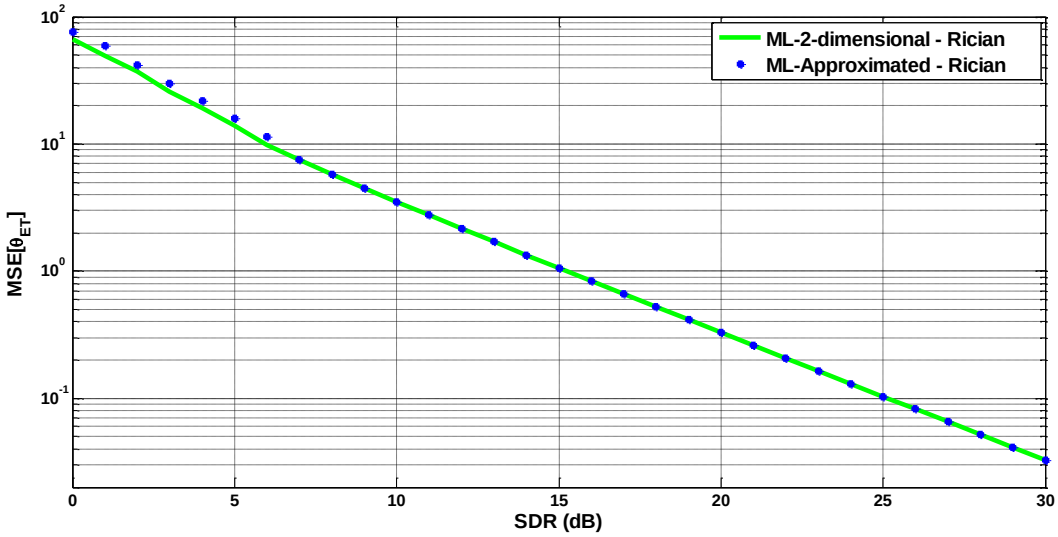

Figure 8. $MSE\{\widehat{\theta}_{ET}\}$ **of the two-dimensional ML estimator versus the approximated ML estimator for the first simulation scenario.** $\theta_B = \theta_{um} = 30^o$, $\theta_{ET} = 15^o$, $N = 32$, $PRI\ \omega_R = 0.9375^o$, $[\theta_{BO}]_1 = 0^o$, $[\theta_{BO}]_N = 29.0625^o$

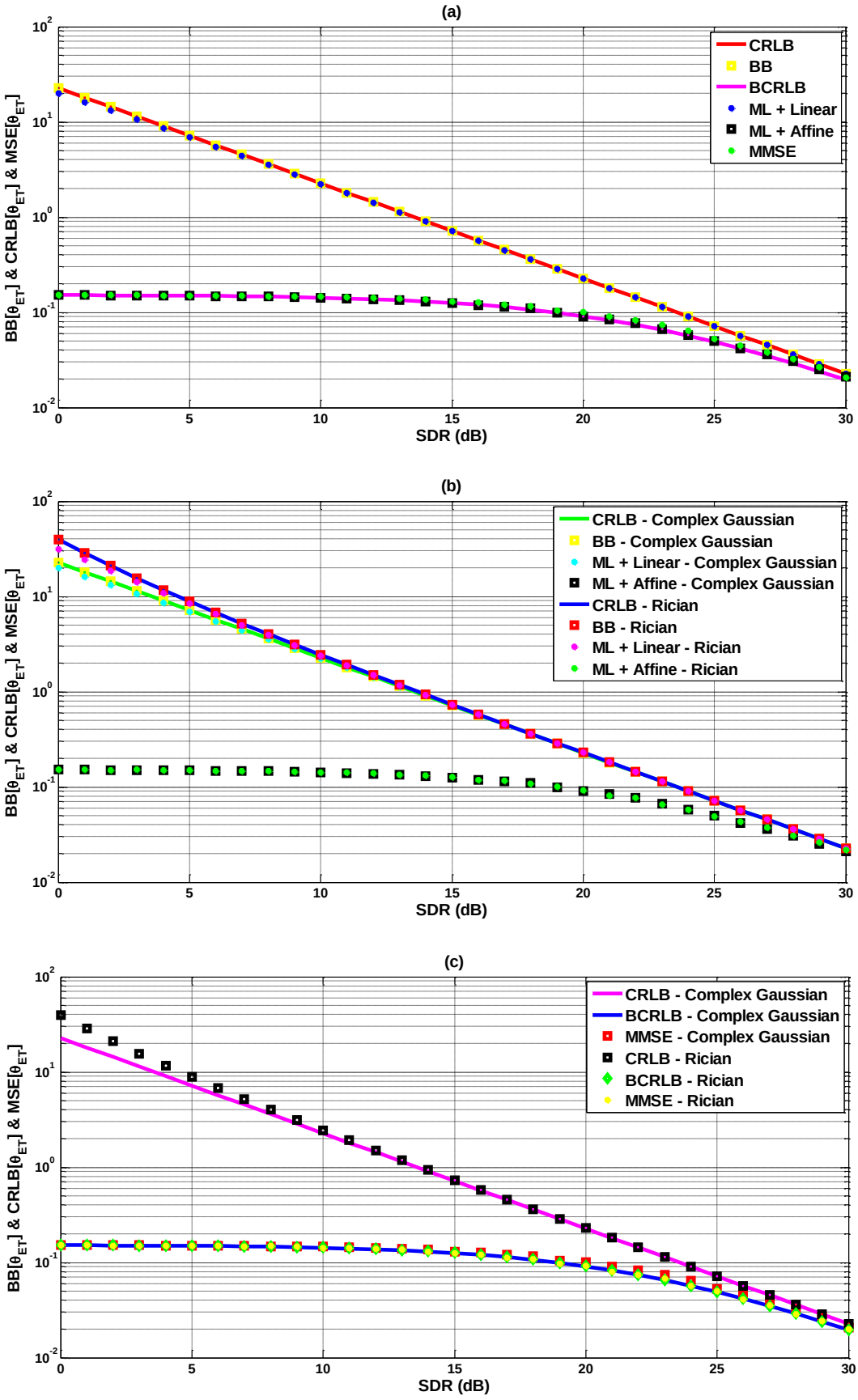

Figure 9. $MSE\{\widehat{\theta}_{ET}\}$ **of the nonrecursive DOA estimators versus the MSE bounds for the second simulation scenario. (a) Transformed ML estimators and MMSE estimator versus the MSE bounds for complex Gaussian distributed data. (b) Transformed ML estimators versus the MSE bounds. (c) MMSE estimators versus the MSE bounds.** $\theta_B = \theta_{um} = 25^o$, $\theta_{ET} = 12.5^o$, $N = 32$, $PRI\ \omega_R = 0.7813^o$, $[\theta_{BO}]_1 = 0^o$, $[\theta_{BO}]_N = 24.2188^o$

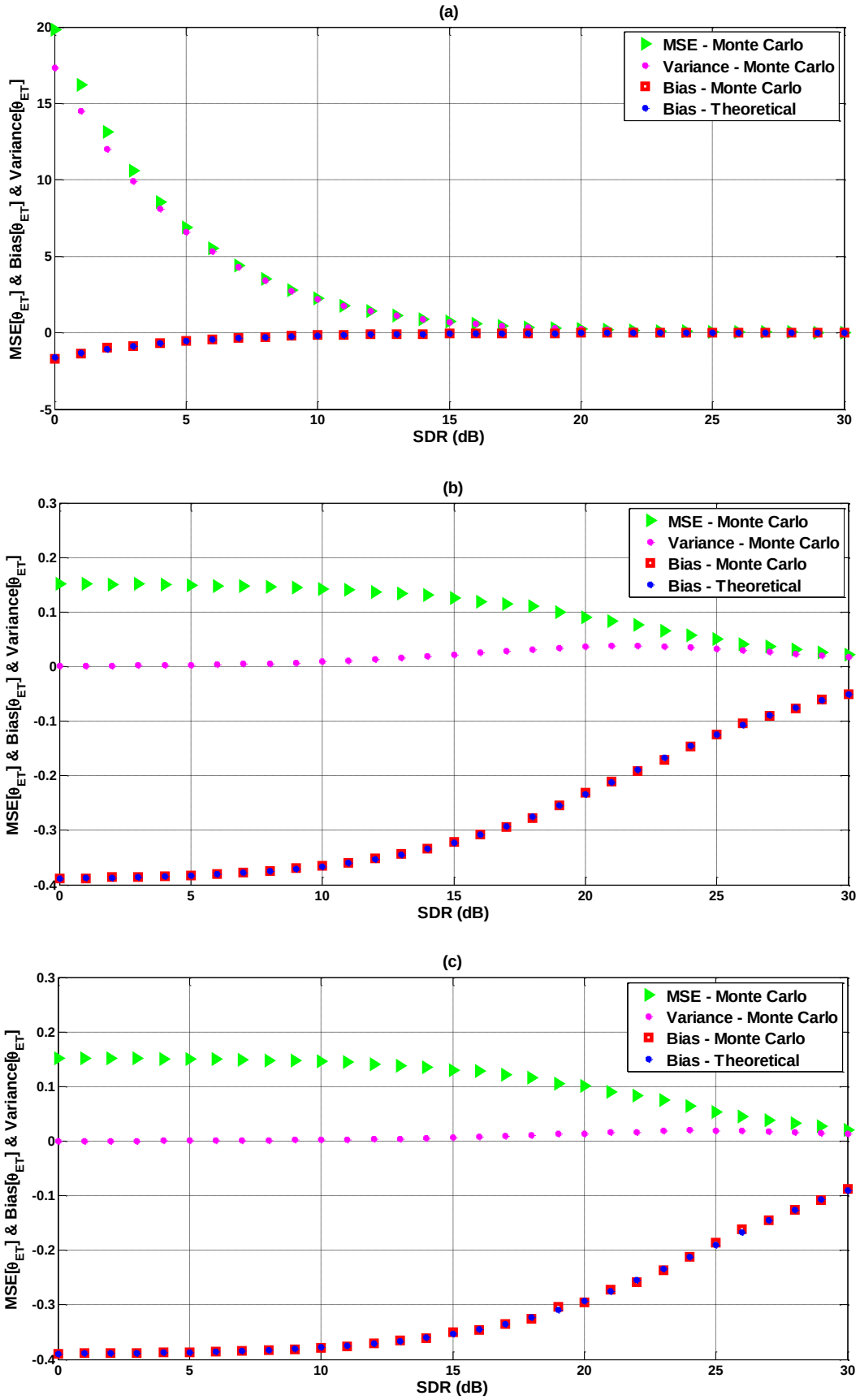

Figure 10. $MSE\{\hat{\theta}_{ET}\}$, $Bias\{\hat{\theta}_{ET}\}$ **and** $Variance\{\hat{\theta}_{ET}\}$ **of the nonrecursive DOA estimators for the second simulation scenario. (a) Linearly transformed ML estimator. (b) Affine transformed ML estimator. (c) MMSE estimator.** $\theta_B = \theta_{um} = 25^o$, $\theta_{ET} = 12.5^o$, $N = 32$, $PRI\ \omega_R = 0.7813^o$, $[\theta_{BO}]_1 = 0^o$, $[\theta_{BO}]_N = 24.2188^o$

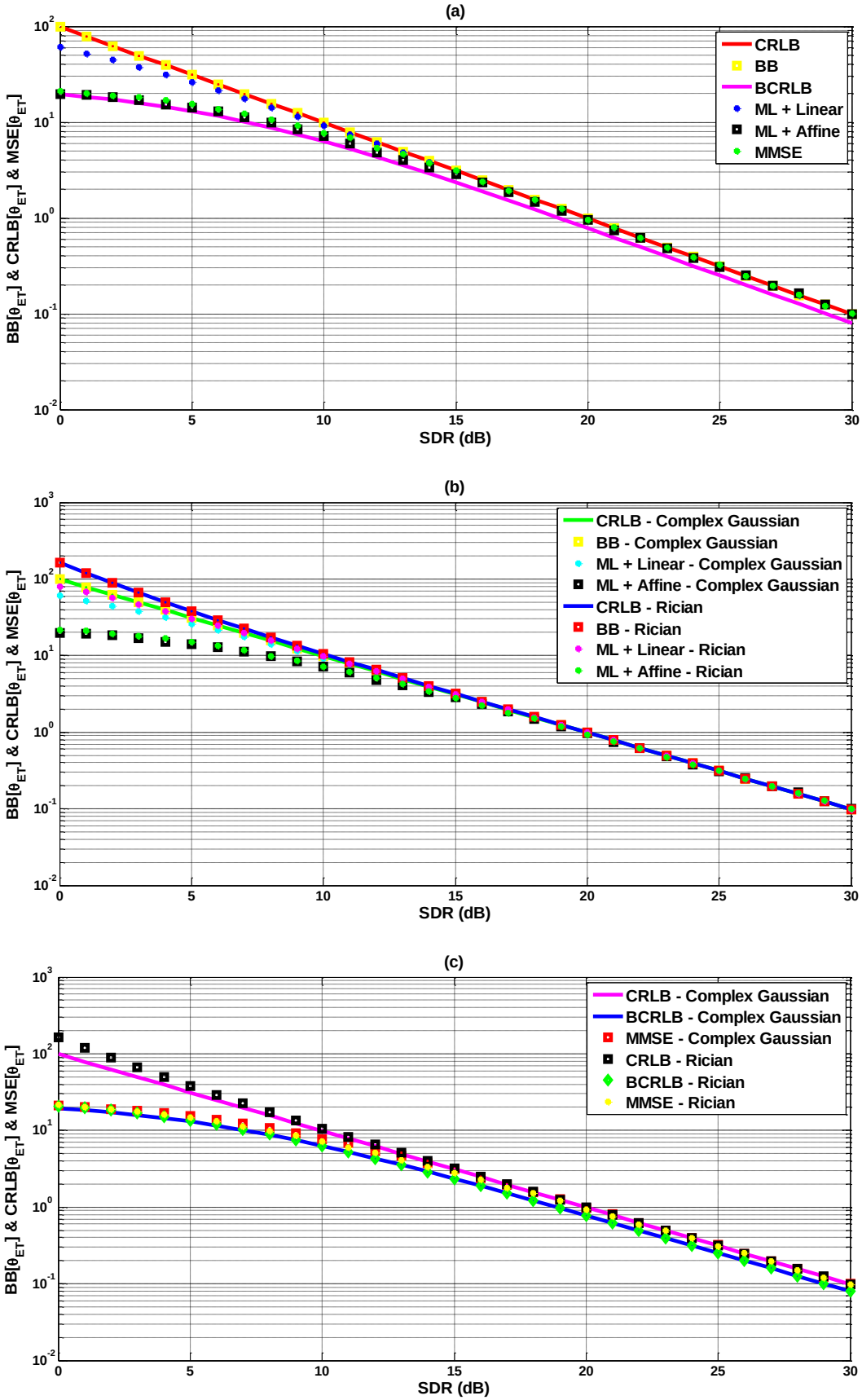

Figure 11. $MSE\{\widehat{\theta}_{ET}\}$ **of the nonrecursive DOA estimators versus the MSE bounds for the third simulation scenario. (a) Transformed ML estimators and MMSE estimator versus the MSE bounds for complex Gaussian distributed data. (b) Transformed ML estimators versus the MSE bounds. (c) MMSE estimators versus the MSE bounds.** $\theta_B = \theta_{um} = 25^o$, $\theta_{ET} = 12.5^o$, $N = 16$, $PRI\ \omega_R = 1^o$, $[\theta_{BO}]_1 = 0^o$, $[\theta_{BO}]_N = 15^o$

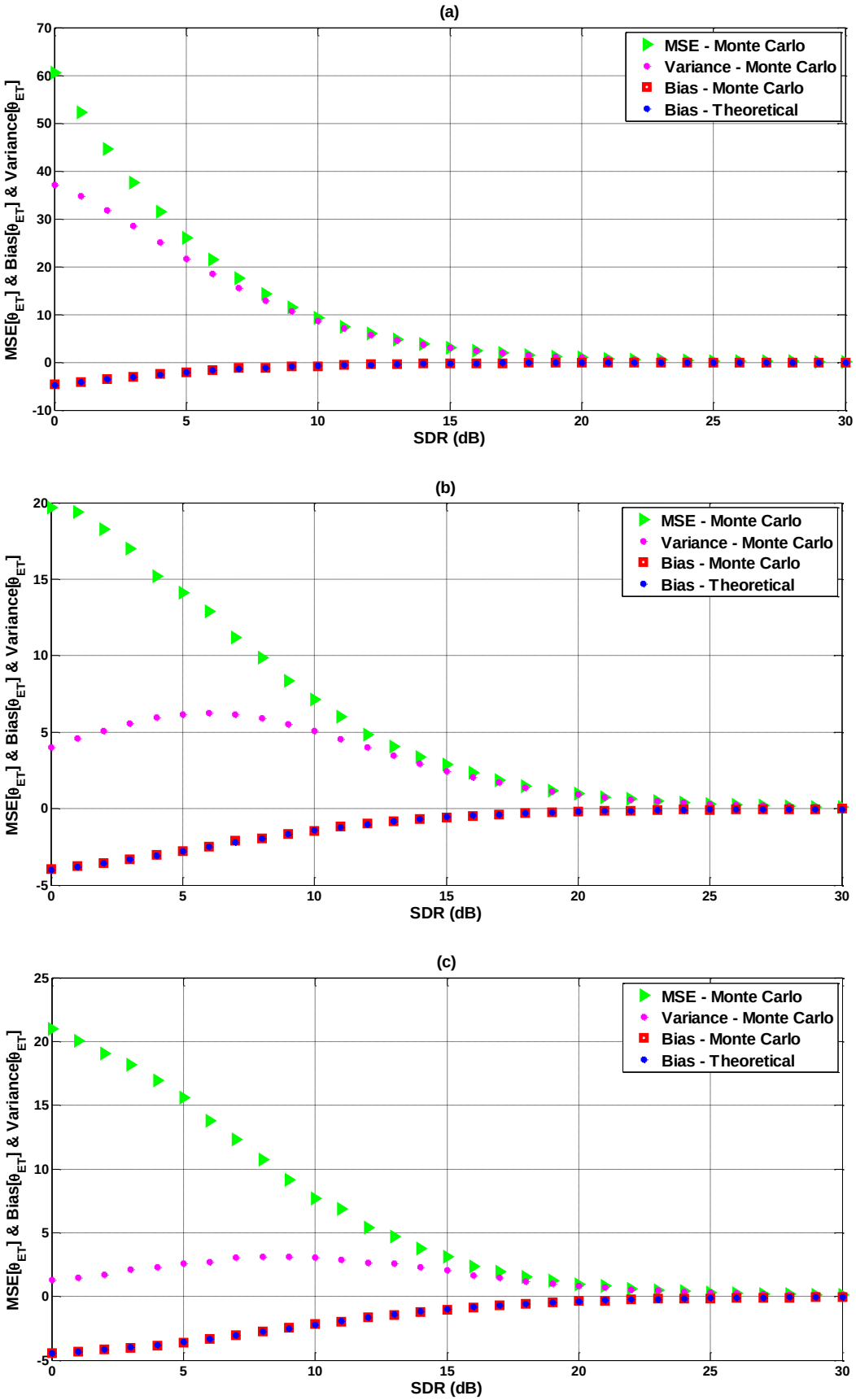

Figure 12. $MSE\{\hat{\theta}_{ET}\}$, $Bias\{\hat{\theta}_{ET}\}$ and $Variance\{\hat{\theta}_{ET}\}$ **of the nonrecursive DOA estimators for the third simulation scenario. (a) Linearly transformed ML estimator. (b) Affine transformed ML estimator. (c) MMSE estimator.** $\theta_B = \theta_{um} = 25^o$, $\theta_{ET} = 12.5^o$, $N = 16$, $PRI\ \omega_R = 1^o$, $[\theta_{BO}]_1 = 0^o$, $[\theta_{BO}]_N = 15^o$

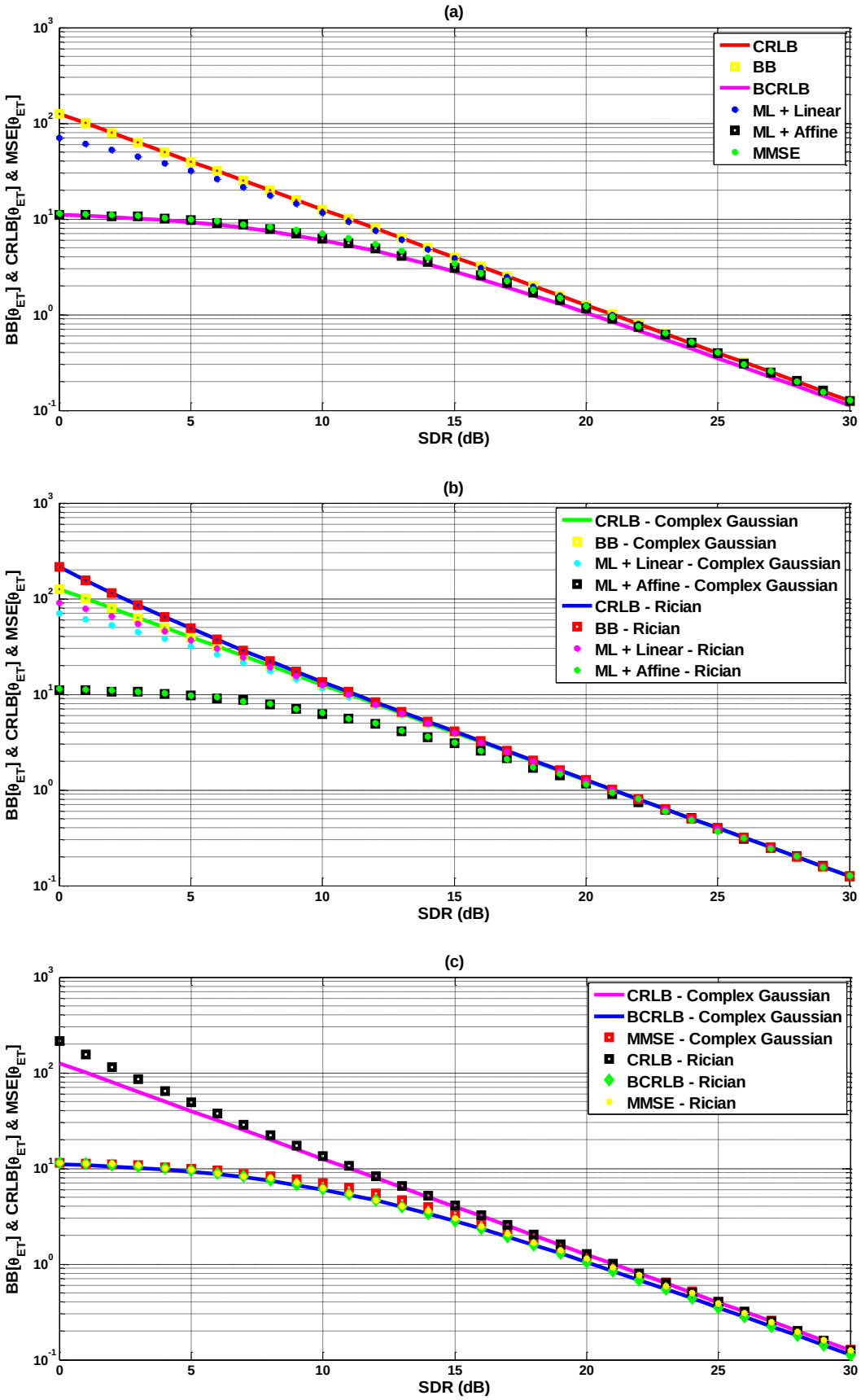

Figure 13. $MSE\{\widehat{\theta}_{ET}\}$ **of the nonrecursive DOA estimators versus the MSE bounds for the fourth simulation scenario. (a) Transformed ML estimators and MMSE estimator versus the MSE bounds for complex Gaussian distributed data. (b) Transformed ML estimators versus the MSE bounds. (c) MMSE estimators versus the MSE bounds.** $\theta_B = \theta_{um} = 25^o$, $\theta_{ET} = 12.5^o$, $N = 8$, $PRI\ \omega_R = 2.5714^o$, $[\theta_{BO}]_1 = 0^o$, $[\theta_{BO}]_N = 18^o$

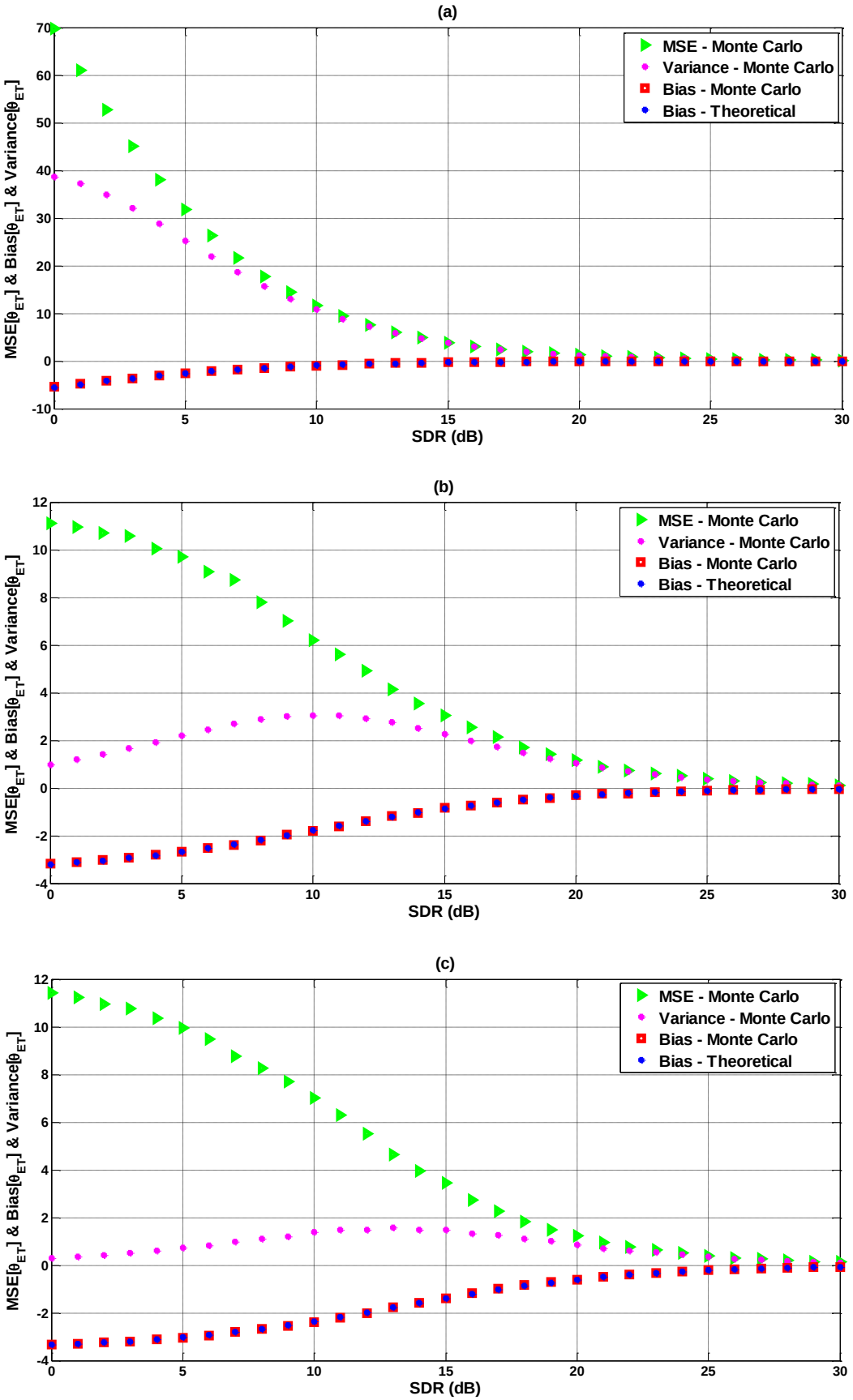

Figure 14. $MSE\{\widehat{\theta}_{ET}\}$, $Bias\{\widehat{\theta}_{ET}\}$ and $Variance\{\widehat{\theta}_{ET}\}$ **of the nonrecursive DOA estimators for the fourth simulation scenario. (a) Linearly transformed ML estimator. (b) Affine transformed ML estimator. (c) MMSE estimator.** $\theta_B = \theta_{um} = 25^o$, $\theta_{ET} = 12.5^o$, $N = 8$, $PRI\ \omega_R = 2.5714^o$, $[\theta_{BO}]_1 = 0^o$, $[\theta_{BO}]_N = 18^o$

4.7.1.2 The recursive estimators

The parameters of the evaluated scenarios are illustrated in Table 5 to Table 9.

The DOA estimation accuracy (as measured by the MSE) for the first simulation scenario is illustrated in Figure 15. The snapshots have equal parameters, and thus have equal MSEs. As shown in Figure 15, the recursive MMSE DOA estimator improved the DOA estimation accuracy by merging the information contained in the three snapshots.

Table 5. The first simulation scenario that is used to evaluate the recursive DOA estimators. Parameters listed are: spinning antenna beamwidth θ_B, unambiguous width θ_{um}, emitter DOA θ_{ET}, number of data samples N, the product of the pulse repetition interval and angular velocity ($PRI\ \omega_R$), antenna boresight directions vector θ_{BO}, reference SDR SDR_R and snapshot SDR SDR_S.

Snapshot	$\theta_B = \theta_{um}$	θ_{ET}	N	$PRI\ \omega_R$	$[\boldsymbol{\theta_{BO}}]_1$	$[\boldsymbol{\theta_{BO}}]_N$	$SDR_R - SDR_S$ (dB)
1	30^o	15^o	32	0.6774^o	0^o	21^o	0
2	30^o	15^o	32	0.6774^o	0^o	21^o	0
3	30^o	15^o	32	0.6774^o	0^o	21^o	0

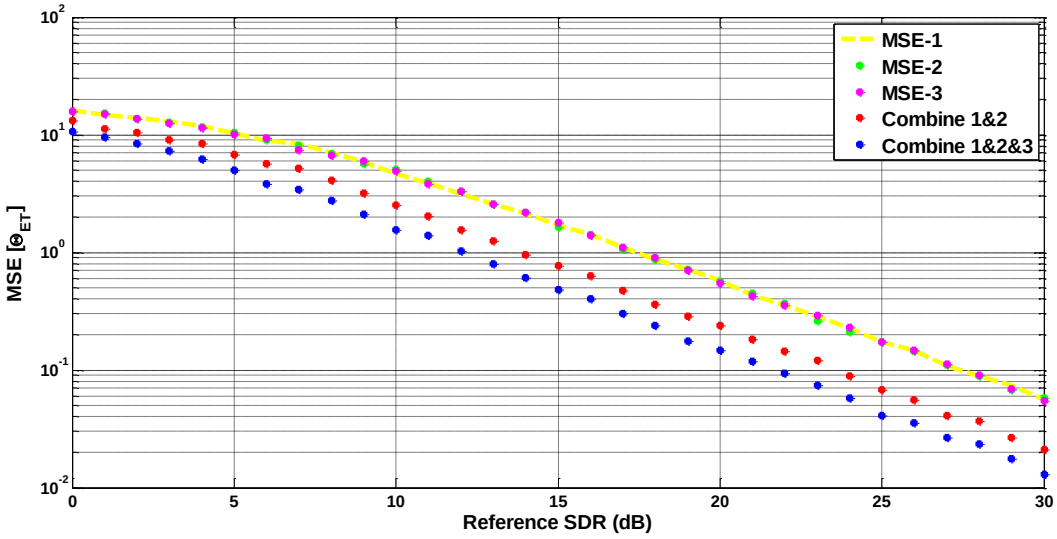

Figure 15. $MSE\{\hat{\theta}_{ET}\}$ of the single snapshots and the combined snapshots for the first simulation scenario (recursive estimators).

The DOA estimation accuracy for the second simulation scenario is illustrated in Figure 16. The snapshots have equal parameters except that the SDR of the third snapshot is 10 dB less than the SDR of the other snapshots. The MSEs of the first and the second snapshots are better than the MSE of the third snapshot due to the SDR. As shown in Figure 16, the recursive MMSE DOA estimator improved the DOA estimation accuracy by merging the information contained in the three snapshots.

Table 6. The second simulation scenario that is used to evaluate the recursive DOA estimators. Parameters listed are: spinning antenna beamwidth θ_B, unambiguous width θ_{um}, emitter DOA θ_{ET}, number of data samples N, the product of the pulse repetition interval and angular velocity ($PRI\ \omega_R$), antenna boresight directions vector θ_{BO}, reference SDR SDR_R and snapshot SDR SDR_S.

Snapshot	$\theta_B = \theta_{um}$	θ_{ET}	N	$PRI\ \omega_R$	$[\boldsymbol{\theta_{BO}}]_1$	$[\boldsymbol{\theta_{BO}}]_N$	$SDR_R - SDR_S$ (dB)
1	30^o	15^o	32	0.6774^o	0^o	21^o	0
2	30^o	15^o	32	0.6774^o	0^o	21^o	0
3	30^o	15^o	32	0.6774^o	0^o	21^o	10

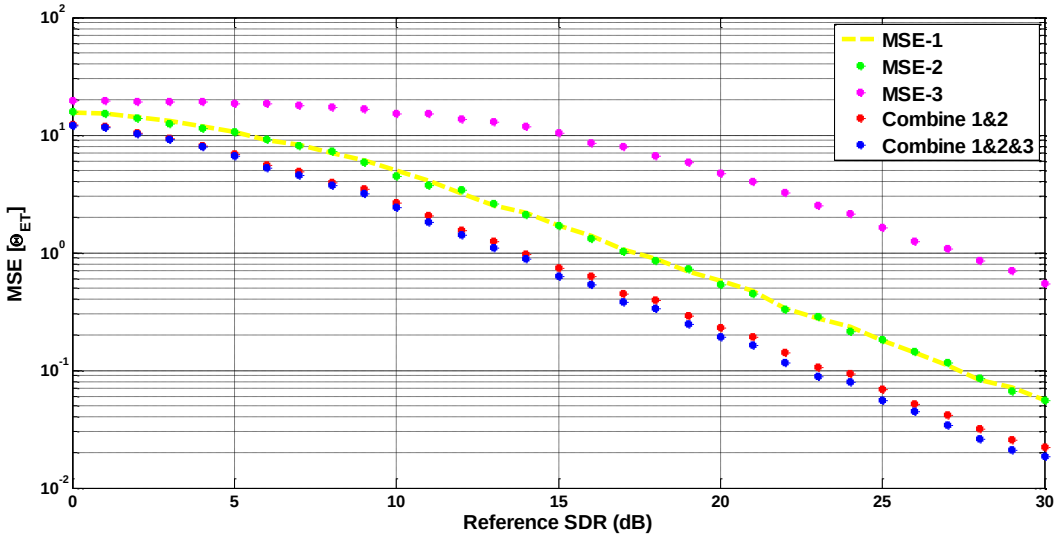

Figure 16. $MSE\{\hat{\theta}_{ET}\}$ of the single snapshots and the combined snapshots for the second simulation scenario (recursive estimators).

The DOA estimation accuracy for the third simulation scenario is illustrated in Figure 17. The three snapshots differ with regard to the emitter steering vector (in terms of boresight directions). The MSEs of the snapshots are almost equal. As shown in Figure 17, the recursive MMSE DOA estimator improved the DOA estimation accuracy by merging the information contained in the three snapshots.

Table 7. The third simulation scenario that is used to evaluate the recursive DOA estimators. Parameters listed are: spinning antenna beamwidth θ_B, unambiguous width θ_{um}, emitter DOA θ_{ET}, number of data samples N, the product of the pulse repetition interval and angular velocity ($PRI\ \omega_R$), antenna boresight directions vector θ_{BO}, reference SDR SDR_R and snapshot SDR SDR_S.

Snapshot	$\theta_B = \theta_{um}$	θ_{ET}	N	$PRI\ \omega_R$	$[\boldsymbol{\theta_{BO}}]_1$	$[\boldsymbol{\theta_{BO}}]_N$	$SDR_R - SDR_S$ (dB)
1	30^o	15^o	16	1.0667^o	0^o	16^o	0
2	30^o	15^o	32	0.3871^o	2^o	14^o	0
3	30^o	15^o	8	3^o	0^o	21^o	0

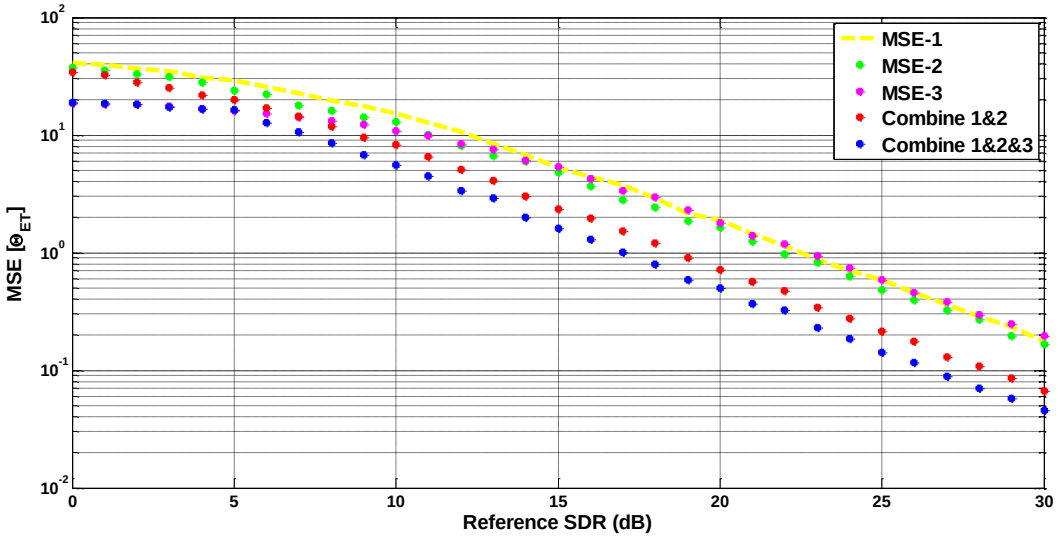

Figure 17. $MSE\{\hat{\theta}_{ET}\}$ of the single snapshots and the combined snapshots for the third simulation scenario (recursive estimators).

The DOA estimation accuracy for the fourth simulation scenario is illustrated in Figure 18. The three snapshots differ with regard to the emitter steering vector (in terms of boresight directions) and SDR. The MSE of the first snapshot is better than the MSE of the second snapshot due to the SDR and wider spread. The MSE of the third snapshot is better than the combined first and second snapshots due to the SDR and wider spread. As shown in Figure 18, the recursive MMSE DOA estimator improved the DOA estimation accuracy by merging the information contained in the three snapshots.

Table 8. The fourth simulation scenario that is used to evaluate the recursive DOA estimators. Parameters listed are: spinning antenna beamwidth θ_B, unambiguous width θ_{um}, emitter DOA θ_{ET}, number of data samples N, the product of the pulse repetition interval and angular velocity ($PRI\ \omega_R$), antenna boresight directions vector θ_{BO}, reference SDR SDR_R and snapshot SDR SDR_S.

Snapshot	$\theta_B = \theta_{um}$	θ_{ET}	N	$PRI\ \omega_R$	$[\boldsymbol{\theta_{BO}}]_1$	$[\boldsymbol{\theta_{BO}}]_N$	$SDR_R - SDR_S$ (dB)
1	30^o	15^o	16	1.0667^o	0^o	16^o	7
2	30^o	15^o	32	0.3871^o	2^o	14^o	10
3	30^o	15^o	8	3^o	0^o	21^o	0

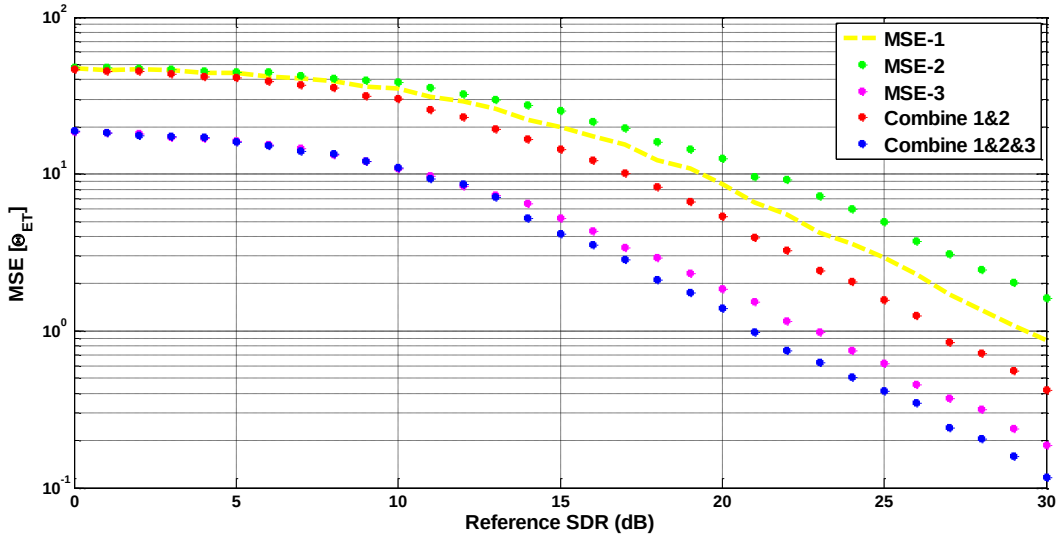

Figure 18. $MSE\{\widehat{\theta}_{ET}\}$ of the single snapshots and the combined snapshots for the fourth simulation scenario (recursive estimators).

In the fifth simulation scenario, a random parameter generator that has a uniform distribution was used to create a partial spread of the data across the spinning antenna mainlobe scenario. The scenario consists of ten snapshots and the generated parameters are illustrated in Table 9. The DOA estimation accuracy of this scenario is illustrated in Figure 19, which shows that the recursive MMSE DOA estimator improved the DOA estimation accuracy by merging the information contained in the ten snapshots.

Table 9. The fifth simulation scenario that is used to evaluate the recursive DOA estimators. Parameters listed are: spinning antenna beamwidth θ_B, unambiguous width θ_{um}, emitter DOA θ_{ET}, number of data samples N, the product of the pulse repetition interval and angular velocity ($PRI\ \omega_R$), antenna boresight directions vector θ_{BO}, reference SDR SDR_R and snapshot SDR SDR_S.

Snapshot	$\theta_B = \theta_{um}$	θ_{ET}	N	$PRI\ \omega_R$	$[\boldsymbol{\theta_{BO}}]_1$	$[\boldsymbol{\theta_{BO}}]_N$	$SDR_R - SDR_S$ (dB)
1	30^o	15^o	24	0.2812^o	0.2767^o	6.7444^o	1.3194
2	30^o	15^o	9	1.0271^o	0.9250^o	9.1415^o	1.5699
3	30^o	15^o	22	0.3739^o	1.9554^o	9.8069^o	4.8676
4	30^o	15^o	18	0.4970^o	3.2656^o	11.7150^o	4.5230
5	30^o	15^o	8	0.8896^o	3.6326^o	9.8595^o	1.9261
6	30^o	15^o	4	2.0939^o	1.9587^o	8.2403^o	4.6094
7	30^o	15^o	22	0.2964^o	0.9947^o	7.2197^o	0.0636
8	30^o	15^o	16	0.7040^o	0.3590^o	10.9194^o	6.2181
9	30^o	15^o	21	0.3030^o	0.3385^o	6.3990^o	6.4866
10	30^o	15^o	24	0.3584^o	0.0403^o	8.2830^o	8.9670

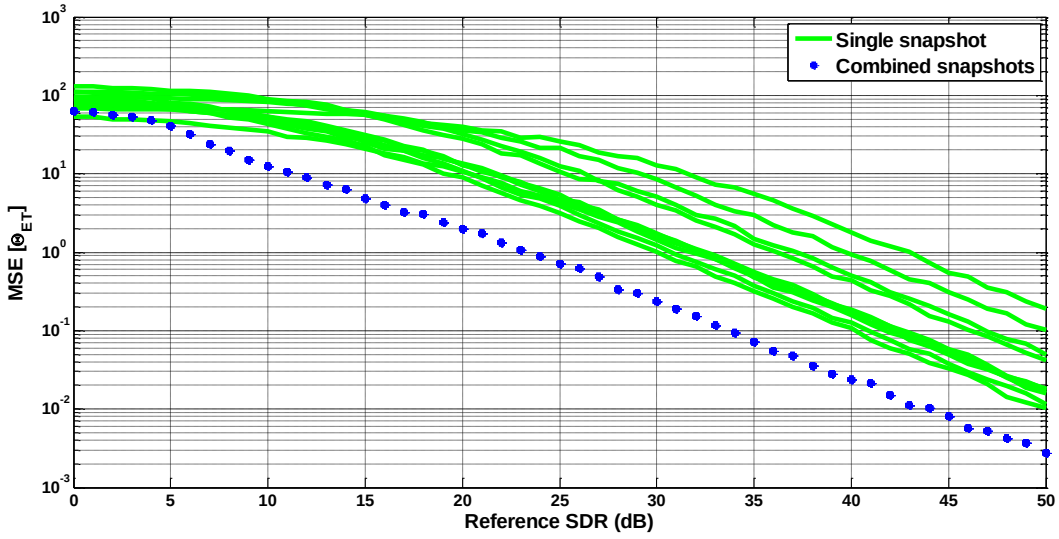

Figure 19. $MSE\{\widehat{\theta}_{ET}\}$ of the single snapshots and the combined snapshots for the fifth simulation scenario (recursive estimators).

We note here that we obtained similar results using the Rician version of the recursive MMSE DOA estimator. We did not include these results for brevity.

4.7.2 Real radar data

The DOA estimation accuracy of the constructed DOA estimators was evaluated using real radar data provided by Reutech Radar Systems [50].

The data was recorded by a mechanically scanning L-band radar that uses three carrier frequencies for transmissions, and sequentially changes the carrier frequency from burst to burst. Each burst consists of 32 pulses, and the pulse repetition frequency (PRF) is 4 KHz. The spinning rate of the radar's antenna is 30 rpm, and the antenna beamwidth is 7.3^{o}.

A transponder beacon that is located 10 km away from the radar retransmits the radar's signal when illuminated by the radar. The retransmitted radar signal is received by a 15 elements phased array and beamformed in the elevation plane to improve the SDR.

The recorded radar signal is modulated by the two-way radar antenna beam pattern, and the spinning antenna mainlobe is fitted to a Gaussian model.

4.7.2.1 The nonrecursive estimators

The parameters of the evaluated scenario are illustrated in Table 10, and the magnitude of the L-band radar's data is illustrated in Figure 20. Each burst in Figure 20 is highlighted by a colour that corresponds to the relevant carrier frequency. The red burst that is pointed at in Figure 20 is extracted and then used to emulate a partial spread of the data across the spinning antenna mainlobe scenario.

The estimated SDR is 15 dB, and synthesised complex white Gaussian noise was injected into the radar's data to obtain different values of SDR. In this setting, the estimated complex amplitude is fixed and the SDR is scaled to calculate the disturbance power $\sigma_d^2 = \frac{b^2}{SDR}$.

In Figure 21 and Figure 22, the MSE, bias and variance of the nonrecursive DOA estimators and the MSE bounds are illustrated. It is evident from Figure 21 that the MMSE estimator and the affine transformed ML estimator outperform the CRLB and the BB, and that the MSE of the MMSE estimator is close to the BCRLB.

Table 10. The real data scenario that is used to evaluate the nonrecursive DOA estimators. Parameters listed are: spinning antenna beamwidth θ_B, unambiguous width θ_{um}, emitter DOA $\boldsymbol{\theta_{ET}}$, number of data samples N, pulse repetition frequency PRF, antenna boresight directions vector $\boldsymbol{\theta_{BO}}$, and estimated SDR after recovering the antenna pattern loss

Scenario	$\theta_B = \theta_{um}$	θ_{ET}	N	PRF (KHz)	$[\boldsymbol{\theta_{BO}}]_1$	$[\boldsymbol{\theta_{BO}}]_N$	SDR (dB)
1	7.3^{o}	134.9582^{o}	32	4	137.8015^{o}	139.2188^{o}	15

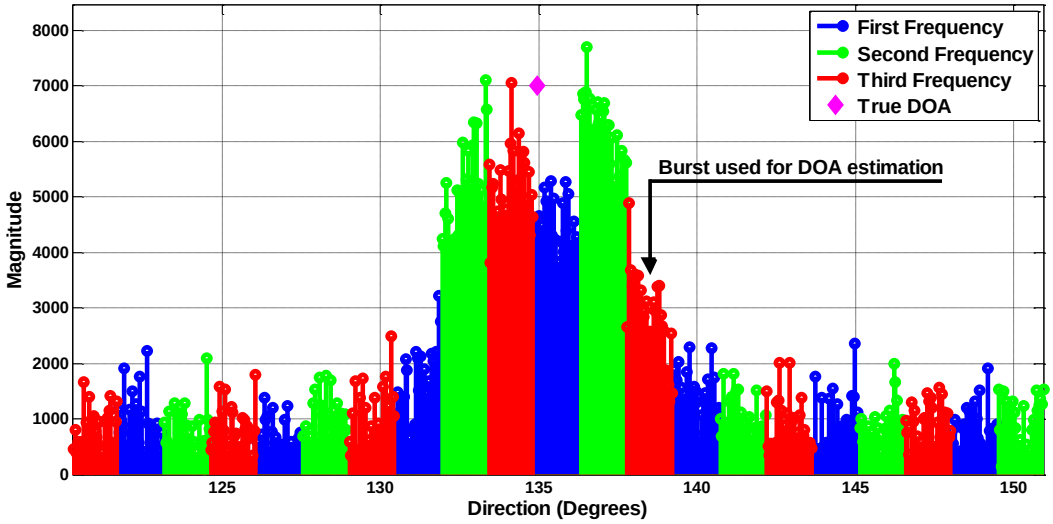

Figure 20. The magnitude of the L-band radar's data. First frequency = 1.235 GHz, second frequency = 1.3 GHz and third frequency = 1.365 GHz. $\theta_B = \theta_{um} = 7.3^o$, $\theta_{ET} = 134.9582^o$, $N = 32$, $PRF = 4\ KHz$, $[\theta_{BO}]_1 = 137.8015^o$, $[\theta_{BO}]_N = 139.2188^o$, $SDR = 15\ dB$

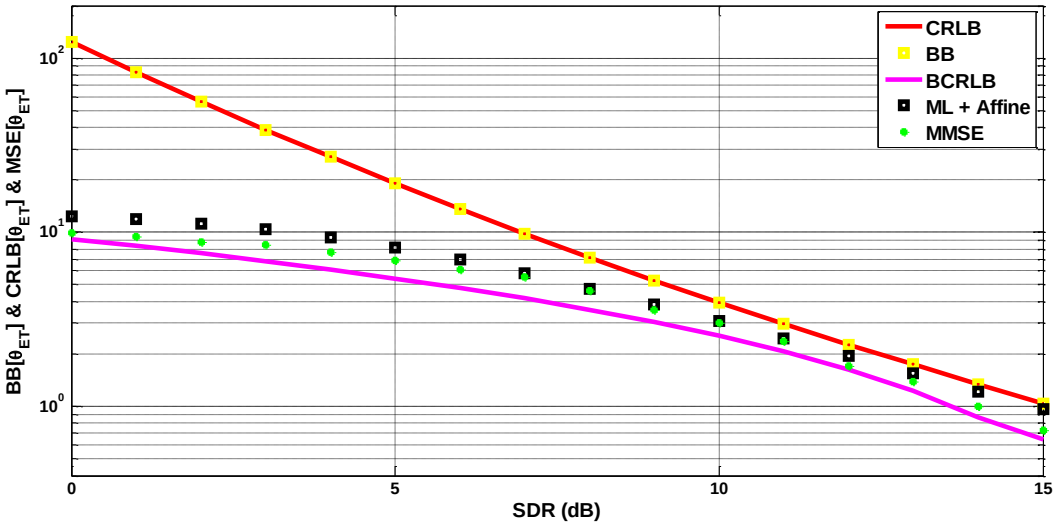

Figure 21. $MSE\{\hat{\theta}_{ET}\}$ **of the nonrecursive DOA estimators versus the MSE bounds using real radar data.** $\theta_B = \theta_{um} = 7.3^o$, $\theta_{ET} = 134.9582^o$, $N = 32$, $PRF = 4\ KHz$, $[\theta_{BO}]_1 = 137.8015^o$, $[\theta_{BO}]_N = 139.2188^o$, $SDR = 15\ dB$

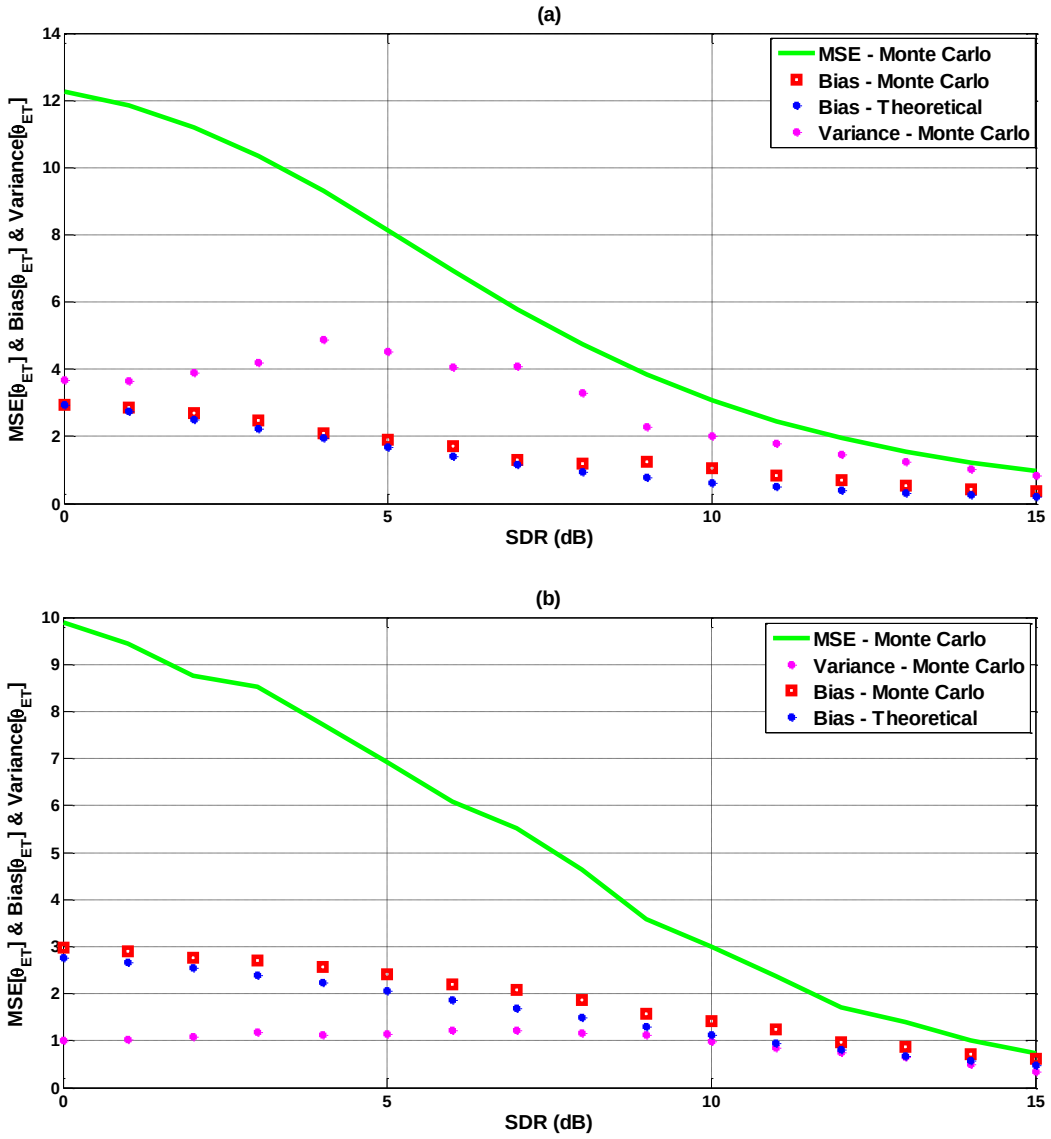

Figure 22. $MSE\{\widehat{\theta}_{ET}\}$, $Bias\{\widehat{\theta}_{ET}\}$ **and** $Variance\{\widehat{\theta}_{ET}\}$ **of the nonrecursive DOA estimators for the real data scenario. (a) Affine transformed ML estimator. (b) MMSE estimator.** $\theta_B = \theta_{um} = 7.3^o$, $\theta_{ET} = 134.9582^o$, $N = 32$, $PRF = 4\ KHz$, $[\theta_{BO}]_1 = 137.8015^o$, $[\theta_{BO}]_N = 139.2188^o$, $SDR = 15\ dB$

4.7.2.2 The recursive estimators

The parameters of the evaluated scenarios are illustrated in Table 11 and Table 12, and the magnitude of the radar's data is shown in Figure 23 and Figure 25. In both scenarios, synthesised complex white Gaussian noise was injected into the radar's data to obtain different values of SDR, while maintaining the initial SDR difference between the snapshots.

The two snapshots for the first real data scenario are shown in Figure 23, and the bursts pointed at in the figure are extracted and then used to emulate a partial-spread scenario. The two snapshots differ with regard to the emitter steering vector (in terms of boresight directions), and the SDR of the second snapshot is slightly better than the SDR of the first snapshot.

The DOA estimation accuracy for the first real data scenario is shown in Figure 24. The antenna boresight directions vector $\boldsymbol{\theta_{BO}}$ provides useful information that is used to set the prior pdf parameters. Thus, the MSE of the first snapshot is better than the MSE of the second snapshot, because $\boldsymbol{\theta_{BO}}$ of the first snapshot is closer to the true DOA than $\boldsymbol{\theta_{BO}}$ of the second snapshot. As shown in Figure 24, the recursive MMSE DOA estimator improved the DOA estimation accuracy by merging the information contained in the two snapshots.

Table 11. The first real data scenario that is used to evaluate the recursive DOA estimators. Parameters listed are: unambiguous width θ_{um}, emitter DOA θ_{ET}, number of data samples N, pulse repetition frequency PRF, antenna boresight directions Vector θ_{BO}, frequency $Freq$ and estimated SDR after recovering the antenna pattern loss.

Snapshot	θ_{um}	θ_{ET}	$Freq$ (GHz)	SDR (dB)	N	PRF (KHz)	$[\boldsymbol{\theta_{BO}}]_1$	$[\boldsymbol{\theta_{BO}}]_N$
1	8.5^o	134.9696^o	1.365	18.8502	32	4	136.0107^o	137.4225^o
2	8.5^o	134.9696^o	1.365	20.2748	32	4	137.3236^o	138.7189^o

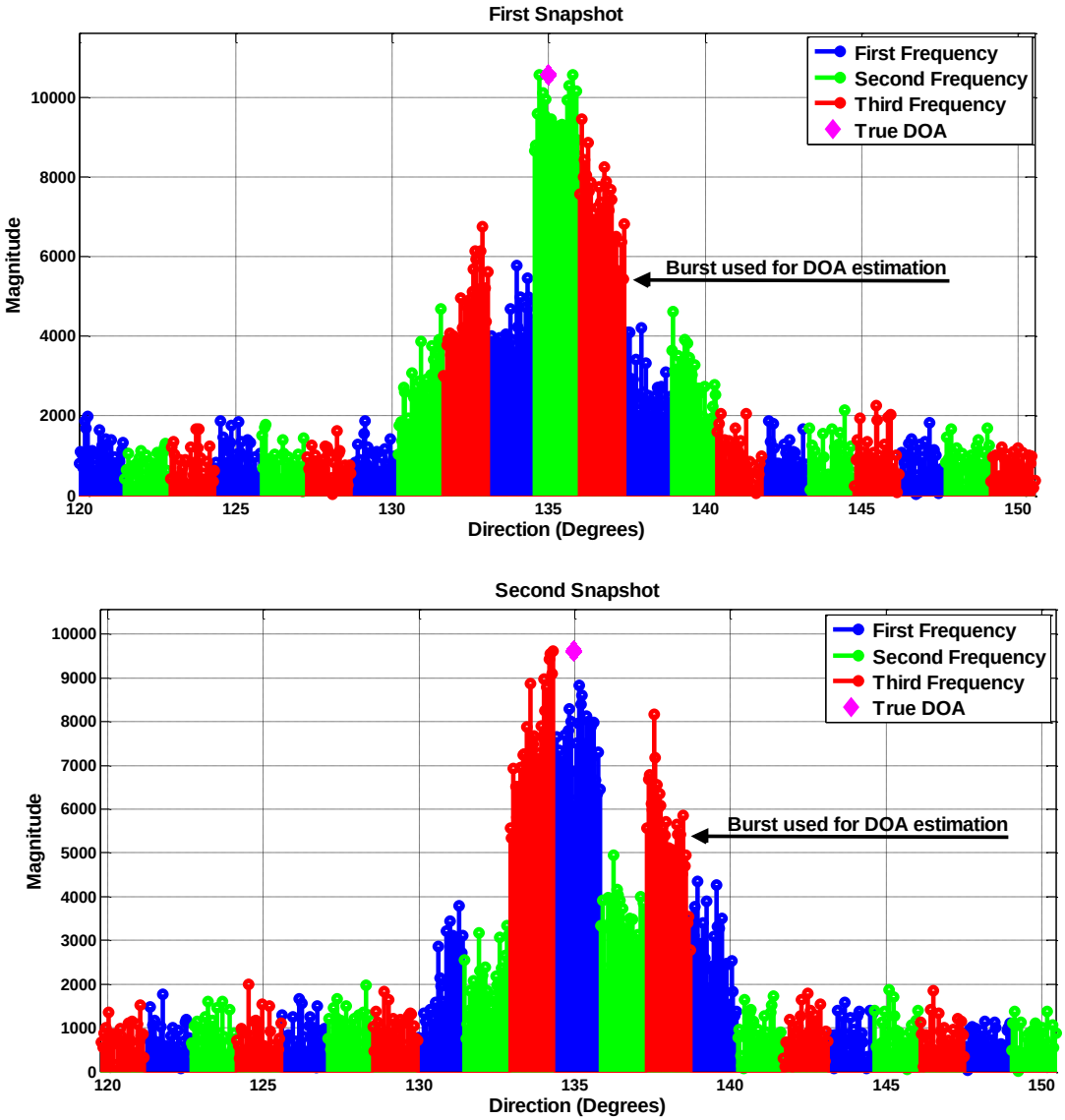

Figure 23. Magnitude of the radar data for the first real data scenario (recursive estimators). First frequency = 1.235 GHz, second frequency = 1.3 GHz and third frequency = 1.365 GHz.

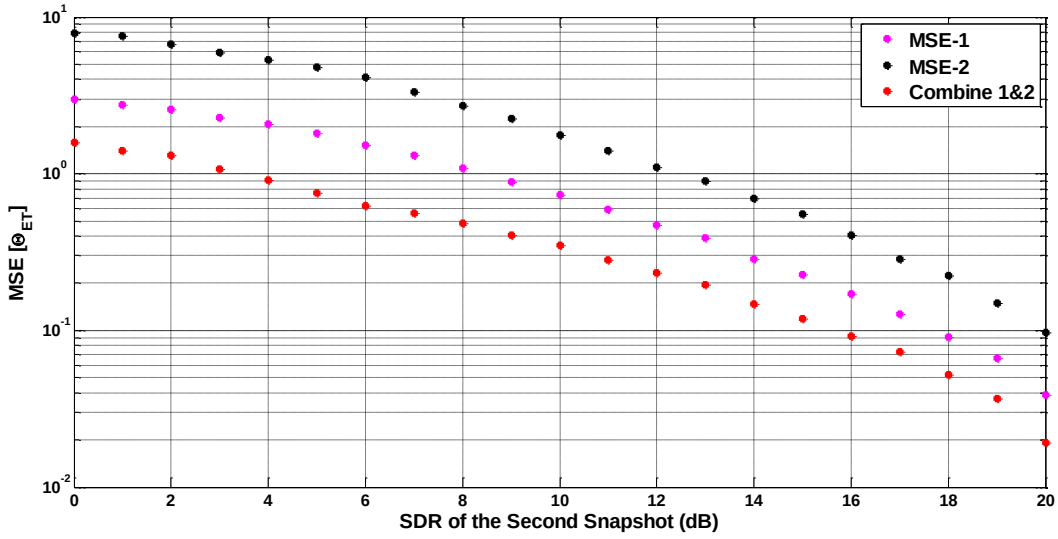

Figure 24. $MSE\{\widehat{\theta}_{ET}\}$ of the single snapshots and the combined snapshots for the first real data scenario (recursive estimators).

The two snapshots for the second real data scenario are shown in Figure 25; the bursts pointed at in the figure are extracted and then used to emulate a partial-spread scenario. The two snapshots differ with regard to the emitter steering vector (in terms of boresight directions and frequency), and the SDR of the second snapshot is better than the SDR of the first snapshot.

The DOA estimation accuracy for the second real data scenario is shown in Figure 26. The MSE of the second snapshot is better than the MSE of the first snapshot, because the second snapshot has a better SDR. As shown in Figure 26, the recursive MMSE DOA estimator improved the DOA estimation accuracy by merging the information contained in the two snapshots.

Table 12. The second real data scenario that is used to evaluate the recursive DOA estimators. Parameters listed are: unambiguous width θ_{um}, emitter DOA θ_{ET}, number of data samples N, pulse repetition frequency PRF, antenna boresight directions vector θ_{BO}, frequency $Freq$ and estimated SDR after recovering the antenna pattern loss.

Snapshot	θ_{um}	θ_{ET}	$Freq$ (GHz)	SDR (dB)	N	PRF (KHz)	$[\boldsymbol{\theta_{BO}}]_1$	$[\boldsymbol{\theta_{BO}}]_N$
1	8.5^o	134.9806^o	1.235	17.8504	32	4	137.1039^o	138.5046^o
2	8.5^o	134.9806^o	1.365	23.2568	32	4	137.7795^o	139.1748^o

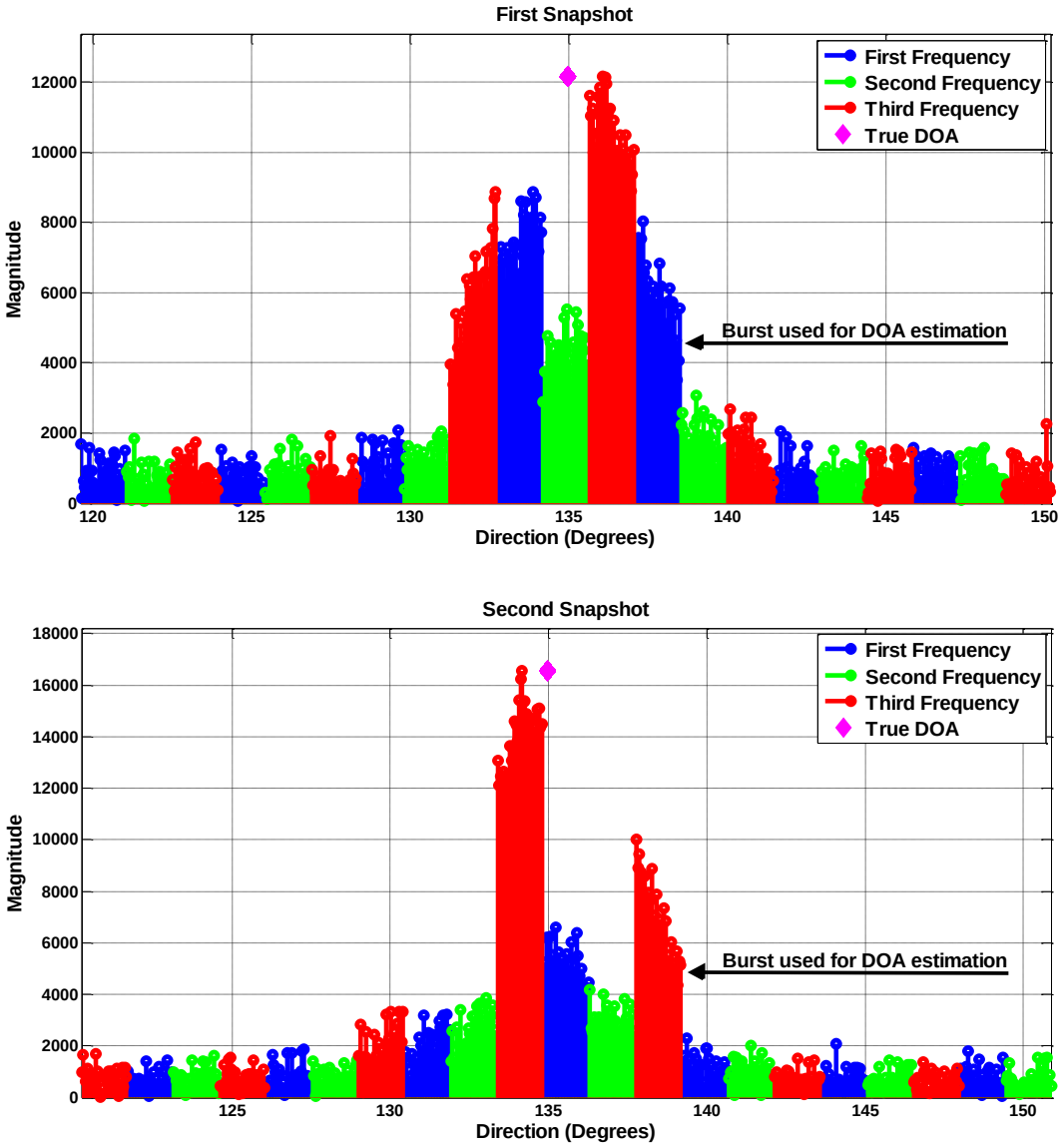

Figure 25. Magnitude of the radar data for the second real data scenario (recursive estimators). First frequency = 1.235 GHz, second frequency = 1.3 GHz and third frequency = 1.365 GHz.

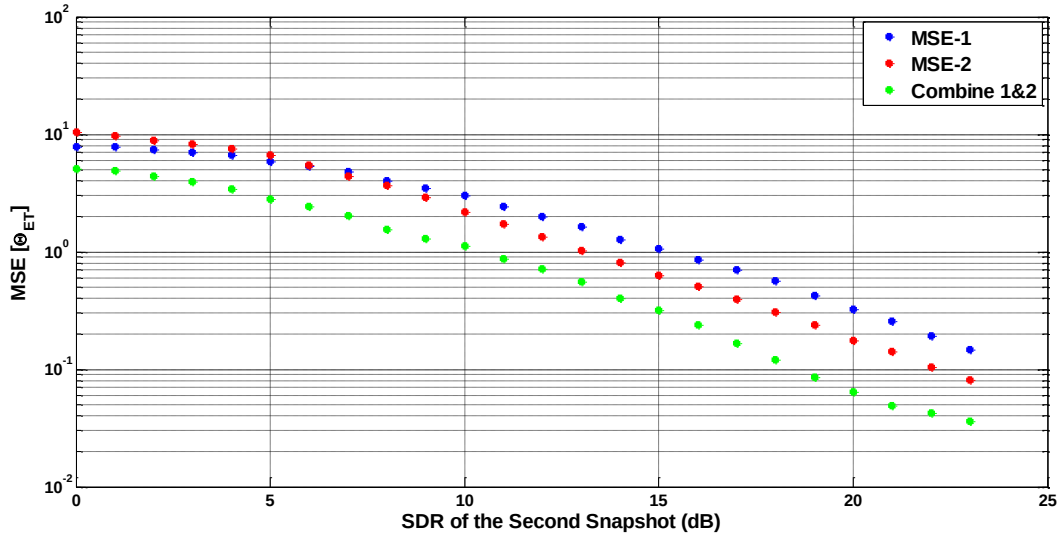

Figure 26. $MSE\{\widehat{\theta}_{ET}\}$ of the single snapshots and the combined snapshots for the second real data scenario (recursive estimators).

4.8 Summary

In this chapter, biased estimators for estimating the DOA of emitters' signals received by a spinning antenna based ELINT system were constructed. Two types of data were considered: 1) complex Gaussian distributed data, and 2) Rician distributed data. The biased DOA estimators were constructed using minimax estimation techniques and Bayesian estimation techniques. The minimax DOA estimators are scaled versions of the ML DOA estimators, while the Bayesian DOA estimators are based on the MMSE form. The BCRLB was derived to provide a performance benchmark for the Bayesian DOA estimators.

The DOA estimation accuracy of the constructed biased DOA estimators was evaluated using Monte Carlo simulation and real radar data. The constructed biased DOA estimators were shown to outperform the CRLB and the BB, and the constructed Bayesian DOA estimators were shown to perform closely to the BCRLB. The recursive Bayesian DOA estimators are based on the sequential form of the MMSE estimator and were shown to improve the DOA estimation accuracy by merging the information contained in several snapshots.

5. Super-resolution

5.1 Introduction

The spatial resolution of a single beam mechanically steered (spinning) antenna is bounded by the Rayleigh limit [58], which is independent of the SDR. Increasing the antenna aperture is a well-known technique for improving the spatial resolution. However, this technique is limited by the size, weight, mechanics and cost constraints.

The spinning directional antenna is the most cost-effective antenna configuration for providing high gain over a wide (multi-octave) frequency range. There is, of course, the concomitant variation of the antenna beamwidth. To keep the antenna size reasonable in terms of the mechanics of spinning, the low frequency will suffer the most in terms of spatial resolution, driving us towards better estimation methods than conventional methods.

To overcome the Rayleigh limit, many super-resolution estimators have been proposed in recent literature to support applications such as forward-looking imaging and microwave radiometry, where most of these super-resolution estimators are inspired by array processing literature. Super-resolution estimators can be beneficial for ELINT applications too, especially in the lower band of the frequency domain, where the antenna beamwidth is wide and frequency interference is high.

Some of the published super-resolution estimators exploit the knowledge about the spinning antenna beam pattern and the Doppler frequencies to resolve the received signals [1]-[2], [48]-[49]. While other super-resolution estimators assume that the Doppler frequencies are unknown and thus use a large number of snapshots to resolve the received signals [27]-[30], [34]-[36]. In [4], [37]-[42], [51]-[55], super-resolution estimators that exploit the knowledge about the spinning antenna beam pattern and that can resolve the received signals with a minimum of a single snapshot were proposed.

Unfortunately, the severely ill-conditioned dictionary associated with the spinning antenna problem imposes limitations on the super-resolution estimators. Thus, to the best of our knowledge, the super-resolution estimators currently available in the literature have shortcomings either in terms of performance or the need for tuning user parameters.

In this chapter, we therefore employ the SBL technique [23]-[24] to construct a user parameter-free super-resolution DOA estimator, because of the ability of the SBL technique to accommodate problems with severely ill-conditioned dictionaries [23]-[24], such as the spinning antenna problem. The constructed SBL DOA estimator exploits the knowledge about the spinning antenna beam pattern and is capable of resolving the received signals using a single snapshot.

We use Monte Carlo simulation to demonstrate the performance enhancement provided by the constructed SBL DOA estimator and to compare the constructed SBL DOA estimator with

a DOA estimator that is constructed using the IAA technique [38], [51]-[53]. The IAA DOA estimator has been shown to outperform existing super-resolution DOA estimators for the spinning antenna problem [38], [51]-[53].

5.2 Data model

The first step to derive the data model is to update the data model presented in Section 3.2 to accommodate sparse signal representation. This is achieved by acknowledging that the number of actual signals is much less than the number of potential signals. Thus, Equation (1) becomes:

$$[\boldsymbol{Z}]_n = \sum_{l=1}^{L} [\boldsymbol{b}]_l \; G([\boldsymbol{\theta_S}]_l, [\boldsymbol{\theta_{BO}}]_n) + [\boldsymbol{d}]_n; \qquad n = 1, \dots N \tag{73}$$

where $[\boldsymbol{b}]_l$ is the complex amplitude (weight) at the lth direction. $[\boldsymbol{\theta_S}]_l$ is the lth direction and L is the maximum number of directions (grid points). The nth component of the N-dimensional steering vector $\boldsymbol{a}([\boldsymbol{\theta_S}]_l, \boldsymbol{\theta_{BO}})$ is:

$$[\boldsymbol{a}([\boldsymbol{\theta_S}]_l, \boldsymbol{\theta_{BO}})]_n = G([\boldsymbol{\theta_S}]_l, [\boldsymbol{\theta_{BO}}]_n); \qquad n = 1 \dots . N \tag{74}$$

The vector form of Equation (73) is:

$$\boldsymbol{Z}(x) = \boldsymbol{A}(\boldsymbol{\theta_S}, \boldsymbol{\theta_{BO}})\, \boldsymbol{b}(x) + \boldsymbol{d}(x); \qquad x = 1, \dots X \tag{75}$$

where X is the number of snapshots and $\boldsymbol{\theta_S} = [\,[\boldsymbol{\theta_S}]_1\, [\boldsymbol{\theta_S}]_2 \dots \dots [\boldsymbol{\theta_S}]_L]^T$ is the $L \times 1$ vector of DOAs. $\boldsymbol{A}(\boldsymbol{\theta_S}, \boldsymbol{\theta_{BO}})$ is the $N \times L$ steering matrix (dictionary), defined as $\boldsymbol{A}(\boldsymbol{\theta_S}, \boldsymbol{\theta_{BO}}) = [\boldsymbol{a}([\boldsymbol{\theta_S}]_1, \boldsymbol{\theta_{BO}})\;\; \boldsymbol{a}([\boldsymbol{\theta_S}]_2, \boldsymbol{\theta_{BO}}) \dots \dots \boldsymbol{a}([\boldsymbol{\theta_S}]_L, \boldsymbol{\theta_{BO}})]^T$, and $\boldsymbol{b} = [\,[\boldsymbol{b}]_1\, [\boldsymbol{b}]_2 \dots \dots \dots [\boldsymbol{b}]_L]^T$ is the $L \times 1$ vector of unknown complex amplitudes (weights).

The goal of sparse signal representation is to estimate $\boldsymbol{b}$ given $\boldsymbol{A}(\boldsymbol{\theta_S}, \boldsymbol{\theta_{BO}})$ and $\boldsymbol{Z}$, such that the elements of $\boldsymbol{b}$ are predominantly zero and satisfy $\boldsymbol{Z} = \boldsymbol{A}(\boldsymbol{\theta_S}, \boldsymbol{\theta_{BO}})\, \boldsymbol{b}$.

We note here that the dependency of $\boldsymbol{A}(\boldsymbol{\theta_S}, \boldsymbol{\theta_{BO}})$ and $\boldsymbol{a}([\boldsymbol{\theta_S}]_l, \boldsymbol{\theta_{BO}})$ on $\boldsymbol{\theta_S}$ and $\boldsymbol{\theta_{BO}}$ was omitted in the next sections for ease of notation.

5.3 The iterative adaptive approach

The IAA is a nonparametric, iterative technique based on weighted least squares for estimating the amplitude and phase in array processing [56]. The IAA has many appealing properties, such as: it has a simple form and a high resolution, and is free of user parameters; it facilitates parallel processing, provides good performance with a single snapshot and arbitrary array geometries, and it can work with coherent, partially correlated and uncorrelated signals [56].

The IAA technique is illustrated in Table 13. The first step is to initialise the estimator using the conventional delay-and-sum estimator. The diagonal elements of the $L \times L$ diagonal matrix $\boldsymbol{\Omega}$ are the power at each direction on a predefined grid. The second step is to compute the covariance matrix $\boldsymbol{R}$. In the third step, the complex amplitudes and the diagonal elements

of matrix $\boldsymbol{\Omega}$ are computed. Then the second and the third steps are repeated until convergence. The IAA typically converges after fifteen iterations [56].

Unfortunately, the severely ill-conditioned dictionary associated with the spinning antenna problem results in an ill-posed problem. Thus, the covariance matrix $\boldsymbol{R}$ cannot be inverted directly, and a method such as the diagonal loading method should be used. By using the diagonal loading method, the second step becomes:

$$\boldsymbol{R} = \boldsymbol{A}\,\boldsymbol{\Omega}\,\boldsymbol{A}^{\boldsymbol{H}} + \lambda\,\boldsymbol{I} \tag{76}$$

where λ is a tuning parameter that is chosen heuristically by the user. We note here that tuning the diagonal loading value becomes difficult, as the problem dimensions grow. A wrong setting of the diagonal loading value affects the performance significantly.

We also note here that the similarity between the dictionary columns is the cause of the high condition number.

Table 13. The IAA technique

$$[\boldsymbol{\Omega}]_{ll} = \frac{1}{(\boldsymbol{a}^{\boldsymbol{H}}\,\boldsymbol{a})^2\,X}\sum_{x=1}^{X}|\boldsymbol{a}^{\boldsymbol{H}}\,\boldsymbol{Z}(x)|^2\,; \qquad l = 1, \dots\dots\dots L$$

$\boldsymbol{Repeat}$

$$\boldsymbol{R} = \boldsymbol{A}\,\boldsymbol{\Omega}\,\boldsymbol{A}^{\boldsymbol{H}}$$

$\boldsymbol{for} \quad l = 1, \dots\dots\dots L$

$$[\boldsymbol{b}(x)]_l = \frac{\boldsymbol{a}^{\boldsymbol{H}}\,\boldsymbol{R}^{-\boldsymbol{1}}\,\boldsymbol{Z}(x)}{\boldsymbol{a}^{\boldsymbol{H}}\,\boldsymbol{R}^{-\boldsymbol{1}}\,\boldsymbol{a}}; \qquad x = 1, \dots\dots\dots X$$

$$[\boldsymbol{\Omega}]_{ll} = \frac{1}{X}\sum_{x=1}^{X}|[\boldsymbol{b}(x)]_l|^2$$

$\boldsymbol{end\ for}$

$\boldsymbol{Until\ convergence}$

5.4 The sparse Bayesian learning technique

The SBL technique was originally derived in regression and classification literature to find robust solutions to sparse signal representation from overcomplete dictionaries ($i.e., rank(\boldsymbol{A}) = N\ and\ L > N$) [23]-[24].

The SBL technique enforces sparsity by incorporating a parameterised prior on the unknown weights [23]-[24]. The vector of hyperparameters $\boldsymbol{\gamma}$ controls the prior variance of each weight, and its elements are estimated from the data using the evidence maximisation procedure [23]-[24].

The SBL technique is presented in [23], [24] and illustrated in Table 14. The SBL technique can be applied directly once the problem is formulated as a sparse signal representation problem. The first step is to initialise σ_d^2 and the vector of hyperparameters $\boldsymbol{\gamma}$. In the second step, the weights and the covariance matrix are computed. In the third step, σ_d^2 and the vector of hyperparameters $\boldsymbol{\gamma}$ are updated. The second and the third steps are iterated until convergence. A hyperparameter can be pruned when it reaches an arbitrarily small threshold.

Table 14. The SBL technique

$\boldsymbol{\gamma} = \mathbf{1}, \quad \sigma_d^2 = 1$

$\boldsymbol{Repeat}$

$\boldsymbol{\Phi} = diag(\boldsymbol{\gamma})$

$\boldsymbol{\Sigma_t} = \boldsymbol{A}\,\boldsymbol{\Phi}\,\boldsymbol{A^H} + \sigma_d^2\,\boldsymbol{I}$

$\boldsymbol{\Sigma} = \boldsymbol{\Phi}\,(\boldsymbol{I} - \boldsymbol{A^H}\,\boldsymbol{\Sigma_t^{-1}}\,\boldsymbol{A}\,\boldsymbol{\Phi})$

$\widehat{\boldsymbol{b}}(x) = \boldsymbol{\Phi}\,\boldsymbol{A^H}\,\boldsymbol{\Sigma_t^{-1}}\,\boldsymbol{Z}(x)\,; \qquad x = 1, \dots \dots \dots X$

$$\sigma_d^2 = \frac{(1/x)\ \sum_{x=1}^{X} \left\| \boldsymbol{Z}(x) - \boldsymbol{A}\,\widehat{\boldsymbol{b}}(x) \right\|_2^2}{N - L + \sum_{l=1}^{L} ([\boldsymbol{\Sigma}]_{ll}/[\boldsymbol{\gamma}]_l)};$$

$$[\boldsymbol{\gamma}]_l = \frac{1}{x} \sum_{x=1}^{X} \frac{\left| \left[\widehat{\boldsymbol{b}}(x)\right]_l \right|^2}{1 - ([\boldsymbol{\Sigma}]_{ll}/[\boldsymbol{\gamma}]_l)}; \qquad l = 1, \dots \dots \dots L$$

$\boldsymbol{Until\ convergence}$

5.5 Performance analysis

In this section, we evaluate the spatial resolution and the DOA estimation accuracy (as measured by the MSE) of the constructed SBL DOA estimator using Monte Carlo simulation. Also, we compare the constructed SBL DOA estimator to the IAA DOA estimator and the popular performance benchmark, namely, the CRLB.

In the Monte Carlo simulations, the received signals are incoherent, the beam pattern of the spinning antenna is Gaussian, and the disturbance consists of complex white Gaussian noise with zero mean. The simulation scenarios are illustrated in Table 15.

Table 15. The simulation scenarios that are used to evaluate the SBL DOA estimator. Parameters listed are: spinning antenna beamwidth $\boldsymbol{\theta_B}$, DOAs, number of data samples $\boldsymbol{N}$, the product of the pulse repetition interval and angular velocity ($\boldsymbol{PRI\ \omega_R}$), antenna boresight directions vector $\boldsymbol{\theta_{BO}}$, SDR.

Scenario	θ_B	$\boldsymbol{DOAs}$	N	$PRI\ \omega_R$	$[\boldsymbol{\theta_{BO}}]_1$	$[\boldsymbol{\theta_{BO}}]_N$	$SDR\ (dB)$
1	1.5°	$[0^o \quad 0.9^o]^T$	32	0.2387°	-3.7°	3.7°	20
2	1.5°	$[-1.2^o \quad 0^o \quad 0.75^o]^T$	512	0.0145°	-3.7°	3.7°	20
3	70°	$[0^o \quad 10^o]^T$	256	1.2549°	-160°	160°	20
4	1.2°	$[0^o \quad 0.8^o]^T$	300	0.0234°	-3.5°	3.5°	Varied
5	30°	15^o	Varied	Varied	-75°	75°	15

In Figure 27 to Figure 29, the results of the first, the second and the third simulation scenarios are illustrated, where the outcomes of ten Monte Carlo iterations are plotted in each figure. In Figure 27 to Figure 29, the SBL DOA estimator outperforms the IAA DOA estimator in terms of spatial resolution.

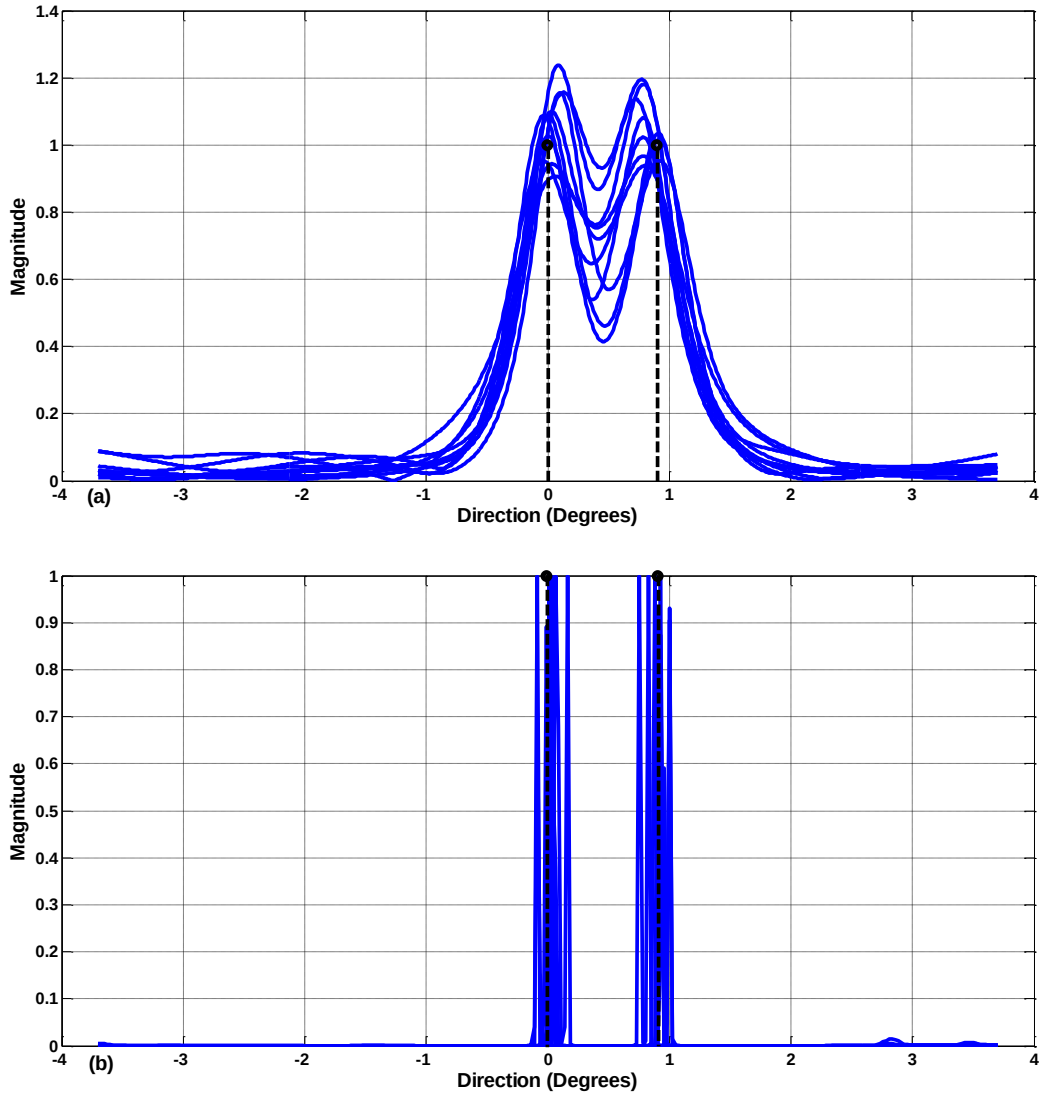

Figure 27. The results of the first simulation scenario that are used to evaluate the SBL DOA estimator and the IAA DOA estimator. (a) The IAA DOA estimator. (b) The SBL DOA estimator. $\boldsymbol{\theta_B = 1.5^o}$, $\boldsymbol{DOAs = [0^o \;\; 0.9^o]^T}$, $\boldsymbol{N = 32}$, $\boldsymbol{PRI\ \omega_R = 0.2387^o}$, $\boldsymbol{[\theta_{BO}]_1 = -3.7^o}$, $\boldsymbol{[\theta_{BO}]_N = 3.7^o}$, $\boldsymbol{SDR = 20\ dB}$

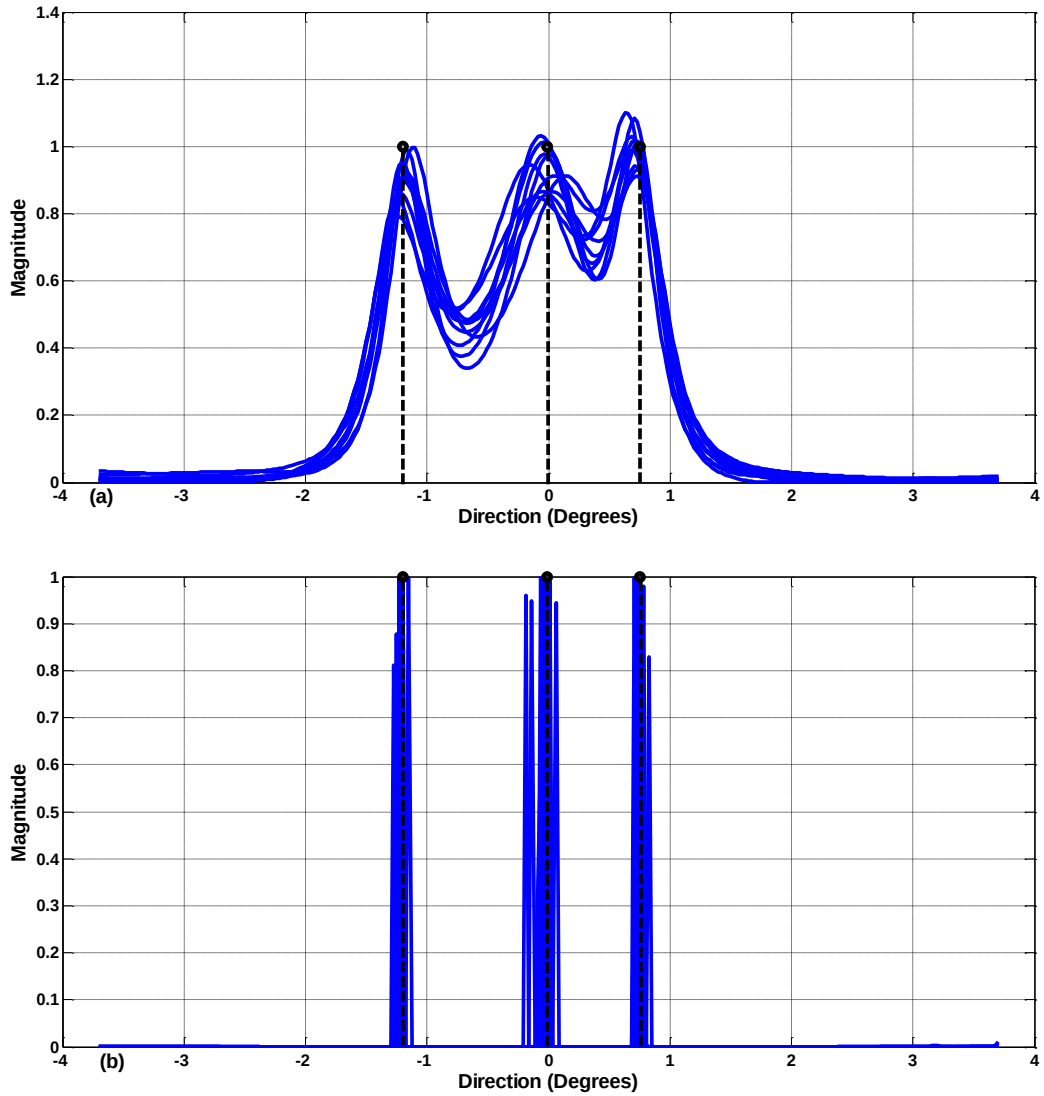

Figure 28. The results of the second simulation scenario that are used to evaluate the SBL DOA estimator and the IAA DOA estimator. (a) The IAA DOA estimator. (b) The SBL DOA estimator. $\boldsymbol{\theta_B = 1.5^o}$, $\boldsymbol{DOAs = [-1.2^o \quad 0^o \quad 0.75^o]^T}$, $\boldsymbol{N = 512}$, $\boldsymbol{PRI\ \omega_R = 0.0145^o}$, $\boldsymbol{[\theta_{BO}]_1 = -3.7^o}$, $\boldsymbol{[\theta_{BO}]_N = 3.7^o}$, $\boldsymbol{SDR = 20\ dB}$

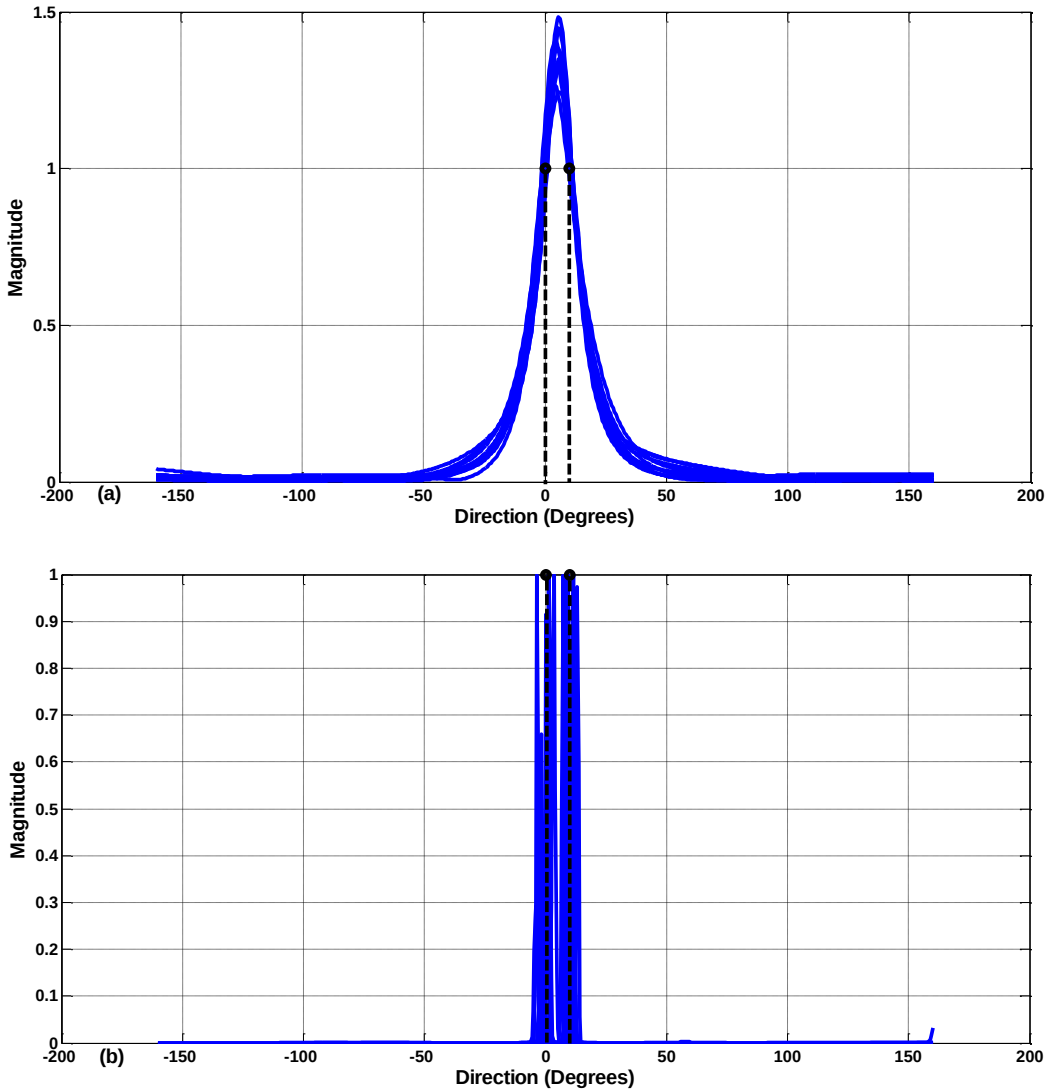

Figure 29. The results of the third simulation scenario that are used to evaluate the SBL DOA estimator and the IAA DOA estimator. (a) The IAA DOA estimator. (b) The SBL DOA estimator. $\boldsymbol{\theta_B = 70^o}$, $\boldsymbol{DOAs = [0^o \;\; 10^o]^T}$, $\boldsymbol{N = 256}$, $\boldsymbol{PRI\ \omega_R = 1.2549^o}$, $\boldsymbol{[\theta_{BO}]_1 = -160^o}$, $\boldsymbol{[\theta_{BO}]_N = 160^o}$, $\boldsymbol{SDR = 20\ dB}$

In Figure 30, the results of the fourth simulation scenario are illustrated, where the MSE of estimating the DOA of a signal that occupies the same Rayleigh resolution cell as another signal is shown. As shown in the Figure 30, the SBL DOA estimator outperforms the IAA DOA estimator in terms of MSE and closer to the CRLB.

In Figure 31, the results of the fifth simulation scenario are illustrated, where the MSE versus the number of data samples is shown. As shown in Figure 31, the SBL DOA estimator outperforms the IAA DOA estimator in terms of MSE and closer to the CRLB.

We note here that the IAA DOA estimator suffers from the large condition number of its covariance matrix [53], and this is because of the severely ill-conditioned dictionary associated with the spinning antenna problem. We tried the regularised version of the IAA [51], but we did not obtain meaningful results. Therefore, we used the conventional method of diagonal loading, which requires tuning the diagonal loading value to obtain optimal

performance. Thus, the adaptivity of the IAA DOA estimator is no longer maintained. Different diagonal loading values should be used depending on the parameters of the encountered scenario. A wrong setting of the diagonal loading value affects the performance significantly. The SBL DOA estimator, in contrast, is user parameter free, and it does not require tuning of user parameters.

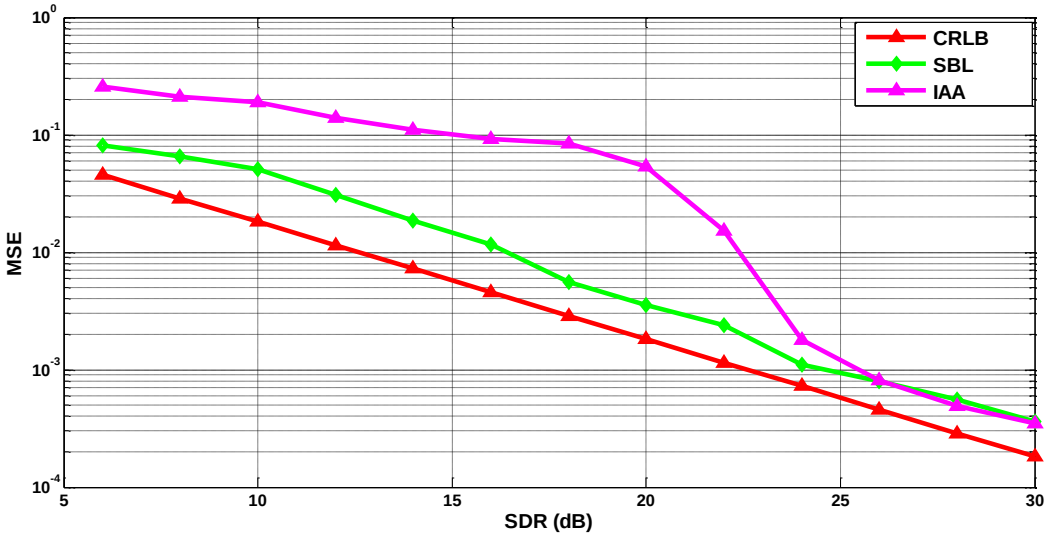

Figure 30. The results of the fourth simulation scenario that are used to evaluate the super-resolution estimators. $\theta_B = 1.2^o$, $DOAs = [0^o \;\; 0.8^o]^T$, $N = 300$, $PRI\ \omega_R = 0.0234^o$, $[\theta_{BO}]_1 = -3.5^o$, $[\theta_{BO}]_N = 3.5^o$

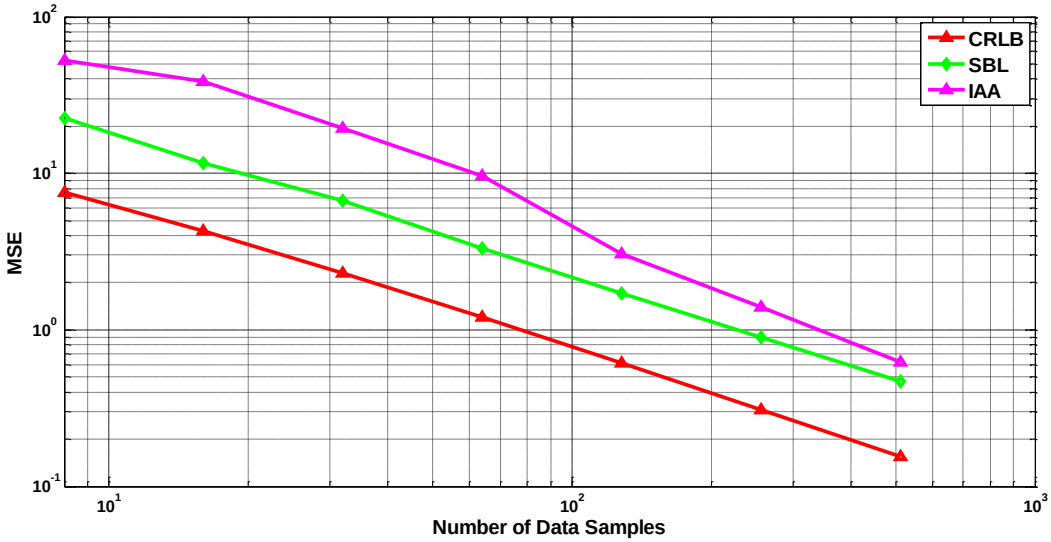

Figure 31. The results of the fifth simulation scenario that are used to evaluate the super-resolution estimators. $\theta_B = 30^o$, $DOAs = \;\; 15^o$, $[\theta_{BO}]_1 = -75^o$, $[\theta_{BO}]_N = 75^o$, $SDR = 15\ dB$

5.6 Summary

In this chapter, a super-resolution DOA estimator for estimating the DOA of signals received by a spinning antenna based system was constructed. The super-resolution DOA estimator was constructed using the SBL technique because of the ability of this technique to accommodate problems with severely ill-conditioned dictionaries, such as the spinning

antenna problem. The spatial resolution and DOA estimation accuracy of the constructed SBL DOA estimator were evaluated and compared to the IAA DOA estimator using Monte Carlo simulation. The SBL DOA estimator was shown to outperform the IAA DOA estimator in terms of spatial resolution and DOA estimation accuracy.

6. Closing remarks

6.1 Conclusion

The spinning directional antenna is the most cost-effective antenna configuration for providing high gain over wide (multi-octave) RF range. Thus, it is the appropriate antenna configuration for increasing the intercept range of an ELINT system.

In the presence of a small SDR, a small number of data samples, a partial spread of the data across the spinning antenna mainlobe, and a wide antenna's beamwidth, it becomes difficult for a spinning antenna based ELINT system to accurately estimate the DOA of the received signals.

DOA estimation is concerned with estimating the DOA of electromagnetic signals or acoustic signals for the purpose of tracking and locating the sources of signals.

In this thesis, we thus investigated the problem of estimating the DOA of emitters' signals received by a spinning antenna based ELINT system, where the goal is to improve the DOA estimation accuracy (as measured by the MSE).

By evaluating the BB and the popular performance benchmark, namely, the CRLB, we showed that the best achievable MSE of the conventional unbiased estimation techniques is insufficient for the kinds of scenarios that spinning antenna based ELINT systems might encounter, i.e., scenarios that are characterised by: the wide beamwidth of the spinning antenna; the partial spread of the data across the spinning antenna mainlobe; the small number of data samples; and a small SDR. Thus, we proposed the use of biased estimation techniques that improve the MSE by introducing a bias.

We first constructed minimax DOA estimators that are transformed versions of the ML DOA estimator, where the transformation parameters are computed by solving minimax optimisation problems. Then, we constructed Bayesian DOA estimators that introduce the bias by imposing prior distributions on the parameters to be estimated. Also, we constructed recursive Bayesian DOA estimators that further improve the MSE by merging the information contained in several snapshots.

Using Monte Carlo simulation and real radar data, we demonstrated the advantages of the constructed biased DOA estimators in terms of the MSE for both complex Gaussian distributed data and Rician distributed data. We demonstrated: that the constructed biased DOA estimators are capable of outperforming the MSE limit specified by the CRLB and the BB; that the constructed Bayesian DOA estimators perform closely to the BCRLB; and that the constructed recursive Bayesian DOA estimators are capable of improving the MSE by merging the information contained in several snapshots. Thus, the constructed biased DOA estimators are believed to be beneficial for practical ELINT applications.

In addition, we investigated the problem of increasing the spatial resolution of a spinning antenna based system beyond the Rayleigh resolution limit, where the goal is to have the

ability to adaptively resolve the received signals and to have an adequate performance in terms of spatial resolution and DOA estimation accuracy (as measured by the MSE).

Our knowledge of the literature indicated that existing spinning antenna based super-resolution DOA estimators have shortcomings either in terms of performance or the need for tuning user parameters. Thus, we proposed the use of the SBL technique because of its ability to accommodate problems with severely ill-conditioned dictionaries, such as the spinning antenna problem, and this, in turn, resulted in an adaptive super-resolution DOA estimator.

Using Monte Carlo simulation, we demonstrated that the constructed SBL DOA estimator is capable of adaptively resolving the received signals using a single snapshot and outperforming the IAA DOA estimator in terms of MSE and spatial resolution. Also, we demonstrated that the SBL DOA estimator is user parameter free, while the IAA DOA estimator requires the tuning of at least one user parameter.

6.2 Future work

In this section, a list of suggested topics for future research is provided.

A potential topic for future research is estimating the DOA of emitters' signals received by a spinning antenna based ELINT system in the presence of correlated disturbance and multipath. Another potential topic for future research is the hardware implementation of the proposed DOA estimators.

The severely ill-conditioned dictionary associated with the spinning antenna problem is a significant limitation. Therefore, the use of super-resolution techniques that cope with the severely ill-conditioned dictionary could be investigated in future research. Also, the investigation of super-resolution techniques that provide better performance in terms of spatial resolution and DOA estimation accuracy can be done in future research.

Bibliography

[1] A. Farina, F. Gini, and M. Greco, "DOA estimation by exploiting the amplitude modulation induced by antenna scanning", IEEE Transactions on Aerospace and Electronic Systems, Vol. 38, pp. 1276-1286, Issue 4, October 2002.

[2] F. Gini, M. Greco, and A. Farina, "Multiple radar targets estimation by exploiting induced amplitude modulation", IEEE Transactions on Aerospace and Electronic Systems, Vol. 39, pp. 1316-1332, Issue 4, October 2003.

[3] M. Greco, F. Gini, A. Farina, and L. Timmoneri, "Direction-of-arrival estimation in radar systems: moving window against approximate maximum likelihood estimator", Radar, Sonar & Navigation, IET, Vol. 3, no. 5, pp. 552-557, September 2009.

[4] Zhang, Q. Wan, and H. Wang, "DOA estimation in mechanical scanning radar systems using sparse signal reconstruction methods", WICOM Conference, Wuhan, China, 2011.

[5] A. Farina, G. Gabatel, and R. Sanzullo, "Estimation of target direction by pseudo-monopulse algorithm", Signal Processing, 80 (2000), 295-310.

[6] G. Galati and F. Studer, "Maximum likelihood azimuth estimation applied to SSR/IFF systems", IEEE Transactions on Aerospace and Electronic Systems, Vol. 26, pp. 27-43, Issue 1, January 1990.

[7] P. Swerling, "Maximum angular accuracy of a pulsed search radar", Proceedings of the IRE, 44, pp. 1146-1155, September 1956.

[8] B. Efron, "Biased versus unbiased estimation", Advanced Mathematics, Vol. 16, pp. 259-277, 1975.

[9] S. Kay and Y.C. Eldar, "Rethinking biased estimation [lecture notes]", Signal Processing Magazine, IEEE, Vol. 25, pp. 133-136, Issue 3, May 2008.

[10] Y. C. Eldar, "Uniformly improving the Cramer-Rao bound and maximum-likelihood estimation", IEEE Transactions on Signal Processing, Vol. 54, pp. 2934-2956, Issue 8, August 2006.

[11] Y. C. Eldar, "MSE bounds with affine bias dominating the Cramer-Rao bound", IEEE Transactions on Signal Processing, Vol. 56, pp. 3824-3836, Issue 8, August 2008.

[12] Y. C. Eldar, Rethinking biased estimation: improving maximum likelihood and the Cramer-Rao bound. Foundations and Trends in Signal Processing, Vol. 1, No. 4, pp. 305-449, 2007.

[13] A. De Martino, Introduction to modern EW systems (radar). Norwood, MA: Artech House, 2012.

[14] S. M. Kay, Fundamentals of statistical signal processing, estimation theory. Englewood Cliffs, NJ: Prentice-Hall, 1993.

[15] J. Tsui, Digital techniques for wideband receivers. Raleigh, NC: SciTech Publishing, 2004.

[16] E. Lipsky, Microwave passive direction finding. Raleigh, NC: SciTech Publishing, 2004.

[17] Electronic warfare and radar systems engineering handbook. Naval Air Systems, Raleigh, ALIAND, 2010.

[18] G.W. Stimson, Stimson's introduction to airborne radar. Edison, NJ: SciTech Publishing, 2014.

[19] D. Adamy, EW 101: a first Course in electronic warfare. Norwood, MA: Artech House, 2001, pp. 154.

[20] M. Skolnik, Radar handbook, Chapter 7. McGraw-Hill, 2008, 3rd edition.

[21] Optimization interface (OPTI) toolbox. [Online] Available at: http://www.i2c2.aut.ac.nz/Wiki/OPTI/.

[22] "ANT-1040G spinning DF antenna unit." [Online] Available at: https://www.rockwellcollins.com/-/media/Files/Unsecure/Products/Product_Brochures/EW-Intelligence/SIGINT/ANT-1040/ANT-1040_data_sheet.ashx

[23] D. Wipf, and D. Rao, "Sparse Bayesian learning for basis selection", IEEE Transactions on Signal Processing, Vol. 52, pp. 2153-2164, Issue 8, July 2004.

[24] D. Wipf, and D. Rao, "An empirical Bayesian strategy for solving the simultaneous sparse approximation problem", IEEE Transactions on Signal Processing, Vol. 55, pp. 3704-3716, Issue 7, June 2007.

[25] A. Farina, and M. Valeri, "Recovery of antenna pattern loss in a search radar", Signal Processing, 65 (1998), 329-336.

[26] P. Stoica, and B. Ottersten, "The evil of superefficiency", Signal Processing, 55 (1996), 133-136.

[27] O. Akhdar, D. Carsenat, C. Decroze and T. Monediere, "A simple technique for angle of arrival measurement", In Proc. Antenna and Propagation Soc. Int. Symp. (AP-S) 2008, pp. 1-4, San Diego, CA, USA.

[28] O. Akhdar, D. Carsenat, C. Decroze and M. Mouhamadou, "A new CLEAN algorithm for angle of arrival denoising", IEEE Antennas Wireless Propag.

Let., Vol. 8, pp. 478-481, 2009.

[29] J. P. Lie, T. Blu, and C. M. S. See, "Single antenna power measurements based direction finding", IEEE Transactions. Signal Processing, Vol. 58, no. pp. 5682-5692, Issue 11, 2010.

[30] J. P. Lie, T. Blu, and C. M. S. See, "Single antenna power measurements based direction finding with incomplete spatial coverage", IEEE International conference on Acoustics, Speech and Signal Processing (ICASSP), pp. 2641-2644, Kyoto, Japan, 2012.

[31] W. P. du Plessis, P. Potgieter, M. Gouws and E-Malan, "Initial results for compressive sensing in electronic support receiver Systems", Electronics, Communications and Photonics Conference (SIECPC), pp. 1-6, Riyadh, Saudi Arabia, 2011.

[32] H. Schultz, "Digital receiver experiment or reality", AOC Aardvark Roost Conference", 2008.

[33] P. Stoica and R. Moses, Introduction to spectral analysis. Raleigh, Englewood Cliffs, NJ: Prentice Hall, 1997, pp. 271.

[34] Yin. Zhang, Y. Zhang, Y. Huang, J. Yang, Y. Zha, J. Wu and H. Yang, "ML iterative superresolution approach for real-beam radar", IEEE Radar Conference, pp. 1192-1196, Cincinnati, OH, USA, 2014.

[35] Yin. Zhang, Y. Xia, W. Li, Y. Huang, and J. Yang, "An improved MUSIC algorithm for angular superresolution in scanning antenna", International Conference on Computational problem solving, pp. 358-361, Jiuzhai, China, 2013.

[36] U. Shikhar and N. Goodman, "Superresolution of coherent sources in real beam data", IEEE Transactions on Aerospace and Electronic Systems, pp. 1557-1566, Issue 3, 2010.

[37] Yin. Zhang, Y. Zhang, Y. Huang, J. Yang, Y. Zha, J. Wu and H. Yang, "An improved Richardson-Lucy algorithm for radar angular super-resolution", IEEE Radar Conference, pp. 406-410, Cincinnati, OH, USA, 2014.

[38] Yin. Zhang, Y. Zhang, Y. Huang, W. Li, Y. Zha, and J. Yang, "Angular superresolution for real beam radar with iterative adaptive approach", IEEE International Geoscience and remote sensing symposium, pp. 3100-3103, Melbourne, VIC, Australia, 2013.

[39] J. Guan, Y. Huang, W. Li, and J. Yang, "Maximum a posterior estimation based angular superresolution for scanning radar imaging", IEEE Transactions on Aerospace and Electronic Systems, pp. 2389-2398, 2014.

[40] Yin. Zhang, Y. Huang, Y. Zha, Y. Wang, and J. Yang, "Real-beam scanning radar angular super-resolution via sparse deconvolution", IEEE

International Geoscience and Remote Sensing Symposium, pp. 3081-3084, Quebec City, QC, Canada, 2014.

[41] Yin. Zhang, Y. Zha, J. Wu, Y. Huang, and J. Yang, "Weighted least squares method for forward looking imaging of scanning radar", IEEE International Geoscience and Remote Sensing Symposium, pp. 714-716, Quebec City, QC, Canada, 2014.

[42] J. Guan, Y. Huang, W. Li, and J. Yang, "Angular super-resolution algorithm based on maximum entropy for scanning radar imaging", IEEE International Geoscience and Remote Sensing Symposium, pp. 3057-3060, Quebec City, QC, Canada, 2014.

[43] Y. Huang, and J. Zhang, "Lower bounds on the variance of deterministic signal parameter estimators using Bayesian inference", IEEE International Conference on Acoustics, Speech, and Signal Processing (ICASSP '03), Vol. 6, pp. VI-745-8, Hong Kong, China, 2003.

[44] P. Forster, and P. Larzabal, "On lower bounds for deterministic parameter estimation", IEEE International Conference on Acoustics, Speech, and Signal Processing, 2002. Proceedings. (ICASSP '02). 2003, pp. II-1137 – II-1140 vol 2, Orlando, FL, USA.

[45] J. Tabrikian, and J.L.Krolik, "Barankin bounds for source localization in an uncertain ocean environment", IEEE Transactions on Signal Processing, Vol. 54, pp. 2917-2927, Issue 11, November 1999.

[46] D. Adamy, EW104: Electronic warfare against a new generation of threats. Norwood, MA: Artech House, 2015.

[47] F. Neri, Introduction to electronic defence. Raleigh, NC: SciTech Publishing, 2006.

[48] F. Gini, M. Greco, A. Farina and M. Gubinelli, "Asymptotic maximum likelihood estimation of multiple radar targets", Proceedings of the IEEE Radar Conference, Huntsville, AL, USA, 2003.

[49] M. Greco, F. Gini and A. Farina, "Joint use of sum and delta channels for multiple radar target DOA estimation", IEEE Transactions on Aerospace and Electronic Systems, Vol. 43, pp. 1146-1154, Issue 3, July 2007.

[50] “Reutech Radar Systems.” [Online] Available at: http://www.rrs.co.za/.

[51] Y. Zhang, W. Li, et al, "A fast iterative adaptive approach for scanning radar angular superresolution", IEEE Journal of Selected Topics in Applied Earth Observations and Remote Sensing, pp. 5336-5345, Vol. 8, Issue 11, July 2015.

[52] Y. Zhang, A. Jakobsson, et al, "Range-recursive IAA for scanning radar angular super-resolution", IEEE Geoscience and Remote Sensing Letters,

pp. 1675-1679, Vol. 14, Issue 10, August 2017.

[53] Yongchao. Zhang, Yin. Zhang, et al, "Angular superresolution for scanning radar with improved regularized iterative adaptive approach", IEEE Geoscience and Remote Sensing Letters, pp. 846-850, Vol. 13, Issue 6, April 2016.

[54] F. Lenti, F. Nunziata, et al, "Two-dimensional TSVD to enhance the spatial resolution of radiometer data", IEEE Transactions on Geoscience and Remote Sensing, pp. 2450 - 2458, Vol. 52, Issue 5, 2014.

[55] F. Lenti, F. Nunziata, et al, "On the spatial resolution enhancement of microwave radiometer data in Banach spaces", IEEE Transactions on Geoscience and Remote Sensing, pp. 1834 - 1842, Vol. 52, Issue 3, 2014.

[56] T. Yardibi, J. Li, et al, "Source localization and sensing: A nonparametric iterative adaptive approach based on weighted least squares", IEEE Transactions on Aerospace and Electronic Systems, Vol. 46, Issue 1, 2010.

[57] “OLYMPIA ELINT/ESM SYSTEM.” [Online] Available at: https://www.l3harris.com/sites/default/files/2020-07/ims_rms_datasheet_mid_Olympia.pdf

[58] A. Farina, Antenna Based Signal Processing Techniques for Radar Systems. Norwood, MA: Artech House, 1992.